CANNABINOIDS REGULATE TYPE 1 CANNABINOID RECEPTOR EXPRESSION IN CELL CULTURE MODELS OF HUNTINGTON'S DISEASE

by

Robert Laprairie

Submitted in partial fulfilment of the requirements
for the degree of Master of Science

at

Dalhousie University
Halifax, Nova Scotia
July 2012

DALHOUSIE UNIVERSITY

DEPARTMENT OF PHARMACOLOGY

The undersigned hereby certify that they have read and recommend to the Faculty of Graduate Studies for acceptance a thesis entitled "CANNABINOIDS REGULATE TYPE 1 CANNABINOID RECEPTOR EXPRESSION IN CELL CULTURE MODELS OF HUNTINGTON'S DISEASE" by Robert Laprairie in partial fulfilment of the requirements for the degree of Master of Science.

Dated: July 30 2012

Supervisor: _____

Readers: _____

_____

_____

DALHOUSIE UNIVERSITY

DATE: July 30 2012

AUTHOR: Robert Laprairie

TITLE: CANNABINOIDS REGULATE TYPE 1 CANNABINOID RECEPTOR EXPRESSION IN CELL CULTURE MODELS OF HUNTINGTON'S DISEASE

DEPARTMENT OR SCHOOL: Department of Pharmacology

DEGREE: MSc. CONVOCATION: October YEAR: 2012

_____

Signature of Author

TABLE OF CONTENTS

LIST OF TABLES

LIST OF FIGURES

ABSTRACT

Type 1 cannabinoid receptor (CB_1) levels decline in the striatum of animal models of Huntington's disease (HD) and in the brains of human patients suffering from HD prior to other pathogenic changes. CB_1 levels can be elevated by treatment with cannabinoids in non-neuronal cells. We wanted to determine: 1) whether cannabinoid treatment could induce CB_1 expression in a striatal cell line, and 2) determine the molecular mechanisms by which cannabinoids and mutant huntingtin regulate CB_1 expression. Treatment of striatal cell lines with CB_1-specific agonists produced a CB_1 receptor-, Akt-, and NF-κB-dependent increase in CB_1 promoter activity and mRNA expression that was attenuated in the presence of mutant huntingtin. Cannabinoid treatment was associated with increased expression of the trophic factor BDNF-2 and the mitochondrial regulator PGC1α in the cell types tested. *In vivo*, cannabinoids may initiate a positive feedback loop increasing receptor expression and restoring cannabinoid-dependent inhibition of neurotransmitter release.

LIST OF ABREVIATIONS USED

111/111	ST*Hdh*$^{Q111/Q111}$ striatal cells
2-AG	2-arachidonyl glycerol
5' UTR	5' untranslated region
7/111	ST*Hdh*$^{Q7/Q111}$ striatal cells
7/7	ST*Hdh*$^{Q7/Q7}$ striatal cells
ACEA	Arachidonyl-2-chloroethylamide
AEA	Anandamide
AM-281	1-(2,4-Dichlorophenyl)-5-(4-iodophenyl)-4-methyl-*N*-4-morpholinyl-1*H*-pyrazole-3-carboxamide
AM-630	1-[2-(morpholin-4-yl)ethyl]-2-methyl-3-(4-methoxybenzoyl)-6-iodoindole
ANOVA	Ananlysis of variance
AP-1	Activator protein 1
BDNF	Brain-derived neurotrophic factor
BMI	Body mass index
BSA	Bovine serum albumin
CalAM	Calcein AM
CB_1	Type 1 cannabinoid receptor
CB_2	Type 2 cannabinoid receptor
CMV	Cytomegalovirus
CNR1	Human type 1 cannabinoid receptor gene
CRE	cAMP response element
DARPP-32	Dopamine and cAMP-regulated phosphoprotein 32 kDa
DCIC	Dorsal colliculus and inferior colliculus of the cerebellum
DMSO	Dimethyl sulfoxide

E_{max}	The maximum effect
EC_{50}	50% effective concentration
eCBs	Endocannabinoids
ECS	Endocannabinoid system
EDTA	Ethylene diaminetetraacetic acid
Egr-1	Early growth-response protein 1
ERE	Estrogen response elements
ERK	Extracellularly-regulated kinase
EthD-1	Ethidium homodimer-1
FAAH	Fatty acid amide hydrolase
GABA	γ-amino butyric acid
GPCR	G-protein coupled receptor
HD	Huntington's disease
HDAC	Histone deacetylase
HPRT	Hypoxanthine ribosyl transferase
Htt	huntingtin protein
HU-308	[(1R,2R,5R)-2-[2,6-dimethoxy-4-(2-methyloctan-2-yl)phenyl]-7,7-dimethyl-4-bicyclo[3.1.1]hept-3-enyl] methanol
IκBα	Inhibitor of kappa B
Iκκ	IκB kinase
KO	Knock-out
LB	Luria broth
mAEA	meth-anandamide
MAPK	Mitogen-activated protein kinase
mHtt	mutant huntingtin protein

MSN	Medium spiny projection neuron
N-mHtt	amino-terminal cleavage product of mutant huntingtin protein
NaB	Sodium butyrate
NF-κB	Nuclear factor κ light chain B
NFAT	Nuclear factor of activated T cells
O-2050	(6a*R*,10a*R*)-3-(1-Methanesulfonylamino-4-hexyn-6-yl)-a,7,10,10a-tetrahydro-6,6,9-trimethyl-6*H*-dibenzo[*b*,*d*]pyran
OD	Optical density
P1	Post-natal day 1
PBS	Phosphate buffered saline
PDE	Phosphodiesterase
PFA	Paraformaldehyde
PGC1α	Peroxisome proliferator activated receptor γ co-activator 1α
polyQ	polyglutamine
ppENK	Pre-proenkephalin
RFLP	Restriction fragment length polymorphism
RT	Reverse transcriptase
S.E.M	Standard error of the mean
SDS	Sodium dodecyl sulfate
SSC	Saline sodium citrate buffer
STAT	Signal transducers and activators of transcription
Tdt	Terminal deoxynucelotidyl transferase
THC	Δ^9-tetrahydrocannabinol
TSA	Trichostatin A
TY	Tryptone/yeast extract broth

URB-597	(3’-(aminocarbonyl)[1,1-bipheynl]3-yl)-cyclohexylcarbamate
WT	Wild-type

ACKNOWLEDGEMENTS

I would like to extend great thanks to my supervisor Dr. Eileen M. Denovan-Wright for her constant support and aid. I would also like to extend my gratitude to Kathleen Murphy, Matthew Hogel, Amina Bagher, Gregory Hosier, and Sarah Hutchings for their constant help and companionship. Thanks to my advisory committee: Drs. Christopher Sinal, Kishore Pasumarthi, and Barbara Karten for their knowledge and assistance. For the provision of certain drugs and animal tissue, thank you Dr. Melanie Kelly. Foremost, I am grateful to God, for in Him are all things possible. I am extremely thankful for the love, help and support of my wife, Kimberly. Without her care and thought this thesis and the work it required would not have been possible. I am appreciative too, for the love and support of my two sons, Ezra and Silas. Finally, I would like to acknowledge the financial support from Dalhousie University, the Canadian Institutes of Health Research (CIHR), the Canadian Consortium for the Investigation of Cannabinoids, the Molly Appeal for Neuroscience Research, and Faith life Financial without which I could not have completed this work.

CHAPTER 1

Introduction

One of the earliest changes that occurs during Huntington's disease progression is a decline in the level of type 1 cannabinoid receptor (CB_1) expression in the striatum. Activation of CB_1 is considered neuroprotective because Ca^{2+}-dependent neurotransmitter release is inhibited and expression of pro-survival genes is increased. Cannabinoid treatment can induce expression of CB_1 in non-neuronal cells. Here, we measured changes in the expression of several components of the endocannabinoid system during Huntington's disease pathogenesis, determined whether cannabinoid treatment could induce CB_1 expression in striatal cell lines, and if so, whether this treatment was beneficial in cells expressing mutant huntingtin. Overall, we wanted to determine if regulating cannabinoid tone and increasing CB_1 expression would be beneficial means of treating Huntington's disease.

1.1 Clinical Characteristics and Management of Huntington's Disease (HD)

Huntington's disease (HD) is a late onset, progressive, neurodegenerative disorder in which patients suffer from motor, cognitive, and psychiatric impairments (Walker, 2007). The global prevalence of HD is approximately 1 in 10,000, although the disease affects people of western European descent to a greater extent than other ethnicities [7 in 10,000; Huntington's disease collaborative research group (HDCRG), 1993]. HD was originally named Huntington's chorea. Chorea is the prominent movement disorder associated with the disease (Newcombe, 1981). Symptoms present as excessive involuntary movement and impaired voluntary movement early in the disease. Excessive involuntary movement describes chorea, whereas impaired voluntary movement causes problems with manual dexterity, swallowing, speech, and balance (Calkins & Van Allen, 1967). During the late phase of HD, excessive movement gives way to bradykinesia, muscular rigidity, and dystonia, similar to impairments observed in patients

suffering from Parkinson's disease (Calkins & Van Allen, 1967). Cognitive deficits affect 'executive functions' such as attention, perception, memory, language, planning and organization (Mestre *et al*., 2009). Psychiatric impairments in HD are quite variable. The incidence of depression among individuals with HD is 40%, compared to 8% in the general population (Thompson *et al.*, 2012). Patients suffering from HD may also suffer anxiety, paranoia, or obsessive-compulsive disorder (van Duijn *et al*., 2007). The symptomatic profile for HD differs in presence and degree of severity from individual to individual.

The progression of HD is variable, but can generally be grouped into three stages: early- middle- and late-symptomatic stages based on the effects of motor symptom severity on quality of life (Rosenblatt *et al*., 2008). Diagnosis of HD, based on chorea, does not usually occur until mid-life, with the median age of onset being between 35 and 55 years, depending on the population studied (Rosenblatt *et al*., 2008). Choreiform movements are the most recognizable symptom in HD, but cognitive and psychiatric abnormalities may be detected prior to motor symptom onset (Orth *et al*., 2010; Rosenblatt *et al*., 2008). After symptom onset, HD symptom severity becomes progressively worse for 15 – 20 years until the patient dies (Rosenblatt *et al*., 2008). The leading causes of death among patients who had been suffering from HD are pneumonia, nutrional deficiencies, and choking (Conneally, 1984).

HD is classified as a neurodegenerative disease because the most obvious, thoroughly studied, pathophysiological change is neuron-specific degeneration. The Vonsattel grading scale is used to determine the degree of progressive atrophy and neurodegeneration, from grades 0 – 4, in the caudate-putamen, globus pallidus, and nucleus accumbens of HD patients (Vonsattel *et al*., 1985). Cresyl-violet staining with quantification of cell numbers in the caudate nucleus of HD patients has been used to demonstrate a 50% reduction of neurons in grade 1 patients and a 95%

reduction of neurons in grade 4 patients compared to age-matched controls (Vonsattel *et al*., 1985). Although the volumes of the caudate and putamen are most severely decreased, the volumes of the internal and external pallidus, cerebellum, and hypothalamus are all decreased in tissue taken from HD patients compared to age-matched controls (Vonsattel *et al*., 2011). In contrast, the volumes of the medial temporal lobe, thalamus, and white matter were not different in HD patients. Although neuronal atrophy is widespread, degeneration of the caudate and putamen regions of the striatum occurs earlier, and is more severe, than in any other brain region (Vonsattel *et al*., 2011).

Neurodegeneration within the striatum is cell-type-specific. The striatum is composed of medium spiny projection neurons (MSN) and aspiny interneurons. Aspiny neurons may be cholinergic, γ-aminobutyric acid (GABA)-ergic, and nitric oxide-containing depending on the type of neurotransmitter they synthesize and release (Vonsattel *et al*., 1985). MSNs are GABA-ergic and subdivided based on the additional type of neurotransmitter they release, the receptors they express, and their projection path (Nestler *et al*., 2001). The direct movement pathway is innervated by MSNs that project from the striatum to the internal segment of the globus pallidus and substantia nigra pars compacta and substantia nigra pars reticulata, produce substance P, and express dopamine D_1 receptors (Nestler *et al*., 2001). The indirect movement pathway is innervated by MSNs that project from the striatum to the external globus pallidus, produce enkephalin, and express dopamine D_2 receptors. Initial observations suggested that MSNs were subject to selective degeneration while aspiny neurons were spared (Ferrante *et al*., 1990). Further investigation has shown that enkephalin-producing neurons of the indirect pathway are more susceptible to degeneration than substance P-producing neurons of the direct pathway (Sapp *et al*., 1995; Fig. 1).

The most prominent pathological change associated with HD occurs in the striatum, yet peripheral pathologies are also present. The most prominent peripheral pathology is weight loss and an inability to gain weight, both of which occur early in HD progression (Djousse *et al.*, 2002). One study examined body mass index (BMI) in HD individuals within 4 years of initial diagnosis and found BMI to be lower in men and women suffering from HD compared to age-matched controls (Djousse *et al.*, 2002). Weight loss occurs in patients suffering HD despite increased appetite and caloric intake (Trejo *et al.*, 2004).

1.1.1 Genetics of HD

The hereditary nature of HD was originally described by George Huntington in 1872 (HDCRG, 1993). George Huntington was able to infer the dominant hereditary nature of HD when he noted that offspring of an individual affected by HD who did not develop HD themselves did not sire future generations affected by the disease (HDCRG, 1993). More than a century later, restriction fragment length polymorphism (RFLP) and Southern blot analyses of DNA from American and Venezuelan HD families narrowed the location of the gene causing HD to the short arm of chromosome 4 (HDCRG, 1993). Hybridization probes were created and used to screen cDNA libraries for the gene within the short arm of chromosome 4. In 1993, the Huntington's disease collaborative research group discovered a cDNA transcript with a polymorphic 5' CAG repeat and high sequence similarity to a region of the short arm of chromosome 4, which they named *IT15* (interesting transcript 15; HDCRG, 1993). This gene has since been renamed *huntingtin*. *Huntingtin* is 13646 bp in length, containing 67 exons, coding for a 3142 amino acid, 348 kDa protein (Li *et al.*, 2006). *Huntingtin* mRNA is detectable in the

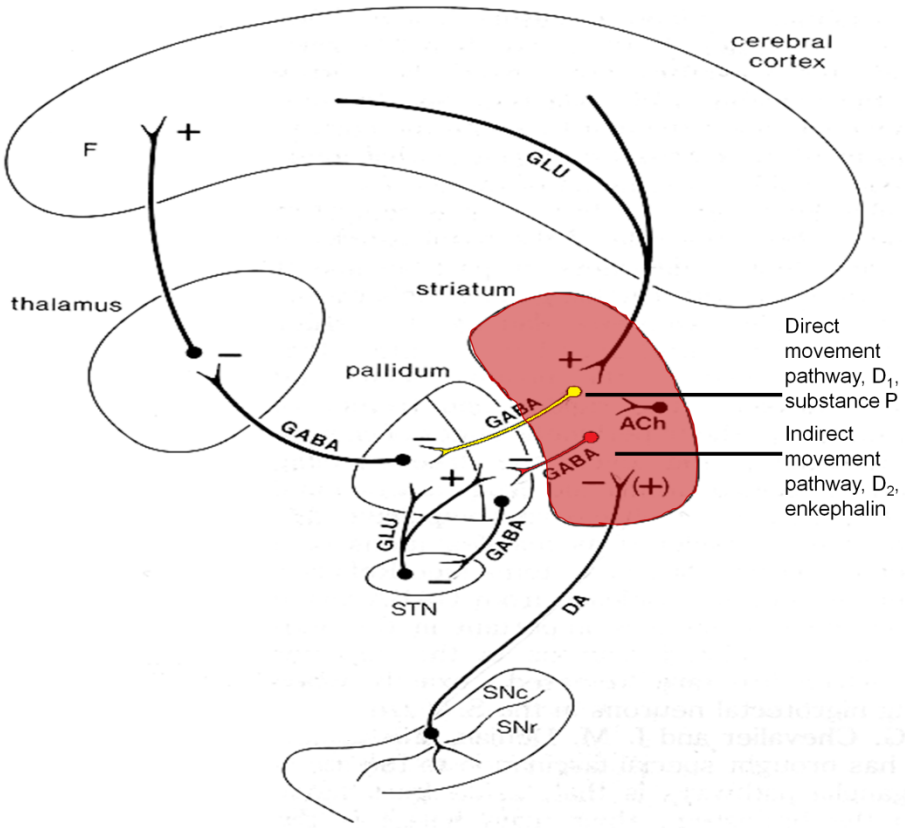

Figure 1. Striatal neurodegeneration during HD progression is cell-specific. HD pathophysiology is associated with a cell-specific degeneration of MSN of the indirect movement pathway that express D_2 receptors and enkephalin, and to a lesser extent MSN of the direct movement pathway that express D_1 receptors and substance P. Here, a schematic of the direct and indirect pathways is illustrated. The striatum is highlighted red, the MSN of the direct pathway are yellow, and the MSN of the indirect pathway are red. SNc, substantia nigra pars compacta; SNr, substantia nigra pars reticulata; DA, dopaminergic neuron; STN, subthalamic neuron; ACh, acetylcholine; GABA, γ-aminobutyric acid; GLU, glutamate; "+", excitatory; "-", inhibitory (modified from Nestler *et al*., 2001).

hippocampus, cerebellar cortex, neocortex, and corpus striatum, as well at lower levels in the pancreas, liver, colon, and spermatocytes in humans (Strong *et al*., 1993). The polymorphic 5' CAG repeat of the *huntingtin* gene encodes an amino (N)-terminal polyglutamine (polyQ) region in the translated huntingtin (Htt) protein (HDCRG, 1993; Lin *et al*., 1993; Strong *et al*., 1993). Several authors examined the CAG repeat length in HD and normal individuals and found that most normal individuals express *huntingtin* genes with 10 – 29 CAG repeats while the *huntingtin* alleles of HD patients had greater than 36 CAG repeats (Kremer *et al*., 1990; HDCRG, 1993; Landwehrmeyer *et al*., 1995). A small percentage of normal, healthy control subjects carried *huntingtin* alleles with 36 – 39 CAG repeats. It has since been demonstrated that the HD phenotype has 'reduced penetrance' when the CAG repeat length is between 36 – 39 such that these individuals have a 40% chance of being HD symptom free at 65 years of age and a 30% chance of being HD symptom free at 75 years of age (Quarrell *et al*., 2007). The number of CAG repeats present in an individual's *huntingtin* allele determines whether an individual will develop HD as well as the age of onset for the disease. CAG repeat length accounts for approximately 50% of the variation in HD age of onset, with a greater number of CAG repeats corresponding to an earlier age of symptom onset. CAG repeat length does not, however, predicate or indicate symptom severity or disease progression (Rosenblatt *et al*. 2006; Ravina *et al*., 2008).

Inheritance of one copy of mutant *huntingtin* does not change Htt protein expression (Sapp *et al*., 1995). Because Htt protein levels are not different in HD *versus* normal individuals, we can assume that altered expression of *huntingtin* does not contribute to HD pathogenesis. The polyQ expansion of mutant Htt (mHtt), therefore, is the mediator of the pathophysiological changes observed in HD. This could either be the result of a loss-of-function or a toxic gain-of-function for mHtt. If loss-of-function were the case, then we would expect deletion of the

huntingtin gene to produce an HD-like phenotype. However, heterozygous deletion of the *huntingtin* allele produces no change in phenotype, and homozygous deletion of the *huntingtin* allele causes embryonic death at day 8.5 in mouse (Dragatsis *et al*., 1998). If gain-of-function were the case, then we would expect that expression of mHtt, even in the presence of wild-type Htt, would produce an HD phenotype. Indeed, two mouse models of HD that overexpress an N-terminal fragment of mHtt in addition to two copies of wild-type Htt, recapitulate the reduced striatal volume, motor and psychiatric deficits associated with HD pathogenesis (Slow *et al*., 2005). Thus, inheritance of a single copy of the mutant *huntingtin* gene containing an expanded CAG repeat, which confers a toxic gain-of-function to the translated mHtt protein, is sufficient to cause HD pathogenesis.

The amino terminus of the Htt protein is a natural substrate for caspase-1, -2, -3, -6, and calpain-mediated cleavage, which releases an N-terminal fragment (N-mHtt; Hermel *et al*., 2004). PolyQ expansion of the Htt protein is associated with polyQ length-dependent increases in cleavage (Gafni *et al*., 2002). Inhibition of caspase or calpain-mediated mHtt cleavage to release N-mHtt is associated with a reduction in the severity of HD symptoms in rodent models of the disease (Hermel, 2004; Graham *et al*., 2006). These data support the hypothesis that N-mHtt is the toxic mediator of HD.

Following cleavage of mHtt, N-mHtt localizes to the nucleus. N-mHtt fragments have been localized to the nuclei of human striatal and cortical cells as well as the nuclei of striatal neurons in transgenic HD mice that overexpress exon 1 of mHtt with 150 CAG repeats (R6/2 HD mice; Gutekunst *et al*., 1999; Meade *et al*., 2002; Van Raamsdonk *et al*., 2005). In contrast, Htt and uncleaved mHtt do not accumulate in the nucleus (Graham *et al*., 2006). Both cleaved and uncleaved mHtt can form insoluble aggregates in the cytoplasm (Hermel *et al*., 2004), which

may facilitate a protective role within the cell (Meade *et al.*, 2004). N-mHtt appears to mediate its toxic effects within the nucleus by entering it passively (Graham *et al*., 2006). Collectively, these data demonstrate that the soluble, nuclear, cleaved, N-terminal, mHtt protein acquires a toxic gain of function that mediates HD pathogenesis.

1.2 Cellular Effects of Mutant Huntingtin Protein

Expression of mHtt is associated with deficits in energy metabolism and mitochondrial function, changes in intercellular signalling and neurotrophic support, and transcriptional dysregulation. With regard to energy metabolism, the concentration of ATP present in cellular lysates derived from HD mouse striatal neurons is lower than the ATP concentration measured in wild-type neurons (Trettel *et al*., 2000; Cui *et al*., 2006). Altered intercellular signalling, specifically excitotoxicty, may also contribute to HD pathology. Excitotoxicity is a degeneration of MSNs caused by either an increase in the amount of glutamate released from cortical neurons onto striatal dendrites or an increase in post-synaptic NMDA-mediated sensitivity of those striatal neurons to glutamate. Injection of the NMDA receptor agonist quinolinic acid into mice expressing full-length huntingtin with 72 glutamines led to a greater degree of striatal neuron degeneration than untreated HD or wild-type mice (Zeron *et al*., 2002). This suggests that HD may be associated with increased susceptibility to excitotoxicity. Treatments that decrease glutamate release may, therefore, have therapeutic potential in HD.

Levels of brain-derived neurotrophic factor (BDNF) are lower in the caudate and putamen of grade 3 HD patients compared to age-matched controls (Zuccato *et al.,* 2008). Cortical BDNF mRNA is less abundant in 6 week old R6/2 (Zuccato *et al*., 2005), and 3 month old YAC72 HD mice (Hermel *et al*., 2004). Striatal BDNF protein is less abundant in 5 month old R6/1 mice that overexpress exon 1 of mHtt containing approximately 115 CAG repeats

compared to controls (Spires *et al*., 2004). Heterozygous or homozygous knockout of BDNF recapitulates the striatal atrophy observed in HD (Strand *et al*., 2007). Intracellular protein signaling *via* extracellularly-regulated kinase (ERK)1/2 is also dysregulated in the presence of mHtt. Gines *et al*. (2010) observed that TrkB-mediated signalling *via* Ras, MAPK, and ERK1/2 (mitogen-activated protein kinases) was reduced in a cell culture model of striatal MSNs expressing two copies of the human mHtt transgene knocked into the mouse *huntingtin* locus (ST*Hdh*$^{111/111}$) compared to wild-type cells, while PI3K/Akt signalling was unaffected. Taken together, these data suggest that decreased neurotrophic support *via* BDNF and altered intracellular signaling contribute to neuronal cell death in HD.

Expression of mHtt is associated with transcriptional dysregulation of a relatively small subset of genes, with the majority remaining unaffected (Luthi-Carter *et al*., 2000). Luthi-Carter *et al*. (2000) found that only 1.7% (6 week old) and 1.2% (12 week old) of the 6000 transcripts analyzed were dysregulated in the presence of mHtt in the striatal tissue of R6/1 HD mice. Microarray analyses of post-mortem brain tissue derived from 44 HD patients (grades 0 – 4) demonstrated that transcriptional dysregulation occurs early in HD progression and is more severe in the caudate nucleus compared to the cerebellum or 2 cortical areas (Hodges *et al*., 2006). These studies demonstrate that cell-specific transcriptional dysregulation in the striatum is associated with mHtt expression and not cell death. Importantly, the cell autonomous affect of mHtt on transcription can be observed in cell culture models of HD (Luthi-Carter *et al*., 2000; Cui *et al*., 2006).

Transcription of type 1 cannabinoid receptor (CB_1) mRNA is reduced early in HD symptom progression in HD patients and all animal models of HD tested to date, relative to age-matched, healthy controls (Pazos *et al*., 2008). In humans, CB_1 mRNA and protein abundance, as

well as receptor binding, are lower in the internal and external segments of the globus pallidus, the substantia nigra pars reticulata, and the caudate and putamen of grades 3 and 4 HD patients relative to age-matched healthy controls and other regions of the brain (Denovan-Wright & Robertson, 2000; Allen *et al*., 2009). The R6/1 and R6/2 HD mouse models exhibit reduced CB_1 mRNA levels in the lateral striatum beginning at 6 and 4 weeks of age, respectively (McCaw *et al*., 2004). Striatal CB_1 mRNA levels are also reduced in the HD94 tetracycline-inducible and the *Hdh* mHtt knock-in models of HD (Lastres-Becker *et al.,* 2002; Blazquez *et al*., 2011). CB_1 mRNA expression is reduced in the presence of mHtt in the ST*Hdh* cell line (Blazquez *et. al*., 2011). Thus, CB_1 mRNA levels are lower in cultured neuronal cell models of HD, which lack intercellular signalling, compared to cells that do not express mHtt (Blazquez *et al*., 2011). McCaw *et al*. (2004) demonstrated that CB_1 transcription was repressed in R6/2 HD mice, in the presence of N-mHtt, by quantifying the number of primary CB_1 mRNA transcripts. Therefore, tissue-, cell-, and developmental stage-specific factors that normally facilitate high-level CB_1 mRNA transcription in the adult striatum are affected by the cell-autonomous overexpression of N-mHtt.

Transcriptional dysregulation can account for other pathogenic features of HD. The transcriptional co-activator peroxisome proliferator activated receptor γ co-activator 1α (PGC1α) controls the expression of several nuclear genes that regulate mitochondrial function (Lin *et al*., 2009). PGC1α mRNA levels are lower in pre-symptomatic HD patients, 3 month old R6/2 transgenic mice, and ST$Hdh^{111/111}$ cell models of HD compared to age-matched healthy individuals or wild-type controls (Trettel *et al*., 2000; Cui *et al*., 2006). BDNF mRNA expression, specifically BDNF-2, is also lower in the presence of mHtt in 6 week old R6/2 mice and HD patients (grades 1 and 2, Sipione *et al*., 2002; Valenza *et al*., 2005). Thus, deficits in

neurotrophic support may be explained by transcriptional dysregulation. mRNA levels of the dopamine and cAMP-regulated phosphoprotein 32 kDa (DARPP-32) are lower in striatal neurons derived from 6 week old R6/1 and R6/2 HD mice compared to wild-type mice (Gomez *et al*., 2006). DARPP-32 is highly expressed within the striatum and lowered DARPP-32 mRNA levels are a unique feature of HD pathogenesis, suggesting that the unique dysregulation of this gene is a direct consequence of mHtt expression. In section 1.3.5, we will discuss how decreased expression of CB_1 may contribute to the late-stage transcriptional dysregulation, excitotoxicity, and changes in motor control and behaviour observed in animal models of HD and in HD patients.

Transcriptional dysregulation is dependent upon the presence of soluble N-mHtt fragments within the nucleus. All models of HD tested to date exhibit some degree of transcriptional dysregulation associated with the expression of mHtt. Transcription is regulated at three levels: chromatin folding and structure, basal transcription machinery, and gene-specific co-activators and co-repressors. N-mHtt can interact with proteins involved at any of these levels to mediate transcriptional dysregulation. However, the gene-specific nature of transcriptional dysregulation in HD is indicative of interactions between N-mHtt and specific transcription factors and co-activators. These interactions squelch co-activation of transcription leading to transcriptional dysregulation. The Sp1 transcription factor interacts with N-mHtt and this interaction is associated with decreased promoter activity for the nerve growth factor receptor and D_2 receptor genes (Li *et al*., 2000). Both wild-type and mutant Htt affect the p50 subunit of the nuclear factor κ light chain B (NF-κB) transcriptional activator (Reijonen *et al.*, 2010). Expression of N-mHtt is associated with decreased levels of p50 (Reijonen *et al*., 2010), while wild-type Htt has been shown to traffic active NF-κB from dendritic spines to the nucleus in

neurons derived from *Hdh*$^{140/140}$ knock-in mice (Marcora *et al*., 2010). Thus, N-mHtt expression yields promoter-specific transcriptional dysregulation in a subset of genes.

1.2.1 Treatment of HD

There is no known cure for HD. All pharmacological treatments of HD attempt to control HD symptoms and progression. The majority of research has focused on therapeutic management of chorea. The only approved therapeutic for HD, tetrabenazine, is a monoamine-depleting agent that also antagonizes D_2 receptors and effectively reduces chorea (Scott, 2011). Neuroleptics and anti-psychotics that antagonize dopamine receptors have also been investigated for their ability to control chorea in patients suffering from HD. Of these, tiapride, haloperidol, flupenazine, perphenazine, pimozide, clozapine, olanzapine, and thiopropazate are able to improve motor impairments in HD during non-randomized, open-label trials (Killoran & Biglan, 2012). The bradykinesia observed during the late-symptomatic stage of HD can be treated by dopamine-replacement therapy, as in Parkinson's disease (Reuter *et al*., 2000; Racette & Perlmutter, 1998). Beyond the treatment of motor impairment, no clinical trials have been undertaken to determine appropriate therapies for improving cognitive or psychiatric impairments in patients with HD. Case reports have described improvements in depression in HD following treatment with imipramine for 3 weeks, mirtazapine for 2 weeks, or venlafaxine for 4 weeks (Whittier *et al*., 1961; Bonelli, 2003). Although numerous drugs exist that may improve motor or cognitive symptoms for those suffering from HD, no holistic, efficacious pharmocological approach has been found to manage this disease (Killoran & Biglan, 2012). Pre-clinical discoveries of promising therapeutic targets, such as gangliosides (Di Pardo *et al*., 2012) or kinase inhibitors (Atwal *et al*., 2011), have not yet been validated clinically. An ideal

therapy for the management of HD symptoms would improve motor coordination, cognition, and weight gain, without inducing unwanted psychoactive effects (Killoran & Biglan, 2012).

1.3 The Type 1 Cannabinoid Receptor

In the past decade, evidence has accumulated indicating that the endocannabinoid system (ECS) plays a critical role in the regulation of numerous biological processes including embryonic development, metabolism, and neurotransmission (Mechoulam & Hanu, 2001; Howlett *et al*., 2002). The ECS consists of endogenously synthesized endocannabinoids [eCBs, anandamide (AEA) and 2-arachidonoylglycerol (2-AG)], their receptors (the type 1 and type 2 cannabinoid receptors), and their anabolic and catabolic enzymes (Martin *et al*., 1999; Matsuda *et al*., 1990; Munro *et al*., 1993; Di Marzo *et al*., 1994; Cravatt *et al*., 1996). In addition to eCBs, phytocannabinoids and synthetic cannabinoids act as cannabinoid receptor ligands. CB_1 mediates cannabinoid-dependent signal transduction in the central nervous system and periphery (Howlett *et al.*, 2002; Basavarajappa *et al.*, 2009), while the type 2 cannabinoid receptor (CB_2) is localized to, and highly inducible in, peripheral haemopoietic cells and glial cells in specific areas of the central nervous system during the inflammatory response (Basavarajappa *et al.*, 2009; Atwood & Mackie, 2012). To date, the majority of CB_1 research has focused on ligand-receptor binding, signal transduction, and protein-protein interactions. In contrast, knowledge of CB_1 gene regulation is limited. CB_1 receptor abundance and the function of the ECS may change in response to altered CB_1 gene expression in different developmental or disease conditions, such as HD, and in response to drug exposure.

1.3.1 Architecture, Splice Variants, and Isoforms of the *CNR1* Gene

The human CB_1 gene (*CNR1*) spans 26.1 kb of chromosome 6 (6q14 – q15). *CNR1* contains 4 exons (Fig. 2A) and the protein coding region of CB_1 is contained entirely within exon 4 (Zhang *et al*., 2004). Outside of the coding region, alternative splicing of CB_1 mRNA produces six 5' untranslated region (5' UTR) splice variants. The precise transcription start sites within exon 1 included in 5' UTR variants 1, 3, 4 and 5 have not been defined, although it appears that multiple transcription start sites may exist within the first 60 bp of exon 1 (Shire *et al*., 1996). Transcription of variant 6 begins within intron 2 and thus the 5' most exon of variant 6 has been redefined as exon 3a. Transcription of variant 2 begins at the 5' end of exon 4. Transcript variants 1, 3, 4, 5, and 6 encode full-length CB_1 that is 472 amino acids in length encoded without interruption by a single region in exon 4. Exon 4, however, can be differentially spliced to remove 102 nts separating the 5' end of exon 4 and a new exon identified as exon 4a. This splicing occurs in transcript variant 2 that encodes the truncated, 439 amino acid, and CB_{1b} protein (Fig. 2D). In CB_{1a}, different intra-exon 4 splice sites result in the loss of 167 nts. Furthermore, two translation start sites are present at the 5' end of exon 4. Translation from the first produces CB_1 and CB_{1b}. Translation from the second is thought to produce the amino-terminal variant CB_{1a}, also known as CB_{1short} (Ryberg *et al.*, 2005). The macaque monkey (*Macaca mulatta*) CB_1 gene is located on chromosome 4. Although the number of exons is not known, the protein coding region of the gene is contained entirely within one contiguous coding region [Fig. 2B; National Institutes of Biotechnology (NCBI), 2011]. The mouse and rat CB_1 genes are located on chromosomes 4 and 5, respectively; both genes contain 2 exons with the protein coding regions existing entirely within the second exon in both species (Fig. 2C; Miller and Devi, 2011).

Figure 2. A) The human CB_1 gene, *CNR1*, spans 26.1 kb on chromosome 6. Six splice variants of the 5' UTR have been identified by sequencing cDNA ESTs. Splice variants are illustrated in blue and numbered on the left. Exons are numbered within the blue boxes. Each splice variant is aligned with respect to its nucleotide sequence in the *CNR1* gene (green, at top). The scale bar represents 5 kb of nucleotides. **B) The non-human primate (*Macaca mulatta*) CB_1 gene is poorly characterized yet it is known that the entire protein coding region is contained within 1 exon (NCBI, 2012).** The protein isoforms CB1a and CB1b have been described in non-human primates (Gustaffson *et al.*, 2008). **C) The rat and mouse CB_1 genes span approximately 20 kb on chromosome 4 and contain 2 exons.** The second exon contains the entire protein coding region. **D) *CNR1* CB_1 coding-region variants.** Three coding regions for protein isoforms of CB_1 have been described in humans and non-human primates: the 472 amino acid, intron-less CB_1, the 439 amino acid CB_{1b}, and the 411 amino acid CB_{1a}. In this figure, position 1 is 300 bp downstream of the 5' end of exon 4 in *CNR1*. Translation of CB_1 and CB_{1b} begins at the same ATG codon located 309 bp downstream of the first nucleotide in exon 4. Translation of CB_{1a} begins 326 bp downstream of the first nucleotide in exon 4. Fifty-nine bp downstream of the CB_{1b} translation start site, CB_{1b} contains a 102 bp intron that is spliced from the pre-mRNA at an atypical intron-exon splice junction (CT/cc and ag/GG). Eighty-eight bp downstream of the CB_{1a} translation start site, CB_{1a} contains a 167 bp intron that is spliced from the pre-mRNA at a typical 5' intron-exon boundary (AG/gt) and an atypical ag/GA 3' splice junction. Downstream of the CB_{1a} intron-exon junction the coding sequences of the three CB_1 isoforms are identical. ATG start codons are bold, Intron sequences are designated by '-'.

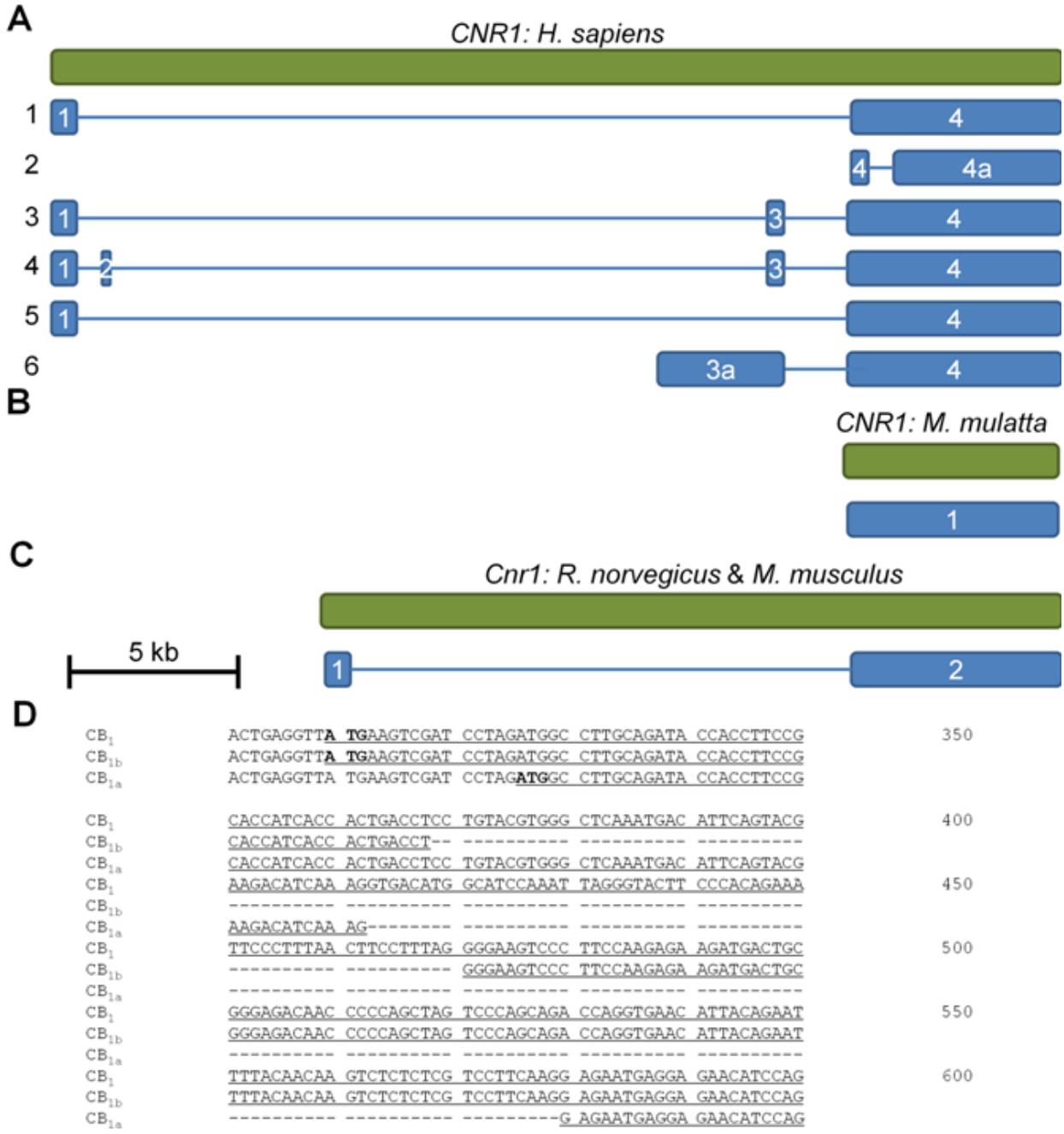
A
CNR1: H. sapiens
1
2
3
4
5
6
4a
3a
B
CNR1: M. mulatta
C
Cnr1: R. norvegicus & M. musculus
5 kb
D
CB1
CB1b
CB1a
ACTGAGGTTA TGAAGTCGAT CCTAGATGGC CTTGCAGATA CCACCTTCCG
CACCATCACC ACTGACCTCC TGTACGTGGG CTCAAATGAC ATTCAGTACG
AAGACATCAA AGGTGACATG GCATCCAAAT TAGGGTACTT CCCACAGAAA
TTCCCTTTAA CTTCCTTTAG GGGAAGTCCC TTCCAAGAGA AGATGACTGC
GGGAGACAAC CCCCAGCTAG TCCCAGCAGA CCAGGTGAAC ATTACAGAAT
TTTACAACAA GTCTCTCTCG TCCTTCAAGG AGAATGAGGA GAACATCCAG
G AGAATGAGGA GAACATCCAG
350
400
450
500
550
600

To date, CB_{1a} and CB_{1b} isoforms have only been identified in humans and higher primates (Ryberg *et al.*, 2005; Gustafsson *et al.*, 2008; Palermo *et al.*, 2009), and some evidence suggests CB_{1a} may be expressed in the rat (Shire *et al.*, 1996). Several authors have demonstrated that CB_1, CB_{1a}, and CB_{1b} receptors signal *via* $G_{i/o}$-type G-proteins and that the amino-terminal variants CB_{1a} and CB_{1b} have reduced affinity for cannabinoid agonists and antagonists (Rinaldi-Carmona *et al.*, 1996; Ryberg *et al.* 2005). However, Xiao and colleagues (2008) did not observe differences in the ligand affinity or localization of the three CB_1 protein isoforms. Moreover, the signalling properties of CB_1 receptor variants may be altered depending on the model system they are being studied in (Straiker *et al.*, 2012), which complicates our ability to understand receptor differences. In the majority of reports, steady-state CB_1 mRNA levels were measured *via* amplification of the common, 3' end, of the CB_1 coding region outside of the 5' region in exon 4 involved in differential splicing. The cell-specific relative abundance of CB_1 *versus* CB_{1a} or CB_{1b} is, therefore, poorly characterized (Gustaffson *et al.*, 2008). Early research suggested that CB_{1a} mRNA accounted for approximately 20% of the CB_1 transcript population (Shire *et al.*, 1996), yet more recent evidence suggests that less than 5% of the total population of CB_1 transcripts obtained from human fetal and adult brain tissue are CB_{1a} or CB_{1b} (Xiao *et al.*, 2008). Studies to define the relative abundance and distribution of the 5' UTR variants, 1 – 6 have measured the levels of expressed sequence tags. The 5' UTR transcript variants 1 (5732 bp), 3 (5863 bp), 4 (5901 bp), and 5 (5776 bp) are most abundant in the brain, lymphocytes, testes, and liver, relative to other tissues (NCBI, 2011); transcript variant 2 (5387 bp mRNA) is expressed at highest levels in the brain and testes (NCBI, 2011); transcript variant 6 (8974 bp mRNA) has only been isolated from brain tissue (NCBI, 2011). Regulation of the transcription of 5' UTR variants and how 5` UTR differences relate to CB_1 mRNA stability and

translation to different CB_1 isoforms has not been characterized. The abundance and activity of the different amino-terminal CB_1 isoforms may be regulated by different physiological conditions, isoform-specific ligand-receptor affinity, and the CB_1 isoform complement expressed in a given cell type (Ryberg *et al*., 2005).

1.3.2 CB_1-mediated Signal Transduction

CB_1 is a G-protein coupled receptor (GPCR) composed of 7 transmembrane α-helices (Stadel *et al*. 2011). The receptor is classically considered to exist on pre-synaptic nerve terminals of GABA-ergic neurons in the central nervous system, but is also present at the pre-synaptic nerve terminals of glutamatergic neurons in the central nervous system (Stadel *et al*., 2011). CB_1 protein is most abundant in pre-synaptic boutons, while the remainder of CB_1 receptors are present at the endoplasmic reticulum or the lysosome (Puente *et al*., 2010; Rozenfeld, 2011). In this setting, CB_1-mediated signal transduction is documented as occurring, most often, *via* coupling with $G_{i/o}$-type G-proteins (reviewed by de Lago & Fernandez-Ruiz, 2007). Following the release of neurotransmitter, the post-synaptic neuron synthesizes and releases the endogenous cannabinoid receptor agonists AEA or 2-AG. The synthesis and release of eCBs occurs on demand by the phospholipase A2 and C enzymes, which are phosphorylated and activated following membrane depolarization in the post-synaptic nerve terminal. The agonists cross the synaptic cleft to activate CB_1 receptors on the pre-synaptic neuron and induce $G_{i/o}$-type signal transduction. CB_1-dependent activation of $G_{i/o}$-proteins causes L-, N-, and P/Q-type Ca^{2+} channel inhibition, protein kinase A inhibition, rectifying K^+ channel activation, ERK activation, and activation of the PI3K/Akt pathway (Fig. 3). Inhibition of Ca^{2+} currents and activation of rectifying K^+ currents causes a decrease in Ca^{2+}-dependent neurotransmitter release. CB_1 activation modulates neurotransmitter release from the pre-synaptic neuron. For this reason, CB_1 activation is considered protective against excitotoxicity due to excessive glutamate release

(de Lago & Fernandez-Ruiz, 2007). Inhibition of protein kinase A yields a downstream decrease in transcription of cAMP response element (CRE)-dependent genes in the pre-synaptic neuron. Active MAPK induces immediate early gene transcription factors, such as *Jun* and *c-Fos*, in the pre-synaptic neuron (reviewed by Howlett *et al*., 2002). Activation of the PI3K/Akt pathway leads to activation of pro-survival signal cascades, phosphorylation of Iκκ, and subsequent activation of NF-κB (Ghose *et al*., 2011; Reijonen *et al*., 2010; Fig. 3). Aside from the predominant $G_{i/o}$-coupled signalling, CB_1 can couple to G_α-proteins to cause an increase in cAMP, G_q-proteins to cause an increase in intracellular Ca^{2+} release, or the non-G-protein factor associated with neutral sphingomyelinase to cause a transient increase in MAPK activity (Bosier *et al*., 2010). Finally, cannabinoid agonists are taken into the cell through the AEA membrane transporter and degraded by the enzymes fatty acid amide hydrolase (FAAH) or monoacylglycerol lipase, which degrade AEA and 2-AG, respectively.

Many GPCRs exist as hetero- or homo-dimers, or as multimers. GPCR oligomerization influences receptor ligand affinity, endocytosis, and G-protein coupling (reviewed by Hudson *et al*., 2010). CB_1 has been shown, in cell culture *via* bioluminescence resonance energy transfer, to form CB_1 homodimers, CB_{1a} and CB_{1b} heterodimers (unpublished data), and D_2 dopamine receptor, β_2-adrenoceptor, and μ- and δ-opiod receptor heterodimers, all of which co-exist and co-localize with CB_1 receptors *in vivo* (Fig. 3; Bortolato *et al*., 2010; Uriguen *et al*., 2009; Pacheco *et al*., 2009; Navarro *et al*., 2008; Rozenfeld *et al*., 2012).

CB_1 receptors can also bind synthetic agonists, antagonists, and inverse agonists. Approximately 85 phytocannabinoids have been isolated from the *Cannabis* plant, the most abundant being Δ^9-tetrahydrocannabinol (THC) and cannabidiol (Huffman, 2000). THC is a full agonist of CB_1 and CB_2. Cannabidiol has been shown to paradoxically inhibit and activate AEA

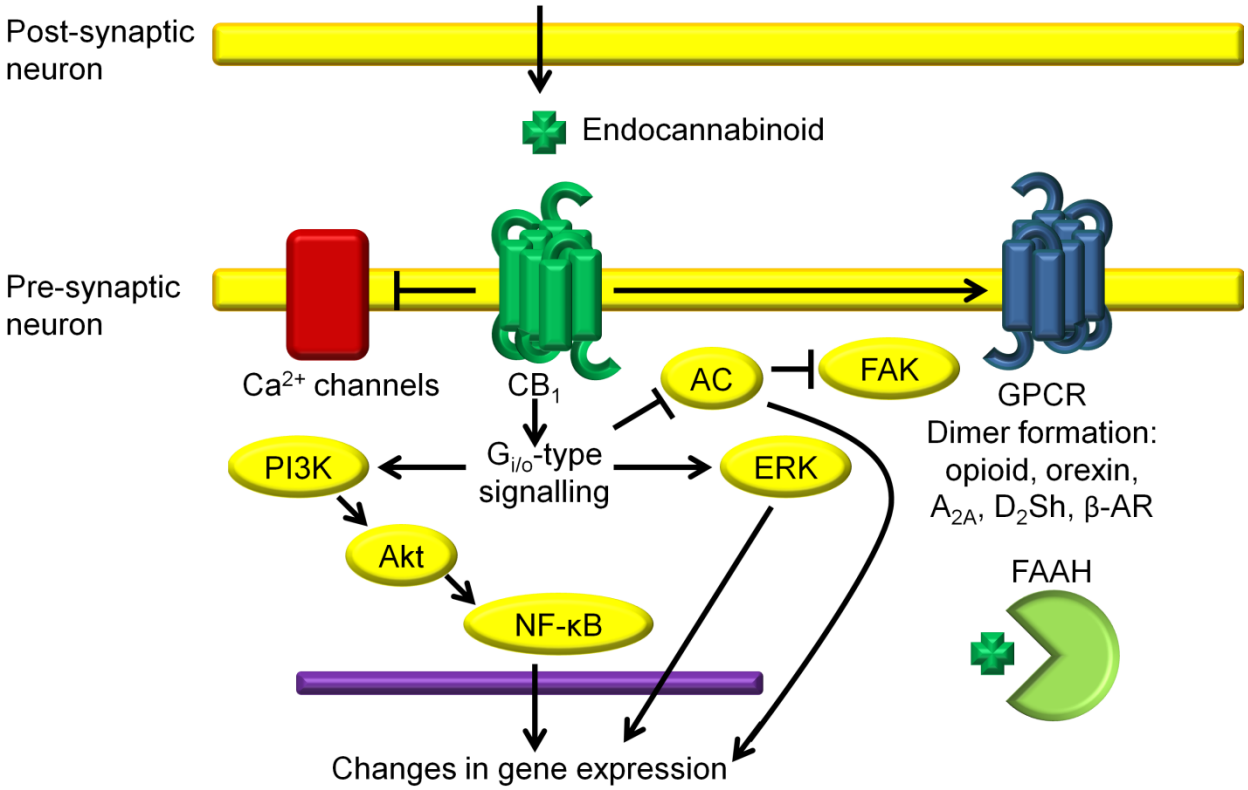

Figure 3. The endocannabinoid system (ECS) and CB_1. The GPCR CB_1 is activated by endocannabinoid ligands such as AEA, which cross the synaptic cleft toward the pre-synaptic neuron in a retrograde direction, and exogenous ligands such as THC. In the central nervous system, activation of CB_1, which is typically coupled to $G_{i/o}$-proteins, inhibits adenylyl cyclase, activates the MAPK and PI3K/Akt pathways, and causes changes in gene expression. Activation of CB_1 also causes inhibition of L-, N-, and P/Q-type Ca^{2+} channels and inhibits focal adhesion kinase (FAK). CB_1 can couple to several other GPCRs, which influences receptor trafficking and ligand affinity. The major catabolic enzyme of cannabinoids is fatty acid amide hydrolase (FAAH).

reuptake in mice by independent research groups, it antagonizes the putative cannabinoid receptor GPR55, and acts as a serotonin 5-HT_{1A} receptor agonist (Russo *et al.*, 2005; Mechoulam *et al*., 2007). Despite the confusion surrounding cannabidiol's mechanism of action, it is currently being investigated for its anticonvulsant, anti-inflammatory, and anxiolytic properties (Mechoulam *et al*., 2007). Synthetic cannabinoids are grouped into 5 classes: classical cannabinoids (structurally related to THC), aminoalkylindoles, diarylpyrazoles, quinolines, and cannabinoid-like eicosanoids (Lambert & Fowler, 2005). Notable synthetic cannabinoid agonists include: arachidonyl-2-chloroethylamide (ACEA), meth-anandamide (mAEA), and WIN 55,212-2, all of which have longer half-lives, and greater affinities for CB_1, than THC or AEA. These cannabinoids are far more potent than their naturally occurring analogs and their medicinal use is typically associated with profound psychoses (Lambert & Fowler, 2005). CB_1 can also be activated indirectly *via* inhibitors of FAAH, the major catabolic enzyme of cannabinoids, such as URB-597 (Hudson *et al.*, 2010) or positive allosteric modulation of the receptor (Ahn *et al.*, 2012). Two important cannabinoid antagonists are the diarylpyrazoles rimonabant (SR141716) and O-2050. Rimonabant was used clinically as an anti-obesity drug as well as an aid to smoking cessation. However, use of rimonabant is associated with severe depression and suicidal tendencies and the drug is no longer available for clinical use (Fong & Heymsfield, 2009). The synthetic inverse agonist AM-281 preferentially binds to CB_1 in its inactive conformation and has been used to study signalling cascades downstream of CB_1.

1.3.3 The *When* and *Where* of CB_1 Expression

In mammals, steady-state levels of CB_1 mRNA vary in different tissues and during different developmental periods. In humans, CB_1 is detected in neocortical progenitor cells and in the subventricular zone during the early cortical plate stages of development (9 to 17 weeks

gestation; Zurolo *et al*., 2010). CB_1 mRNA is also abundant at 19 weeks gestation in humans in white matter, which is nearly devoid of CB_1 expression in adulthood (Zurolo *et al*., 2010). In the human visual cortex, CB_1 mRNA levels rise during early development and plateau approximately 1 year after birth (Pinto *et al*., 2010); from the steady-state CB_1 mRNA plateau achieved 1 year after birth, CB_1 mRNA levels increase further in the visual cortex to reach a new steady-state level during adolescence, after which, CB_1 mRNA abundance declines throughout adulthood (Pinto *et al.* 2010). In the non-human primate, *Macaca mulatta*, high levels of CB_1 mRNA have been observed in the prefrontal cortex during neonatal development (Eggan *et al*., 2010); CB_1 mRNA abundance increases in the prefrontal cortex until reaching a steady-state at P5 (Eggan *et al.*, 2010). In the same manner as is observed in the human visual cortex, a higher steady-state level of CB_1 mRNA is observed in the *Macaca mulatta* prefrontal cortex during adolescence, and steady-state CB_1 mRNA levels decline in the prefrontal cortex following adolescence (Eggan *et al*., 2010). In mice, CB_1 mRNA is detectable during embryonic development at the four-cell and eight-cell/morula stages (Paria *et al.*, 1995), and can still be detected at E12 in glutamatergic neurons of the cerebral cortex and hippocampus (Vitalis *et al*., 2008). CB_1 mRNA is abundant in the adult mouse thalamus, amygdala, dorso-lateral prefrontal cortex, hypothalamus, and pituitary (NCBI, 2011). Further, CB_1 expression is enriched in the striatum, relative to other brain regions, within the adult mouse central nervous system (Fernandez-Ruiz *et al.*, 2004; McCaw *et al*., 2004). It is within the striatum that high steady-state levels of CB_1 expression are dysregulated in Parkinson's disease and HD (Zeng *et al.*, 1999; Denovan-Wright & Robertson, 2000). The temporal and anatomical distribution of CB_1 expression during early development is similar in mice and rats (NCBI, 2011). Six to 8 week-old rats, which are sexually mature, have lower levels of CB_1 mRNA in the limbic/associative brain

areas compared to adolescents (Heng *et al*., 2011). Following periods of peak neurodevelopment associated with high CB_1 levels, CB_1 mRNA abundance declines in these brain regions (Heng *et al*., 2011). Taken together these data demonstrate that, in mammals, CB_1 mRNA levels peak during adolescence within the prefrontal cortex, limbic/associative areas, and visual cortex and subsequently decrease with age. Early development and adolescence represent critical developmental windows where the regulation of CB_1 expression changes in order for higher levels of expression to be achieved. It is likely that developmental stage-specific transcription factors or modifiers regulate the different steady-states of CB_1 expression.

High levels of CB_1 expression are related to the establishment of neuronal circuitry; during critical development periods, areas associated with neurogenesis and synapse formation, such as the subventricular zone, are enriched for CB_1 yet these areas are depleted of CB_1 expression in adulthood. The activity or abundance of the factors that enabled high steady-state CB_1 levels during development and adolescence may decrease in concentration or activity as part of the aging process (Eggan *et al*., 2010; Heng *et al*., 2011). Greater expression and subsequent activation of CB_1 receptors facilitates higher expression of several genes required for brain development, including tyrosine hydroxylase (TH), preproenkephalin (ppENK), the neural adhesion molecule L1, and Bcl-2/Bax genes involved in apoptotic regulation of development (reviewed in Fernandez-Ruiz *et al*., 2004). Mice lacking CB_1 exhibit altered dendritic morphology and lower synapse density in the prefrontal cortex (Fitzgerald *et al.*, 2012), impaired locomotor activity (Zimmer *et al*., 1999), and increased anxiety (Hill *et al*., 2011) compared to wild-type littermates. Thus, the developmental stage-specific expression of CB_1 facilitates the proper establishment of neuronal circuitry and the consequent normalization of behaviour (Fernandez-Ruiz *et al*., 2004). In adulthood, expression of CB_1 is cell-specific within the central

nervous system. Striatal MSNs and interneurons are enriched for CB_1 mRNA expression, relative to other cell populations, within the basal ganglia (Fernandez-Ruiz *et al*., 2004). Consistent with central nervous system anatomical distribution, CB_1 appears to be involved with aspects of motor coordination, mechanisms of reward and motivation, emotion, and central endocrine regulation during adulthood (Fernandez-Ruiz *et al*., 2004).

1.3.4 CB_1 mRNA Expression is Induced by Inflammation

Although CB_2 receptors are considered the major eCB receptor in the periphery, particularly as regulators of inflammation (Rajesh *et al*., 2007; reviewed in Atwood & Mackie, 2010), CB_1 receptors also contribute to regulation of the inflammatory response. Pro-inflammatory molecules induce CB_1 and CB_2 mRNA expression in cells that mediate the inflammatory responses (Gutierrez *et al*., 2006; Borner *et al*., 2008). The involvement of CB_1 in the inflammatory response was first examined in rat dorsal root ganglia (DRG), where complete Freund's adjuvant increased CB_1 mRNA abundance in glial cells of the DRG 4 hours post-treatment, relative to untreated controls (Amaya *et al*., 2006). Freund's adjuvant produces an inflammatory response and activates such transcription factors as nuclear factor of activated T cells (NFAT) and NF-κB in glial cells (Amaya *et al*., 2006; Borner *et al*., 2007a). Activation of NFAT and NF-κB is dependent on the endogenous pro-inflammatory cytokines CD3/28 and interleukin-4 (Borner *et al*., 2007a). CD3/28 and interleukin-4 induce CB_1 mRNA expression in human peripheral T cells and immortalized Jurkat cells (Borner *et al.*, 2007a, 2008). Borner and colleagues (2007a) examined CD3/28- or interleukin-4-mediated induction of CB_1 *via* a promoter-reporter plasmid in which chloramphenicol acetyl transferase activity was driven by a 3 kb fragment of the *CNR1* promoter. Short, double-stranded, decoy oligonucleotides containing the consensus sequences normally bound by NFAT or NF-κB were used to titrate NFAT or NF-

κB enhancers of transcription away from their endogenous promoters (Borner *et al*., 2007a). NFAT and NF-κB facilitate a CD3/28- or interleukin-4-dependent increase in CB_1 expression (Borner *et al*., 2007a). Using the same techniques, it was found that activator protein 1 (AP-1) and the signal transducers and activators of transcription 5 and 6 (STAT5 and STAT6) are also recruited to the *CNR1* promoter to mediate increased mRNA expression in Jurkat cells (Borner *et al*., 2007b and 2008). Together, these data demonstrate that pro-inflammatory cues mediate an increase in CB_1 mRNA level from an initial steady-state to a second, higher state through common mechanisms.

1.3.5 CB_1 Expression is Reduced in the Presence of mHtt

As mentioned earlier (Section 1.2), CB_1 mRNA and protein levels decline early in the pathogenesis of HD. In human grades 3 and 4 HD patients, CB_1 protein abundance is lower in the caudate and putamen compared to other brain regions and age-matched controls (Denovan-Wright & Robertson, 2000). The synthetic cannabinoid positron emission tomography tracer $^{[18F]}$MK-9470 was used to demonstrate that CB_1 receptor binding was reduced in the striatum of early-symptomatic HD rats and rats lesioned with quinolinic acid (Casteel *et al*., 2010). More recently, it has been shown that CB_1 receptor levels are decreased in GABA-ergic striatal neurons to a greater extent than glutamatergic striatal neurons in 4 week-old R6/1 mice (Chiodi *et al*., 2012).

Decreased CB_1 receptor function may contribute to progressive decline in HD. Separate research groups bred two different mouse models of HD with homozygous CB_1 knock-out mice ($CB_1^{-/-}$; Mievis *et al*., 2011; Blazquez *et al*., 2011). Both research groups found that mice over-expressing N-mHtt and having reduced CB_1 levels ($Htt^{+/+}$/mHtt *x* $CB_1^{+/-}$) exhibited an earlier HD symptom onset, a more rapid disease progression, and a greater degree of MSN degeneration

than wild-type mice or mice over-expressing N-mHtt with a full complement of CB_1 (Mievis *et al*., 2011; Blazquez *et al*., 2011). Their findings suggest CB_1 normally performs a neuroprotective role in the striatum and loss of this receptor contributes to HD pathogenesis.

Some additional evidence exists that suggests the ECS as a whole is dysregulated during HD pathogenesis. FAAH mRNA and protein abundance are higher in striatal neurons derived from late-symptomatic R6/1 and R6/2 mice compared to age-matched wild-type controls (Blazquez *et al*., 2011). More importantly, FAAH protein levels are higher in grade 3 HD patients compared to age-matched controls (Blazquez *et al*., 2011). Additionally, eCB levels are dysregulated in HD patients and mouse models. 2-AG levels are higher in the cortex of 12 week-old R6/1 mice, while AEA levels are reduced in the striatum and hippocampus of these mice (Dowie *et al*., 2009). AEA, not 2-AG, is considered the predominant endogenous ligand of striatal CB_1 receptors (Dowie *et al*., 2009). Further, evidence suggests that binding of 2-AG to the CB_1 receptor is associated with receptor desensitization and AEA binding is associated with $G_{i/o}$-type signal transduction (Dowie *et al*., 2009). Therefore, several components of the ECS may be dysregulated during HD pathogenesis, all of which may exacerbate the disease.

If CB_1 receptor levels are decreased, but not lost, then cannabinoid-based therapeutics may relieve some symptoms of HD (Dowie *et al*., 2009). In cell culture it has been shown that treatment with THC or the synthetic cannabinoid agonist HU-210 reduces cell death in PC12 cells over-expressing exon 1 of mutant *huntingtin* and ST*Hdh*$^{111/111}$ cells (Scotter *et al*., 2010; Blazquez *et al*., 2011). In the PC12 model of HD, the protective benefit was conferred *via* $G_{i/o}$-coupling because co-administration of Pertussis toxin eliminated the protective benefit (Scotter *et al*., 2010). Treatment of quinolinic acid or 3-NP lesion models of HD with cannabidiol or the synthetic CB_1 agonist WIN 55,212-2 reduces striatal neurodegeneration (Pinto *et al*., 2006;

Sagredo *et al*., 2007). Moreover, treatment of 3-NP-lesioned mice with AM-404, a cannabinoid reuptake inhibitor, reduces hyperkinesias relative to untreated controls (Lastres-Becker *et al*., 2002). Environmental enrichment increases CB_1 receptor levels in the striatum of R6/1 mice and is associated with delayed symptom onset and slower HD progression (Glass *et al.*, 2004). Dowie *et al*. (2010) observed that chronic THC or synthetic cannabinoid HU-210 treatment (8 weeks) of R6/1 mice beginning at 6 weeks of age had no affect on CB_1 receptor binding, CB_1 mRNA level, motor control, or striatal atrophy compared to untreated controls. However, treatment with the FAAH inhibitor URB-597 was associated with higher striatal CB_1 receptor binding in R6/1 mice compared to age-matched, wild-type controls (Dowie *et al*., 2010). From this, the authors concluded that extremely potent CB_1 agonists may not be suitable for treatment of HD symptoms, but manipulation of eCB levels for the treatment of HD remains an intriguing option. A more recent study, performed on symptomatic R6/2 mice, demonstrated that chronic treatment with THC (3 weeks) improved motor coordination, as measured by rotarod performance, and reduced striatal atrophy, compared to untreated controls (Blazquez *et al*., 2011). Thus, preclinical evidence suggests that CB_1 remains a promising target for HD treatment, although the potency and exposure to a given cannabinoid molecule will have a great affect on the outcome of the treatment.

1.3.6 CB_1 mRNA Level is Modulated by Cannabinoids

Cannabinoids modulate steady-state CB_1 mRNA abundance. Chronic treatment with THC has been shown to decrease CB_1 mRNA levels in the central nervous system of rodents. Repeated exposure to THC, once daily for 14 days by intra-peritoneal injection, decreases CB_1 mRNA levels in the caudate and putamen of adult male rats (Corchero *et al*., 1999). The extent of CB_1 mRNA decrease correlates to the number of repeated exposures. Cannabinoids have also

been shown to increase CB_1 mRNA levels in primary and immortalized cell culture systems (Borner *et al.*, 2007a; Mukhopadhyay *et al.*, 2010; Proto *et al.*, 2011). Treatment of primary mouse hepatic stellate cells with 2-AG induces CB_1 mRNA, up to 30-fold relative to basal expression in untreated cells (Mukhopadhyay *et al.*, 2010). 2-AG-mediated CB_1 induction is retinoic acid receptor (RAR)γ- and CB_1 receptor-dependent in this model system (Mukhopadhyay *et al.*, 2010). AEA has been reported to increase CB_1 mRNA levels in DLD-1 and SW620 cells (Proto *et al.*, 2011). This effect was estrogen receptor- and RARα-dependent. Finally, THC, mAEA, and the CB_2-selective agonist JWH-015 induce CB_1 mRNA expression in Jurkat cells in a CB_2-dependent manner (Borner *et al.*, 2008). Borner and colleagues (2008) observed that CB_2 activation leads to phosphorylation of STAT5/6 – thereby inducing CB_1 promoter activity (Borner *et al.*, 2008). Thus, in some systems, cannabinoid-dependent activation of CB_1 and CB_2 receptors stimulates the activity of specific transcription factors, such as the estrogen receptor, RARα, and STAT6 and augments steady-state CB_1 mRNA level above basal levels. In other systems, cannabinoid exposure down-regulates CB_1 mRNA levels (Corchero *et al.*, 1999). Cannabinoid treatment therefore, as in various pathological conditions, is associated with, malleable, context-specific regulation of CB_1 expression.

In vivo, repeated exposure to cannabinoid agonists is associated with receptor tachyphylaxis (Corchero *et al.*, 1999); whereas in cell culture, single acute doses of cannabinoid agonists induce CB_1 mRNA expression (Mukhopadhyay *et al.*, 2010; Borner *et al.*, 2008). From these observations, it is clear that the response of CB_1 mRNA level to cannabinoid treatment depends on the nature of treatment, chronic *versus* acute, as well as the potency and efficacy of the ligand. For example, CB_1 mRNA expression may be inducible in *in vivo* studies examining

acute doses of cannabinoids, indirect cannabinoid agonism *via* FAAH inhibitors (Kim & Alger, 2010), or allosteric modulation of CB_1 receptor activity (Ahn *et al*., 2012; Navarro *et al*., 2009).

CB_1 protein levels are also increased following acute cannabinoid-dependent induction of CB_1 mRNA levels (Mukhopadhyay *et al*., 2010; Proto *et al*., 2011). This increase is modest (4 – 5-fold) compared to the increased mRNA expression (29 – 30-fold) observed (Mukhopadhyay *et al*., 2010; Proto *et al*., 2011), yet represents an increase in the pool of CB_1 receptors. In these studies, CB_1 protein abundance was quantified *via* western blot. Therefore, it is not known whether cannabinoid-mediated CB_1 induction affects the localization or functionality of CB_1 receptors.

1.4 Objectives of this Study

From the existing literature, it appears that CB_1 expression is decreased in HD, and this decrease may be implicated in the pathogenesis of HD (Mievis *et* al., 2011). There is no cure for HD and existing treatment strategies have limited efficacy. CB_1 receptor activation enhances pro-survival signalling pathways and modulates neurotransmitter release. These effects improve neuronal health, and modulate appetite, motor coordination, cognition, and mood. Preclinical evidence suggests that cannabinoid-based therapeutics may be a useful means of treating HD patients (Blazquez *et al*., 2011). However, no study has yet determined how manipulation of the ECS as a whole may affect HD pathogenesis nor determined whether cannabinoids can increase expression of their cognate receptors in neuronal cell populations.

The objectives of my research were 1) to determine whether expression of mHtt was associated with changes in the ECS, such as cortical FAAH mRNA levels, striatal CB_2 mRNA levels, and cortical and region-specific striatal CB_1 mRNA levels, 2) to establish whether cannabinoid treatment can or cannot induce CB_1 mRNA and protein expression, and if

cannabinoid treatment was associated with increased CB_1 levels, to determine the molecular mechanism by which this occurred, 3) to examine the affect of decreased expression of CB_1, in the absence of mHtt, on transcriptional regulation, and 4) to determine if cannabinoid treatment, and subsequent CB_1 receptor induction, were associated with improved cellular viability and ameliorated transcriptional dysregulation in the presence of mHtt.

We analyzed the mRNA expression of components of the ECS in R6/1 and R6/2 HD mice and age-matched wild-type littermates *via in situ* hybridization and quantitative reverse transcriptase PCR (qRT-PCR). *In situ* hybridization allowed us to monitor tissue-specific and time-dependent changes in the abundance and distribution of mRNAs over the course of the animal's lifespan in two well-characterized mouse models of HD. We chose to analyze the regulation of CB_1 levels, the mechanism of cannabinoid-mediated CB_1 induction, and changes in cell viability in the ST*Hdh* cell culture model of HD.

Given that modulation of the CB_1 levels and the ECS may represent a viable means of treating HD symptoms, the primary aim of this research is to better understand changes in the ECS during HD progression. Specifically, I sought to characterize the regulation and malleability of CB_1 in the presence of mHtt.

CHAPTER 2

Materials and Methods

2.1 Animal Care, Tissue Collection, and Preparation

Animal care and handling protocols were in accordance with the guidelines provided by the Canadian Council on Animal Care, and were approved by the Carleton Animal Care Committee at Dalhousie University. Mice were terminally anaesthetized by injection of sodium pentobarbital and their pedal reflexes were monitored. Adults were decapitated and brains were removed, and post-natal day 1 (P1) mice were killed by an overdose of sodium pentobarbital. Tissue was stored at -80°C. Fourteen micrometer coronal brain tissue sections (adult mice), or 14 µm whole-body sagittal sections (P1 mice), were made from previously frozen tissue using a 2800 Frigocut Reichard-Jung cryostat. Sections were thaw mounted onto Superfrost slides (Fisher Scientific, Ottawa, ON). Mounted tissue sections were archived at -80°C for future use.

Archived tissue from R6/1, R6/2, or $CB_1^{+/-}$ and wild-type littermate mice was collected. R6/1 and R6/2 mice were previously genotyped *via* PCR amplification of the human *huntingtin* transgene, using DNA extracted from an ear punch (Hebb *et al*., 2004). $CB_1^{+/-}$ mice were genotyped *via* PCR amplification of the *Cnr1* coding region, using primers flanking this coding region (Table 1), according to the instructions provided in the Extract-N-Amp blood PCR kit (Sigma-Aldrich, Oakville, ON). Tissue was obtained from four animals in each of the four disease stages identified for R6/1 mice [pre- (4 week), early- (8 week), mid- (14 week), and late- (26 week) symptomatic], and each of the three disease stages identified for R6/2 mice [pre- (3 week), early- (6 week), and late- (11 week) symptomatic], 4 P1 R6/2 mice, and 3 10 week-old heterozygous CB_1 ($CB_1^{+/-}$) knock-out mice. Tissue derived from wild-type, age-matched, littermates were used as controls.

Table 1. Sequence, annealing temperatures, and target PCR products of primers used in RT-PCR and qRT-PCR analyses of gene expression

Target	Oligonucleotide Sequence (5' - 3')	Annealing Temperature (°C)	$MgCl_2$ (mM)	Reference
CB_1 genotype	GTACCCATCACCACAAGACCTCC GGATTCAGAATCATGAAGCAC (WT) AAGAACGAGATCAGCAGCCTC (KO)	58	1	Self-designed
CB_2	GGATGCCGGGAGACAGAAGTGA CCCATGAGCGGCAGGTAAGAAAT	57	2	Self-designed
CB_1	GGGCAAATTTCCTTGTAGCA GGCTAACGTGACTGAGAAA	58	1	Blazquez *et al*., 2011
BDNF-2	AGTCTCCAGGACAAGGATGAAC AAGGATGGTCATCACTCTTCTCA	58	1	Blazquez *et al*., 2011
PGC1α	TTGCTAGCGGTCCTCACAGA GGCTCTTCTGCCTCCTGA	60	2	Cui *et al*., 2006
DARPP-32	AGGAGGCCTCTCCACATCAG CCGTATGGGCAGATTGAGTA	58	2	Yamamoto *et al*., 2009
β-actin	AAGGCCAACCGTGAAAAGAT GTGGTACGACCAGAGGCATAC	59	2	Blazquez *et al*., 2011
HPRT	GCTGGTGAAAAGGACCTCT CACAGGACTAGAACACCTGC	59	3	McCaw *et al*., 2004

CB_1, type 1 cannabinoid receptor; CB_2, type 2 cannabinoid receptor; BDNF, brain-derived neurotrophic factor; PGC1α, peroxisome proliferator activated receptor γ co-activator 1α; DARPP-32, dopamine and cAMP regulted phospho-protein of 32 kDa; HPRT, hypoxanthine ribosyl transferase. WT, wild-type CB_1 genotype reverse primer; KO, knock-out CB_1 genotype reverse primer.

2.2 *In situ* Hybridization

In situ hybridization was performed on coronal sections of mouse brains (spanning Bregma 1.7 to -2.2 mm; Paxinos and Franklin, 2004) or whole-body mounts of P1 mice using radiolabelled oligonucleotide probes specific to several mRNAs (Table 2). Synthetic oligonucleotide probes (Sigma-Aldrich) were 3'-end labelled with [α-P^{33}]dATP (3000 Ci/mmol; Perkin Elmer, Waltham, MA) as follows: oligonucleotide probe (0.4 μM), 20% terminal deoxynucleotidyl transferase (Tdt) buffer, Tdt enzyme (30 U, Promega, Madison, WI), and [α-P^{33}]dATP (600 Ci/mmol) were added together in RNase- and DNase-free dH_2O to a final volume of 25 μL. The end-labelling reaction was carried out at 37°C for 90 min. Ethylene diaminetetraacetic acid (EDTA, 0.05 M, Sigma-Aldrich) was added to stop the reaction and RNase- and DNase-free dH_2O was added to a final volume of 50 μL. Unincorporated radionucleotides were removed from the labelled oligonucleotide probes via gel exclusion chromatography with Microspin G-25 spin columns (Amersham Biosciences, Piscataway, NJ) which were used according to the manufacturer's instructions and were discarded. Eluted radiolabelled olgionucleotides were used for hybridization.

Selected slides were removed from storage at -80°C and allowed to reach room temperature. All reagents used to make solutions were RNase-free and obtained from Sigma-Aldrich, unless otherwise noted. Tissue was fixed in 4% paraformaldehyde (PFA) for 5 min. Slides were rinsed twice for 5 min each in 1X phosphate-buffered saline (PBS; 0.137 M NaCl, 0.027 M KCl, 0.014 M KH_2PO_4, 0.043 M Na_2HPO_4•7 H_2O) and once for 20 min in 2X saline sodium citrate buffer (SSC; 0.3 M NaCl, 30 mM tri-sodium citrate, pH 7.0) at room temperature.

Table 2. Sequence and target mRNA transcripts of oligonucleotides used for *in situ* hybridization.

Target	Oligonucleotide Sequence (5'- 3')	Reference
CB_1	ATGTCTCCTTTGATATCTTCGTACTGAATGTCATTTG	McCaw *et al*., 2004
CB_2	GGCGTAATACGACTCACTATAGGGCCTTTATTAGGGAGGCTGA	Munro *et al*., 2004
FAAH	GTCAGCCAGATAGGAGGTCACACAGTTGGTCCCTTTGTTCACTT	Self-designed
DARPP-32	TCCACTTGGTCCTCAGAGTTTCCATCTCTC	Gomez *et al*., 2006
PDE10A	GACCAATGTCAAAGTGGAATAGCTCGATGTCCCGGC	Hebb *et al., 2004*
PDE1B	CATGTAGCGCAGCAGAGACCGTAGCTTAATCCACA	Hebb et al., 2004
Egr-1	CCGTTGCTCAGCAGCATCATCTCCTCCAGTTTGGGGTAGTTGTCC	Rodriguez-Lebron *et al.,*2005
ppENK	TCCACTTGGTCCTCAGAGTTTCCATCTCTC	Rodriguez-Lebron *et al.*, 2005
D_2	GGCAGGGTTGGCAATGATACACTCATTCTGGTCTGTATT	Rodriguez-Lebron *et al.*, 2005
PGC1α	AATAGGCCATCCATGGCTAGTCC	McKee *et al*., 2005
Dynamin	CACTGGCTTTCTCTTTGTCCCCAAGAGGCTC	Rodriguez-Lebron *et al.*, 2005
β-actin	TCCACTTGGTCCTCAGAGTTTCCATCTCTC	Rodriguez-Lebron *et al.*, 2005

CB_2, type 2 cannabinoid receptor; FAAH, fatty acid amide hydrolase; DARPP-32, dopamine and cAMP-regulated phospho-protein 32 kDa; PDE10A, phosphodiesterase 10A; PDE1B, phosphodiesterase 1B; Egr-1, early growth-response protein 1; ppENK, pre-proenkephalin; D_2, type 2 dopamine receptor; PGC1α, peroxisome proliferator activated receptor γ co-activator 1α.

Slides were allowed to dry for 60 min. Hybridization buffer, consisting of 5X SSC (0.75 M NaCl, 75 mM tri-sodium citrate, pH 7.0), 2% Denhardt's solution, 0.02 M Na_3PO_4 (pH 6.8), 0.2% sodium dodecyl sulfate (SDS), 5 mM M EDTA, 10 µg/mL polyA oligonucleotides, 50 µg/mL salmon sperm DNA, 50 µg/mL Yeast tRNA, and 10% (w/v) dextran sulphate was made up to a final volume of 100 mL in dH_2O. The hybridization buffer was boiled for 10 min and rapidly chilled. The entire 50 µL radiolabelled oligonucleotide probe was added to the chilled hybridization buffer. The solution was mixed on a rocking platform for 10 min. Once the slides had dried for 60 min, 200 µL of hybridization buffer containing approximately $1x10^6$ cpm of labelled probe were added to each slide. Individual slides were placed in 10 cm petri dishes and covered in parafilm. Petri dishes were placed in Tupperware containers with a piece of wet filter paper. Containers were sealed and incubated overnight at 42°C. Following hybridization, slides were subjected to twelve, 30 min, 55°C, consecutive washes: four in 1X SSC (0.15 M NaCl, 15 mM tri-sodium citrate, pH 7.0), four in 0.5X SSC (0.075 M NaCl, 7.5 mM tri-sodium citrate, pH 7.0), and four in 0.25X SSC (0.0375 M NaCl, 3.75 mM tri-sodium citrate, pH 7.0). Slides were dipped once in dH_2O and allowed to dry overnight at room temperature.

All slides were exposed to Kodak Biomax MR film (Simga-Aldrich), in a light-tight case for 4 weeks at room temperature. Following X-ray autoradiography, the tissue on the slides was counter-stained with cresyl violet to visualize anatomical structures. Autoradiographic films were scanned using a flat bed scanner and stored as digital images. mRNA distribution and densitometry were analyzed using Kodak 3D imaging software (version 3.6.1). Optical density (OD) of the mRNA hybridization signals was measured in various regions of the mouse brain or post-natal mouse body. Local film background was subtracted from each of the mRNA hybridization measurements to account for variability between sections and background signal.

mRNA hybridization was measured in each of the wild-type, R6/1, R6/2, and $CB_1^{+/-}$ mice in the lateral striatum. CB_1 mRNA expression was also measured in the cortex, dorsomedial and ventromedial striatum. FAAH, early growth-response protein 1 (Egr-1), and dynamin expression were measured in the cortex (Fig. 4). mRNA hybridization measurements were averaged at each disease stage to attain a measurement of mRNA level in the mouse brains.

2.3 ST*Hdh* Cell Culture

The ST*Hdh* cell lines are derived from striatal precursor cells obtained from embryonic day 14 wild-type mice [ST$Hdh^{Q7/Q7}$ (7/7)] or knock-in mice expressing one copy [ST$Hdh^{Q7/Q111}$ (7/111)] or two copies [ST$Hdh^{Q111/Q111}$ (111/111)] of exon 1 of the human *huntingtin* allele in the mouse *huntingtin* locus that have been transduced with a defective SV40 retrovirus containing the temperature-sensitive A58/U19 large T antigen and geneticin-resistance genes, which confers conditional immortalization (Coriell Institute, Camden, NJ; Trettel *et al*., 2000; Paoletti *et al*., 2008). Cells were maintained at the permissive temperature of 33°C, at 5% CO_2, 95% O_2, in Dulbecco's modified eagle's medium (DMEM) supplemented with 10% fetal bovine serum, 2 mM L-glutamine, $1x10^4$ U/mL penicillin/streptomycin, and 400 µg/mL geneticin in cell-culture treated flasks or 0.01% poly-D-lysine-coated wells (Invitrogen, Burlington, ON; Paoletti *et al*., 2008). Cells were not maintained past the fifth passage. Multi-well plates were coated with 0.01% poly-D-lysine to provide an adherent substrate for growing cells. Wells were rinsed once with dH_2O, incubated with 0.01% poly-D-lysine for 2 h at 37°C, rinsed twice with 1X PBS, and allowed to air-dry overnight at room temperature before being stored at 4°C.

2.3.1 Serum Deprivation and Drug Treatments

ST*Hdh* cells normally exist in a permissive, dividing state. Temperature shift to 39°C inactivates the temperature-sensitive large T antigen and causes ST*Hdh* cells to exit the cell cycle

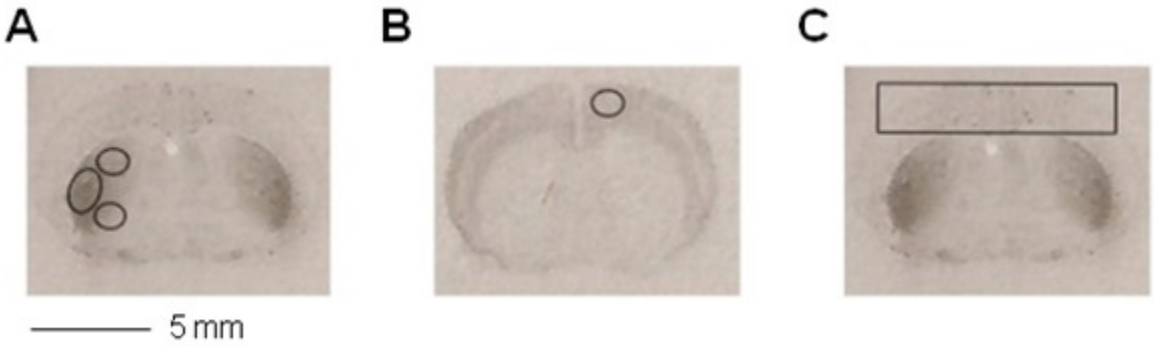

Figure 4. mRNA hybridization was quantified in several regions of the mouse brain. Representative coronal sections derived from R6/2 mice illustrate the specific brain regions used to quantify mRNA hybridization. The OD of hybridization signal specific to several mRNAs was measured in the areas outlined in each panel. A) mRNA hybridization measurements were taken from the lateral, dorsomedial, and ventromedial striatum (Bregma 1.7 to -2.2 mm) for CB_1, and the lateral striatum for all other mRNAs, B) with the exceptions of Egr-1, FAAH, and dynamin, which were measured in the cortex. C) CB_1 mRNA expression was measured in the cortex by counting CB_1-positive neurons because cortical hybridization was punctate.

and differentiate into cells whose phenotype resembles glia (Trettel *et al*., 2000). Serum deprivation also causes ST*Hdh* cells to exit the cell cycle. However, serum deprivation is associated with increased neurite outgrowth, flattening of cells, and expression of DARPP-32 and D_2 receptors (Trettel *et al*., 2000; Paoletti *et al*., 2008). Therefore, the phenotype of serum-deprived ST*Hdh* cells resembles that of 'adult' striatal MSNs (Paoletti *et al*., 2008; Blazquez *et al*., 2011). Here, serum-deprived ST*Hdh* cells were used as models of MSNs. ST*Hdh* cells were normally maintained in serum-containing media. Media was aspirated from cells and the cells were rinsed once with 1X PBS. Media lacking serum, but otherwise equivalent to ST*Hdh* media described above, was then added and cells were allowed to grow for an additional 24 h. These cells are considered 'post-mitotic' and referred to in the remainder of this text as 'untreated'. Also, cells are referred to according to their specific genotype for the remainder of the text, that is, 7/7, 7/111, or 111/111.

All drugs were obtained from Tocris Bioscience (Ellisville, MI). The CB_1 agonists ACEA, mAEA, and AEA, and the FAAH inhibitor (3'-(aminocarbonyl)[1,1-bipheynl]3-yl)-cyclohexylcarbamate (URB-597) were dissolved in ethanol and added directly to cell media to achieve the correct dose. The pan-HDAC inhibitor sodium butyrate (NaB), the type 1 HDAC inhibitor trichostatin A (TSA), D_2 receptor agonist quinipirole, the $D_{1/2}$ receptor agonist apo-morphine, the CB_2 agonist [(1R,2R,5R)-2-[2,6-dimethoxy-4-(2-methyloctan-2-yl)phenyl]-7,7-dimethyl-4-bicyclo[3.1.1]hept-3-enyl] methanol (HU-308), the CB_2 antagonist 1-[2-(morpholin-4-yl)ethyl]-2-methyl-3-(4-methoxybenzoyl)-6-iodoindole (AM-630), and the CB_1 antagonists 1-(2,4-Dichlorophenyl)-5-(4-iodophenyl)-4-methyl-*N*-4-morpholinyl-1*H*-pyrazole-3-carboxamide (AM-281) and (6a*R*,10a*R*)-3-(1-Methanesulfonylamino-4-hexyn-6-yl)-a,7,10,10a-tetrahydro-6,6,9-trimethyl-6*H*-dibenzo[*b*,*d*]pyran (O-2050) were dissolved in dimethyl sulfoxide (DMSO)

and added directly to cell media to achieve the correct dose. ST*Hdh* cells appear morphologically distinct within 4 – 6 h of serum deprivation (Trettel *et al*., 2000). Therefore, cells were treated with drug 6 h post serum-deprivation.

2.4 Plasmid Manipulation and Cloning

In order to study transcriptional regulation of CB_1 in the presence of mutant huntingtin a promoter-reporter construct containing 904 bp of the human *CNR1* promoter driving expression of the *Renilla* luciferase gene was used. In this way, promoter activity could be quantified using the dual luciferase assay (Promega). In addition, promoter-reporter constructs containing 5 tandem repeat estrogen response elements (ERE) or NF-κB response elements driving firefly luciferase activity were used to study CB_1 promoter activity and cannabinoid-mediated signal transduction. Plasmids were propagated in electrocompetent cells, which were prepared as follows. *Escherichia coli* [*E. coli* strain IVNαF' DH1 (K-12); Invitrogen] were grown overnight at 37°C on luria broth (LB) plates. A single colony was chosen and inoculated in 25 mL Tryptone/Yeast extract (TY) broth, and was incubated overnight at 37°C, 250 rpm. Five millilitres of this culture were added to 500 mL fresh TY broth. Cell growth was monitored by absorption spectrophotometry at 600 nm until an A_{600} of 0.4 was achieved. The 500 mL culture was incubated on ice 30 min, centrifuged at 1000 *x g* for 15 min, and the supernatant was discarded. The pellet was resuspended in 250 mL sterile dH_2O, centrifuged at 1000 *x g* for 20 min, and the supernatant was discarded. The pellet was resuspended in 125 mL sterile dH_2O, centrifuged at 1000 *x g* for 20 min, and the supernatant was discarded. The pellet was resuspended in another 125 mL sterile dH_2O, centrifuged at 1000 *x g* for 20 min, and the supernatant was discarded. The pellet was resuspended in 20 mL 10% glycerol, centrifuged at 1000 *x g* for 20 min, and the supernatant was discarded. The pellet was resuspended in 1.5 mL

10% glycerol, distributed in 40 µL aliquots, and the cells were stored at -80°C. For electroporation, 10 ng of plasmid were added to 40 µL of electrocompetent *E. coli*. This solution was placed in an electroporation cuvette and an electric pulse was applied, followed by immediate addition of 410 µL LB. The solution was transferred to a sterile tube and incubated for 1 h at 37°C, 250 rpm. Cells were cultured on LB media containing carbenicillin (50 µg/mL, Invitrogen) overnight at 37°C. Carbenicillin-resistant colonies were selected and plasmids were purified using the GenElute Plasmid MidiPrep system according to the manufacturer's instructions (Sigma-Aldrich).

2.4.1 pLight_Switch *CNR1* Promoter-*Renilla* Luciferase Construct

The pLight_Switch *CNR1* promoter-*Renilla* luciferase construct (pCNR1) was purchased from SwitchGear Genomics (Menlo Park, CA). This plasmid is a 3656 bp variant of the pGL3-basic (Promega) line of promoters. The plasmid contains the following features, which are illustrated in figure 5A: the 904 bp *CNR1* promoter sequence inserted into the multiple cloning site between the *Mlu*I and *Bgl*II restriction sequences, the *Renilla* luciferase gene and SV40 late poly-adenylation signal, an origin of replication site, and an ampicillin resistance gene. An empty vector, pLS_Empty (pELS), was made from pCNR1 to serve as a negative control. The *CNR1* promoter was restriction enzyme digested from 500 ng pCNR1 in 1 U FastDigest® *Hind*III, 1 U FastDigest® *Sac*I, and 20% FastDigest® Green Buffer in dH_2O to a final volume of 20 µL at 37°C for 15 min (Fermentas Canada, Burlington, ON). The reaction was heat inactivated at 80°C for 5 min. The 2656 bp product was resolved on a 0.7% agarose gel, the DNA was purified using the GenElute Gel Extraction Kit (Sigma). Five and 3' overhangs were removed from the entire volume of gel-purified DNA *via* mung bean nuclease (4 U) in 5% mung bean nuclease buffer in dH_2O to a final volume 50 µL at 30°C for 30 min (New England Biolabs, Pickering, ON). Mung

bean nuclease was inactivated by the addition of 0.01% SDS and the DNA was purified by phenol/chloroform extraction. Two hundred nanograms of plasmid were circularized using T4 DNA ligase (400 U; New England Biolabs) in 10% T4 DNA ligase buffer in dH_2O to a final volume of 20 µL at 16°C over-night. The resulting pELS plasmid was chilled on ice and used to transform electrocompetent *E. coli* as described above. An aliquot of pELS was sequenced by GeneWiz Inc. (South Plainfield, NJ) to confirm the removal of the *CNR1* promoter.

2.4.2 Firefly Luciferase Constructs

The pGL3-basic cytomegalovirus (CMV) promoter-firefly luciferase construct (pCMV) was used as a control for the dual luciferase assay because activity of this promoter had been characterized in 7/7, 7/111, and111/111 cells (Hogel, 2011; Promega). This plasmid is a 6600 bp variant of the pGL3-basic (Promega) line of promoters. The plasmid contains the following features, which are illustrated in figure 5B: an 825 bp CMV immediate early enhancer/promoter sequence inserted into the multiple cloning site, followed immediately by the firefly luciferase gene and SV40 late poly-adenylation signal, an SV40 early enhancer/promoter driving expression of the hygromycin resistance gene, an origin of replication site, and an ampicillin resistance gene.

The pTL-basic (pTL) promoter-firefly luciferase construct was purchased from Panomics (Santa Clara, CA). This plasmid is a 4800 bp variant of the pGL3-basic (Promega) line of promoters. The plasmid contains the following features, which are illustrated in figure 5C: a multiple cloning site, followed immediately by the firefly luciferase gene and SV40 late poly-adenylation signal, an origin of replication site, an ampicillin resistance gene, and an f1 origin of replication. Two tandem repeat promoter-reporter constructs were derived from the pTL promoter (Panomics). These were the NF-κB construct (pNF) and the ERE construct (pERE),

which contain 5 tandem repeat response elements for their respective transcription factors inserted between the *Bgl*II and *Hind*III restriction sites of the pTL plasmid (Panomics).

2.4.3 pEGFP Construct

The pEGFP construct was purchased from Promega. This plasmid is a 4700 bp variant of the pGL3-basic (Promega) line of promoters. The plasmid contains the following features, which are illustrated in figure 5D: an 825 bp CMV immediate early enhancer/promoter sequence inserted into the multiple cloning site, followed immediately by the enhanced green fluorescent protein (*Aequorea victoria*) gene and SV40 late poly-adenylation signal, an SV40 early enhancer/promoter driving expression of the kanamycin/neomycin resistance gene, an origin of replication site, and an ampicillin resistance gene.

2.5 Transfection of Vectors into Cells and the Dual Luciferase Assay

The pCNR1 or pELS plasmids were transfected alone or co-transfected with pERE, pNF or pTL plasmids into 7/7, 7/111, and 111/111 cells. Promoter activity was then quantified by measuring firefly and *Renilla* luciferase activity in cell lysates *via* the dual luciferase assay. The pCMV plasmid was transfected into 7/7, 7/111, and 111/111 cells as a control because the activity of this promoter in the presence of mHtt in 7/111 and 111/111 cells had been previously characterized (data not shown; Hogel, 2011). The pEGFP plasmid was transfected into all cells in order to visually estimate transfection efficiency by fluorescence microscopy.

Transfections were performed using Lipfectamine 2000® reagent according to the manufacturer's instructions (Invitrogen). Transfections were performed on cells grown in 24-well plates. Briefly, 1 µL Lipofectamine 2000® reagent was mixed with 50 µL opti-MEM media (Invitrogen), per transfection, and incubated at room temperature for 20 min. In a separate tube, promoter-reporter plasmids were mixed with 50 µL opti-MEM media, per transfection, and

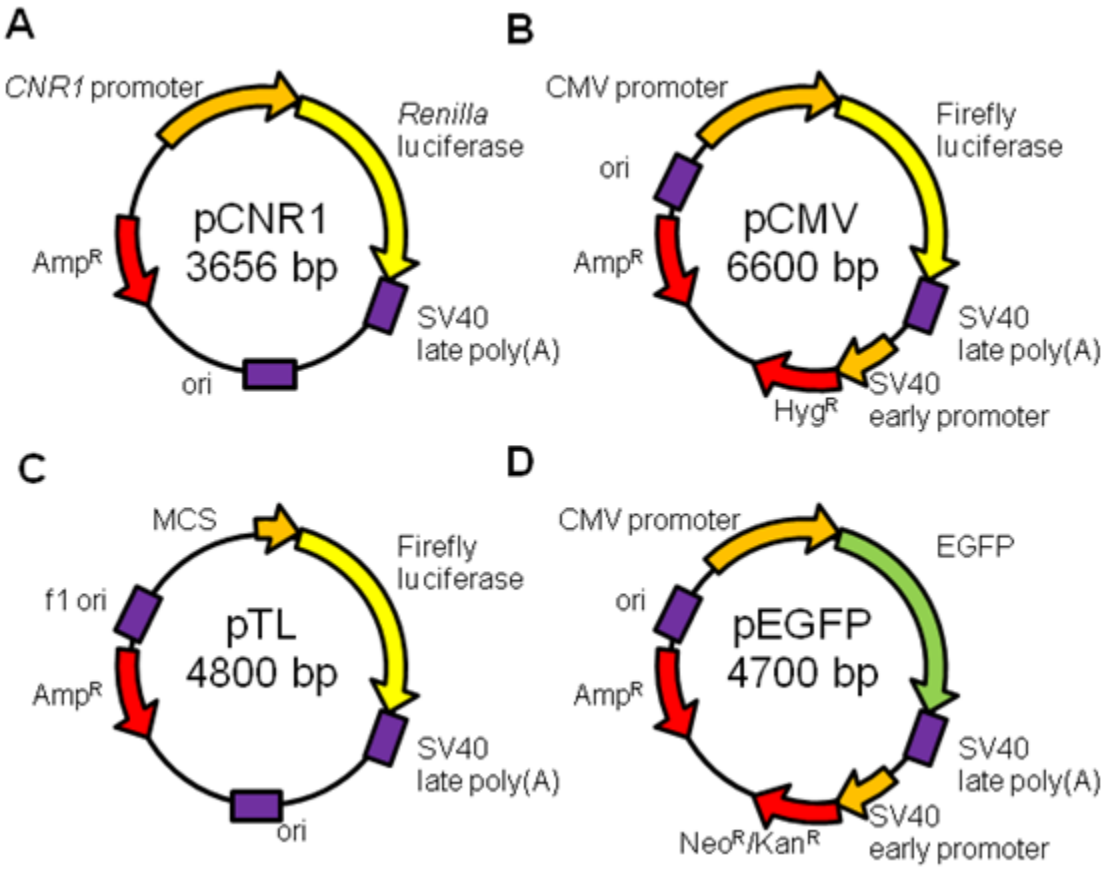

Figure 5. Several plasmids were transfected into 7/7, 7/111, and 111/111 cells to study the CB_1 promoter activity. A) The pCNR1 plasmid (SwitchGear Genomics) contains 904 bp of the CB_1 promoter driving expression of the *Renilla* luciferase gene. B) The pCMV plasmid contains the CMV promoter driving expression of the firefly luciferase gene. D) pTL is a minimal promoter plasmid from which the tandem repeat ERE and NF-κB response element promoters (pERE and pNF) are built. C) The pEGFP plasmid (Promega) was used to visually assess transfection efficiency and contains the CMV promoter driving EGFP gene expression. Amp^R, ampicillin resistance; ori, origin of replication; Hyg^R, hygromycin resistance; Neo^R, neomycin resistance; Kan^R, kanamycin resistance; MCS, multiple cloning site.

incubated at room temperature for 5 min. Plasmid concentrations were: 400 ng pCNR1 or pELS, 200 ng pERE, pNF, or pTL, or 50 ng pCMV, and 50 ng pEGFP. The plasmid and Lipofectamine 2000® solutions were combined and allowed to incubate for 30 min at room temperature. Media was aspirated from cells, cells were washed twice with 1X M PBS, and were then given 500 µL antibiotic-free media. The combined Lipofectamine 2000®/plasmid solution was added to each well (100 µL/well) and cells were incubated at 33°C for 24 h.

The dual luciferase assay protocol was adapted from the manufacturer's instructions (Promega). The protocol is described here for 1 well in a 24-well plate. Media was aspirated from cells and they were washed once with 1X M PBS. One hundred microlitres of 20% passive lysis buffer (PLB) were added and this solution was allowed to incubate for 30 min at room temperature with shaking. The cell lysate was scraped and collected into a 0.5 mL eppendorf tube. The luciferase assay substrate was resuspended in luciferase assay buffer II to make luciferase assay reagent. Ten microlitres of cell lysate solution were added to 50 µL luciferase assay reagent and firefly luciferase activity measured on a GloMax-20/20^{n} single tube luminometer (Promega). The Stop&Glo® substrate was diluted 1 in 50 in Stop&Glo® buffer to make Stop&Glo® reagent. Fifty microlitres of Stop&Glo® reagent were added to the cell lysate/luciferase assay solution, this was rapidly mixed, and *Renilla* luciferase activity measured on the luminometer.

Luciferase activity data were normalized to total protein content in cell lysates. This was done because nearly all promoters tested to date are affected to some degree by expression of mHtt (Hogel *et al.*, 2011), protein concentration accounts for differences in cell growth and number, and normalizing to total protein is a verified method of analyzing luciferase data (Krainc *et al.*, 2007; Schagat *et al.*, 2007). Four microlitres of cell lysate solution were added to

796 µL dH_2O and 200 µL Bradford dye reagent (Bio-Rad, Mississauga, ON). This solution was mixed for 5 min at room temperature. Protein concentrations were then determined by measuring absorption at 595 nm and comparing absorption values to those generated by a series of bovine serum albumin (BSA) solutions with known concentrations between 0.05 and 10 µg/µL protein.

2.6 Quantitative Reverse Transcriptase (qRT)-Polymerase Chain Reaction (PCR)

qRT-PCR was employed in order to measure the endogenous levels of several genes in the 7/7, 7/111, and 111/111 cells.

2.6.1 Trizol Harvest of RNA from Cell Culture

RNA was harvested from 7/7, 7/111, and 111/111 cells grown to approximately 80% confluency in 24-well plates using the Trizol® (Invitrogen) extraction method. Media was aspirated from cells and cells were washed once in 1X PBS. Cells were lysed with 200 µL Trizol®, and lysates were incubated on ice for 3 min. Forty microlitres of chloroform were added and samples were centrifuged at 12,000 *x g* for 20 min at 4°C. The aqueous upper layer was drawn off and mixed with 100 µL isopropanol. This solution was incubated on ice for 10 min and centrifuged at 12,000 *x g* for 10 min at 4°C. The supernatant was discarded and the pellet resuspended in 200 µL ice-cold, 75% ethanol. This solution was incubated on ice for 10 min and centrifuged at 7,500 *x g* for 5 min at 4°C. The supernatant was discarded, the pellet was incubated on ice for 10 min, to evaporate any remaining ethanol, and resuspended in 10 µL dH_2O. RNA samples were stored at -80°C.

2.6.2 Reverse Transcriptase Reaction

Reverse transcription reactions were used to synthesize cDNA from an mRNA template. Reactions were carried out with SuperScript III® reverse transcriptase (+RT, Invitrogen), or without (-RT) as a negative control for use in subsequent PCR experiments. The concentration of

RNA was determined by absorption spectrophotmetry at 260 nm. Based on the concentration of RNA determined by spectrophotometry, 2 μg of RNA were added to the reverse transcriptase reaction containing 0.5 μM dNTPs and 7.5 μM oligo-$d(T)_{12-18}$ (Invitrogen) in dH_2O to a final volume of 13 μL for +RT reactions, or 14 μL for –RT reactions. This solution was incubated at 65°C for 5 min then chilled on ice for 1 min. Twenty percent SuperScript buffer, 5% RNase OUT (RNase inhibitor cocktail), 5 mM dithiothreitol, and 200 U SuperScript III® reverse transcriptase (Invitrogen) were added to the reaction, which was incubated for 1 h at 50°C, followed by 15 min at 70°C to end the reaction. The reaction was diluted 1 in 2 in dH_2O and stored at -20°C.

2.6.3 RT-PCR

One microlitre of cDNA produced *via* RT reaction was added to 10% PCR buffer, 0.3 mM dNTPs, 0.5 μM forward and 0.5 μM reverse primers, and 0.75 U *Pfu* DNA polymerase in dH_2O to a final volume of 20 μL (Fisher Scientific, Ottawa, ON). The PCR program was: 95°C for 3 min, 35 cycles of 95°C 30 s, a primer-specific annealing temperature (Table 1) for 30 s, and 72°C for 30 s, and 72°C for 4 min. PCR products were mixed with 0.2% xylene cyanol and bromophenol blue (1:1, v/v) and resolved by electrophoresis on 2% (w/v) agarose gels at 80 V for 120 min.

2.6.4 LightCycler® SYBR Green qRT-PCR

mRNA expression of several genes was quantified *via* real-time PCR using cDNA synthesized from RT reactions. qRT-PCR was conducted using the LightCycler® system and software (version 3.0; Roche, Laval, QC). cDNA abundance was measured using SYBR Green (Roche), contained in the PCR buffer, which intercalates with double-stranded DNA and fluoresces green. Fluorescence is then quantified by the LightCycler® on a per-sample basis

during each round of PCR amplification of cDNA. qRT-PCR reactions were composed of a primer-specific concentration of $MgCl_2$, 0.5 μM each of forward and reverse primers, 2 μL of LightCycler® FastStart Reaction Mix SYBR Green I [0.3 mM dNTP, 10% SYBR Green I dye, 1.2 U FastStart *Taq* DNA polymerase], and 1 μL cDNA to a final volume of 20 μL with dH_2O (Roche). The PCR program was: 95°C for 10 min, 50 cycles of 95°C 10 s, a primer-specific annealing temperature (Table 1) for 5 s, and 72°C for 10 s. Melting curve analysis was performed immediately after the PCR program to determine the purity of the PCR product produced. The melting curve program was 95°C for 10 s, 60°C for 30 s, a ramp to 99°C at 0.20°C/s, and 40°C for 30 s. qRT-PCR experiments always included sample-matched –RT controls, a no-sample dH_2O control, and a standard control containing 1 μL of product-specific cDNA of a known concentration in copies/μL. Expression data were quantified by comparing the crossing points (*i.e.* the cycle number during PCR amplification at which the amount of product measured began to increase at a logarithmic rate) of each sample to a product-specific standard curve generated by plotting the crossing points of known standards against their respective concentrations in copies/μL.

2.7 Immunocytochemistry

7/7, 7/111, and 111/111 cells were grown to approximately 50% confluency on 0.01% poly-D-lysine coated cover-slips in 24-well plates. Media was aspirated from wells and cells were washed twice in 1X PBS. Cells were fixed for 10 min at room temperature with 4% PFA and washed three times with 1X M PBS, 5 min each, with shaking. Cells were incubated with blocking solution [1X PBS, 5% normal goat serum, 0.3% TritonX-100 (Sigma-Aldrich) in dH_2O] for 1 h at room temperature, with shaking. Following blocking, cells were washed with primary antibody solutions of anti-N-CB_1 (polyclonal rabbit anti-amino-terminal CB_1 IgG,

Cayman Chemical, Ann Arbor, MI) diluted 1:500 in antibody dilution buffer [1X PBS, 1% (w/v) BSA, 0.3% TritonX-100 (Sigma-Aldrich) in dH_2O] overnight at 4°C, with shaking. Cells were washed three times with 1X PBS, 5 min each, with shaking. Cells were incubated in Cy^2 (cyanine-conjugated polyclonal goat anti-rabbit IgG, Jackson ImmunoResearch, West Grove, PA) diluted 1:500 in antibody dilution buffer for 1 h at room temperature, protected from light, with shaking. Cells were washed three times with 1X M PBS, 5 min each, with shaking. Cover-slips were removed from wells and placed on SuperFrost slides with 2 µL Hoescht nuclear stain (Sigma-Aldrich) and 2.5 µL Fluorsave® reagent (Calbiochem via Cedarlane, Burlington, ON). Immunofluorescence was visualized with a Zeiss Axioplan II MOT fluorescent microscope, images were captured using Axionvision Rel. Version 4.8.2 and an Axiocam HRC Colour Camera (Carl Zeiss Canada, Toronto, ON). Immunofluorescence was also visualized with a Zeiss 510 Upright Laser Scanning Microscope, images were captured using Zen Image Capture 2009 edition (Carl Zeiss Canada). The following excitation/emission filters were used to visualize fluorescence: for Cy^2 492 nm/510 nm, and for Hoescht nuclear staining 350 nm/461 nm. For confocal analysis, 24 images were captured using Zen Image Capture with a section thickness of 0.35 µm. Individual cells were analyzed as follows. A line 50 µm long, passing through the nucleus, was drawn across the cell. The Zen program quantified fluorescence along that line per µm. Data were then binned into 5 µm segments, and the value of each bin calculated as the mean fluorescence within each 5 µm segment (*i.e.* 5 µm/bin; Fig. 6). For each treatment group fifty cells were analyzed and the mean of each 5 µm segment was calculated.

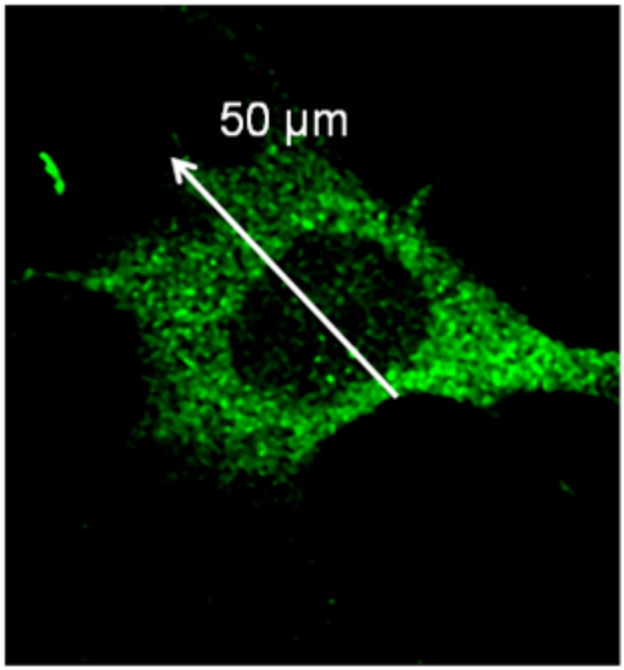

Distance (µm)		F_{645}	Mean F_{645}	St Err F_{645}
Bin 1	1	528.6		
	2	478.7		
	3	546.1		
	4	472.9		
	5	471.3	499.5	15.7
Bin 2	6	132.5		
	7	173.7		
	8	198.5		
	9	196.9		
	10	132.7	166.9	14.7
Bin 3	11	125.8		
	12	116.0		
	13	259.6		
	14	139.7		
	15	198.0	167.8	27.0

Figure 6. The cellular distribution of CB_1 was analyzed by measuring fluorescence intensity along a line transecting a cell. Confocal images acquired using the Zen Image Capture software were analyzed as illustrated here. Cells were grown on cover-slips for the immunocytochemical detection of CB_1. A 50 µm line transecting the nucleus was drawn over 50 cells per treatment group. Fluorescence intensity along this line was quantified per cell per µm and the mean of each 5 µm segment was calculated. Here, a 7/111 cell incubated with anti-N-CB_1 and Cy^2 secondary antibody (green) is depicted and the corresponding data for the first 15 µm is provided to the right.

2.8 On- and In-cell Western Analyses Using the Odyssey Imaging System

7/7, 7/111, and 111/111 cells were grown to approximately 90% confluency in 0.01% poly-D-lysine coated 96-well plates. Media was aspirated from wells and cells were washed twice in 1X PBS. Cells were fixed for 10 min at room temperature with 4% PFA and washed three times with 1X M PBS, 5 min each, with shaking. For on-cell assays, cells were incubated with blocking solution (as described in 2.7, without TritonX-100) for 1 h at room temperature, with shaking. Following blocking, cells were washed with primary antibody solutions directed against N-CB_1 diluted 1:500, pERK2(Tyr204) diluted 1:200 [polyclonal mouse anti-pERK(Tyr204) IgG, Santa Cruz Biotechnology, Santa Cruz, CA], ERK2 diluted 1:200 (polycloncal rabbit anti-ERK2 IgG, Santa Cruz Biotechnology), pAkt(Ser473) diluted 1:200 [polyclonal mouse anti-pAkt(Ser473) IgG, Cell Signalling Technology, Danvers, MA), panAkt diluted 1:250 [polyclonal rabbit anti-Akt IgG, Cell Signalling Technology), or β-actin diluted 1:2000 (monoclonal mouse anti-β-actin IgG, Millipore) in antibody dilution buffer (as described in 2.7, for on-cell assays) overnight at 4°C, with shaking. Cells were washed three times with 1X PBS, 5 min each, with shaking. Cells were incubated in $IR^{CW700dye}$ [infrared dye-conjugated polyclonal goat anti-mouse IgG (red)] and/or $IR^{CW800dye}$ [infrared dye-conjugated polyclonal anti-rabbit IgG (green), Rockland Immunochemicals, Gilbertsville, PA] diluted 1:500 in antibody dilution buffer (without TritonX-100) for 1 h at room temperature, protected from light, with shaking. Cells were washed three times with 1X PBS, 5 min each, with shaking. Cells were allowed to air-dry overnight, protected from light. On-cell western analyses were then conducted using the Odyssey Imaging system and software (version 3.0; Li-Cor, Lincoln, NE). Image acquisition and quantification were completed using the default settings for the Microplate2 and Multi-96well programs, respectively.

In-cell assays followed the completion of on-cell assays. The process described above was repeated, but TritonX-100 was added to all blocking and dilution solutions to permeabilize cells.

2.9 Cell Viability Assay

The Live/Dead® cell viability assay (Invitrogen) employs the dyes calcein AM (CalAM) and ethidium homodimer-1 (EthD-1). CalAM is cleaved to produce the green fluorophore calcein by enzymatic activity of esterases in metabolically active cells. Cells staining positive for EthD-1 have become permeable to the dye, which cannot passively enter cells, and the dye fluoresces red upon intercalation with nucleic acids. Cells can exist along a continuum of CalAM and EthD-1 staining from positive for CalAM and negative for EthD-1 to *vice versa*, but not negative or positive for both stains. The intensity of green and red fluorescence are therefore directly and indirectly correlated measures of general cell viability, respectively. Cells were grown to approximately 90% confluency on 0.01% poly-D-lysine-coated cover-slips in 24-well plates or in 0.01% poly-D-lysine-coated 96-well plates. Media was aspirated from wells and cells were washed twice in 1X PBS. Cells were incubated with 2 μM EthD-1 and 4 μM CalAM (diluted in 1X PBS) for 45 min, at room temperature, with shaking. Following incubation, cells were washed once with 1X PBS. 7/7 cells grown in serum-containing media were used as a positive control for CalAM staining and a negative control for EthD-1 staining. 7/7 cells incubated for 45 min with 70% methanol prior to dye incubation were used as a positive control for EthD-1 staining and a negative control for CalAM staining. Cover-slips were removed from wells, placed on SuperFrost slides, and fluorescence was visualized with a Zeiss Axioplan II MOT fluorescent microscope, images were captured using Axionvision Rel. Version 4.8.2 and an Axiocam HRC Colour Camera (Carl Zeiss Canada). For cells grown in 96-well plates,

fluorescence was quantified using a SynergyHT fluorescent/luminescent plate reader (Promega) set to read from the bottom of the plate with a sensitivity setting of 50. Fluorescence readings were acquired twice for each sample. The following excitation/emission filters were used to visualize fluorescence: for EthD-1 528 nm/617 nm, and for CalAM 494 nm/517 nm.

2.10 CellTiter-Glo® ATP Quantification

The CellTiter-Glo® cell viability assay (Promega) measures ATP concentration in a cell culture solution. Firefly luciferase enzymes require ATP to catalyze a light-yielding reaction. In this assay, the firefly luciferase protein and its substrate, luciferin, are mixed with cells grown in culture, and the ATP endogenously produced by the cells is the limiting reagent in the luciferase reaction. Thus, the amount of light produced is directly proportional to the concentration of ATP present. Cells were grown to approximately 90% confluency in 0.01% poly-D-lysine-coated 96-well plates. Fifty microlitres of media were aspirated from wells. Fifty microlitres of CellTiter-Glo® reagent (resuspended in CellTiter-Glo® buffer according to the manufacturer's instructions) were added to the wells. Cells were incubated with CellTiter-Glo® reagent for 2 min, at room temperature, with shaking, followed by 10 min incubation at room temperature without shaking. Luminescence was quantified using a SynergyHT fluorescent/luminescent plate reader (Promega) set to read from the bottom of the plate with a sensitivity setting of 200. Luminescence readings were acquired twice for each sample. The excitation and emission filters used were Lum/E and 645 nm, respectively. Background luminescence was collected using a cell-free well containing 50 µL of media and 50 µL CellTiter-Glo® reagent and subtracted from each sample reading. For each experiment, an ATP standard curve was created with ATP concentrations from 1 nM to 100 µM in a final volume of 50 µL cell culture media and 50 µL

CellTiter-Glo® reagent. This standard curve was used to calculate ATP concentration in each sample.

2.11 Statistical Analyses

The *in situ* hybridization OD values for mRNA expression in wild-type, R6/1, R6/2 and mice were analyzed by two-way analysis of variance (ANOVA). The factors considered were genotype and disease stage. Fold-change values derived from *in situ* hybridization OD values for mRNA expression in $CB_1^{+/-}$ mice were analyzed by two-tailed Student's *t*-test. Data produced from viability assays, dual luciferase assays, qRT-PCR, and on- and in-cell western assays, were analyzed by one- or two-way ANOVA, as indicated. *Post-hoc* analyses were performed using the Tukey's Honest Significance Test. Homogeneity of variance was confirmed using Bartlett's Test. The level of significance was set to $P < 0.001$, < 0.01, or < 0.05, as indicated, and all results are reported as the mean ± standard error of the mean (S.E.M). Analyses were performed, and graphs were constructed, using Microsoft Excel (2011) and GraphPad (version 5.04, Prism, La Jolla, CA).

CHAPTER 3

Results

3.1 CB_1, Fatty Acid Amide Hydrolase (FAAH), and CB_2 mRNA Levels were Dysregulated in R6/1 and R6/2 HD Transgenic Mice.

To determine whether the observation that CB_1 mRNA abundance is reduced in the striatum of adult transgenic HD mice reflected a uniform or region-specific decrease in CB_1 mRNA level (Denovan-Wright & Robertson, 2000), we used *in situ* hybridization to examine CB_1 mRNA levels in the lateral, ventromedial and dorsomedial striatum, and cortex of HD mice relative to age-matched, wild-type controls. We chose to examine both the R6/1 and R6/2 transgenic HD mouse lines. R6/1 mice express exon 1 of the mHtt transgene containing approximately 115 CAG repeats and develop HD motor symptoms at approximately 8 weeks of age when their performance in the rotarod task is poorer than similarly aged wild-type littermates (Li *et al*., 2005). Motor control progressively deteriorates in R6/1 mice until death at approximately 30 weeks of age (Mangiarini *et al*., 1996). R6/2 mice express exon 1 of the mHtt transgene containing approximately 150 CAG repeats (Li *et al.*, 2005). HD progression is more rapid in R6/2 mice than R6/1 mice and rotarod performance declines in R6/2 mice at approximately 4 weeks of age (Li *et al*., 2005). R6/2 mice die at approximately 12 weeks of age (Bjorkqvist *et al.*, 2005). Thus, the two models experience the same order of development of HD symptoms over different time periods and can be compared to examine how disease pathogenesis correlates with molecular phenomena such as transcriptional dysregulation (Zuccato *et al*., 1998). We also examined cortical FAAH mRNA levels *via in situ* hybridization in R6/1 and R6/2 HD mice, relative to age-matched wild-type controls. Following autoradiography, the optical density (OD) corresponding to mRNA hybridization with the radiolabeled probe was measured at ages corresponding to four stages of disease progression [pre- (4 week), early- (8

week), mid- (14 week), and late- (26 week) symptomatic] in R6/1 and three stages of disease progression [pre- (3 week), mid- (6 week), and late- (11 week) symptomatic] in R6/2 mice. These measurements were compared to age-matched wild-type littermates. Representative sections illustrating CB_1 and FAAH hybridization are presented in figure 7. CB_1 mRNA levels were lower in the lateral striatum, but unchanged in the dorsomedial and ventromedial striatum, of 26 week-old wild-type mice compared to 4 week-old wild-type mice ($n = 4$; $P < 0.05$; Fig. 8A,B,C). The number of CB_1-labelled cortical neurons was greater in 26 week old wild-type mice compared to 4 week-old wild-type mice ($n = 4$; $P < 0.05$; Fig. 8D). In wild-type mice, then, there was a decrease in the lateral striatum, and an increase in the cortex, in CB_1 mRNA abundance with age. There was no difference in CB_1 mRNA abundance in the lateral, ventromedial, and dorsomedial striatum, and the number of cortical neurons in pre-symptomatic R6/1 mice compared to wild-type littermates at the 'pre' stage. A lower level of CB_1 mRNA was observed at early-, mid-, and late-symptomatic disease stages in the lateral, ventromedial, and dorsomedial striatum of R6/1 mice, relative to age-matched wild-type littermates and pre-symptomatic R6/1 mice ($n = 4$; $P < 0.05$; Fig. 8A,B,C). The number of CB_1-labelled cortical neurons was lower in R6/1 mice at early-, mid-, and late-symptomatic disease stages, relative to age-matched wild-type littermates and pre-symptomatic R6/1 mice ($n = 4$; $P < 0.05$; Fig. 8D). Cortical FAAH mRNA levels were lower in 26 week-old wild-type mice compared to 4 week-old wild-type mice ($n = 4$; $P < 0.05$; Fig. 9). In R6/1 mice, cortical FAAH mRNA levels were lower in mid- and late-symptomatic stages compared to the pre-symptomatic period ($n = 4$; $P < 0.05$; Fig. 9). FAAH mRNA levels were higher in late-stage symptomatic R6/1 mice than in age-matched wild-type littermates ($n = 4$; $P < 0.05$; Fig. 9).

Similar to the wild-type littermates of R6/1 mice, CB_1 mRNA levels were lower in the lateral striatum, but unchanged in the ventromedial and dorsomedial striatum, of 11 week-old wild-type littermates of R6/2 mice compared to 3 week-old wild-type mice ($n = 4$; $P < 0.05$; Fig. 10A,B,C). Further, the number of CB_1-labelled cortical neurons was greater in 11 week-old wild-type mice compared to 3 week-old littermates (n = 4; $P < 0.05$; Fig. 10D). In R6/2 mice, CB_1 mRNA abundance was reduced at mid- and late-symptomatic stages in the lateral, dorsomedial, and ventromedial striatum of R6/2 mice compared to age-matched wild-type littermates and 3 week-old R6/2 mice ($n = 4$; $P < 0.05$; Fig. 10A,B,C). The number of CB_1-labelled cortical neurons was lower in R6/2 mouse cortical neurons at mid-, and late-symptomatic disease stages compared to age-matched wild-type littermates and 3 week-old R6/2 mice ($n = 4$; $P < 0.05$; Fig. 10D). Cortical FAAH mRNA levels were lower in 11 week-old wild-type and 6 and 11 week-old R6/2 mice compared to 3 week-old littermates ($n = 4$; $P < 0.05$; Fig. 11). FAAH mRNA abundance was greater in pre-, mid-, and late-symptomatic disease stages of R6/2 mice compared with age-matched wild-type littermates ($n = 4$; $P < 0.05$; Fig. 11). CB_1 mRNA abundance was decreased in the lateral striatum and increased in cortical neurons as part of the aging process in wild-type littermates of R6/1 and R6/2 mice. CB_1 mRNA levels declined early in HD symptom onset in 3 regions of the striatum, and in cortical neurons. Cortical FAAH mRNA levels were lower in aged wild-type, R6/1, and R6/2 mice compared to young mice of the same genotype. Cortical FAAH expression was higher in aged HD mice than age-matched wild-type littermates. If FAAH levels are higher in HD mice than in wild-type mice, then eCB tone (AEA abundance) may be lower in older HD mice compared to similarly aged wild-type mice because FAAH is the major catabolic enzyme of AEA (Navarro *et al.*, 2009).

We also wanted to determine whether expression of CB_2 was altered during HD disease progression in R6/2 mice. We were unable to specifically detect CB_2 mRNA using *in situ* hybridization (data not shown). Instead, CB_2 was quantified *via* qRT-PCR. CB_2 mRNA abundance was greater in late-symptomatic stage R6/2 mice compared to pre-symptomatic R6/2 mice and age-matched wild-type littermates ($n = 4$; $P < 0.05$; Fig. 12). Expression of CB_2 mRNA is inducible in the presence of pro-inflammatory cytokines such as interleukin-1β, and TNFα (Borner *et al*., 2007a). Therefore, inflammation occurring at the late stages of HD progression may be responsible for induction of CB_2 levels.

CB_1 mRNA levels decline during adulthood in the presence of mHtt (Denovan-Wright & Robertson, 2000). To determine whether CB_1 mRNA levels were different in the central nervous system of HD mice relative to wild-type mice early in development, we probed sections from P1 wild-type and HD R6/2 mice for CB_1 using *in situ* hybridization. No differences were observed in CB_1 mRNA abundance or distribution between genotypes in the central nervous system and specifically in the primary and secondary motor cortices, lateral striatum, or dorsal coliculus and inferior coliculus (DCIC; Fig. 13). Importantly, the anatomical distribution of CB_1 mRNA at P1 was distinct from that of adulthood. In adulthood, CB_1 mRNA levels were highest in the striatum, relative to other tissues (Fig. 7; Denovan-Wright & Robertson, 2000). Therefore, the factors that facilitate high steady-state CB_1 mRNA levels in the striatum during adulthood are not present in the striatum at P1. In HD, during adulthood, the factors that facilitate high steady-state CB_1 mRNA levels are dysregulated in the presence of mHtt.

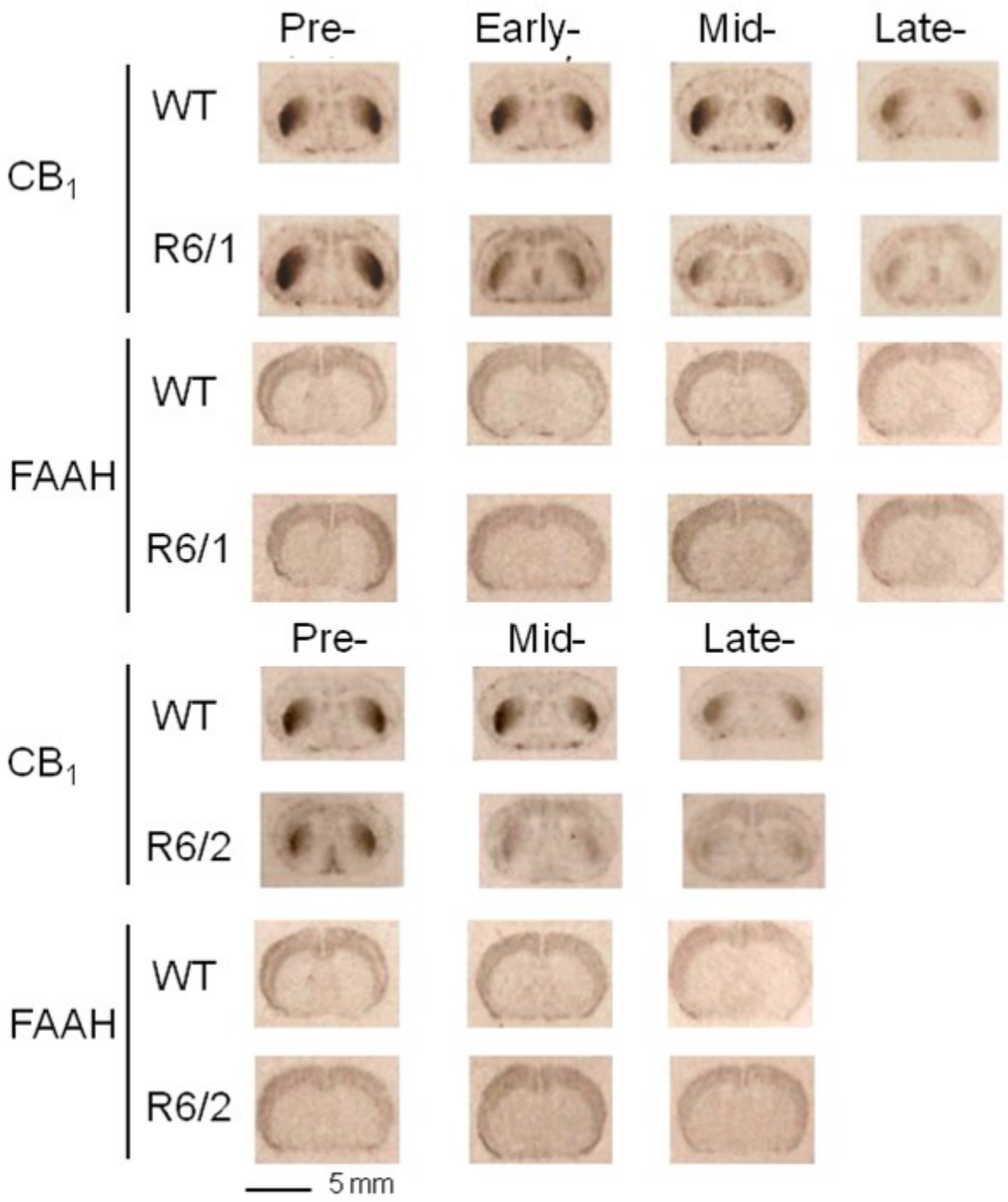

Figure 7. CB_1 mRNA levels were lower and FAAH mRNA levels were higher in HD mice compared to age-matched wild-type (WT) littermates. *In situ* hybridization was used to determine the distribution and relative abundance of CB_1 and FAAH mRNAs in WT, R6/1, and R6/2 mice. This figure presents representative sections of each disease stage for WT and HD mice. Disease stage is indicated above each section. Mouse line and probe used are indicated to the left.

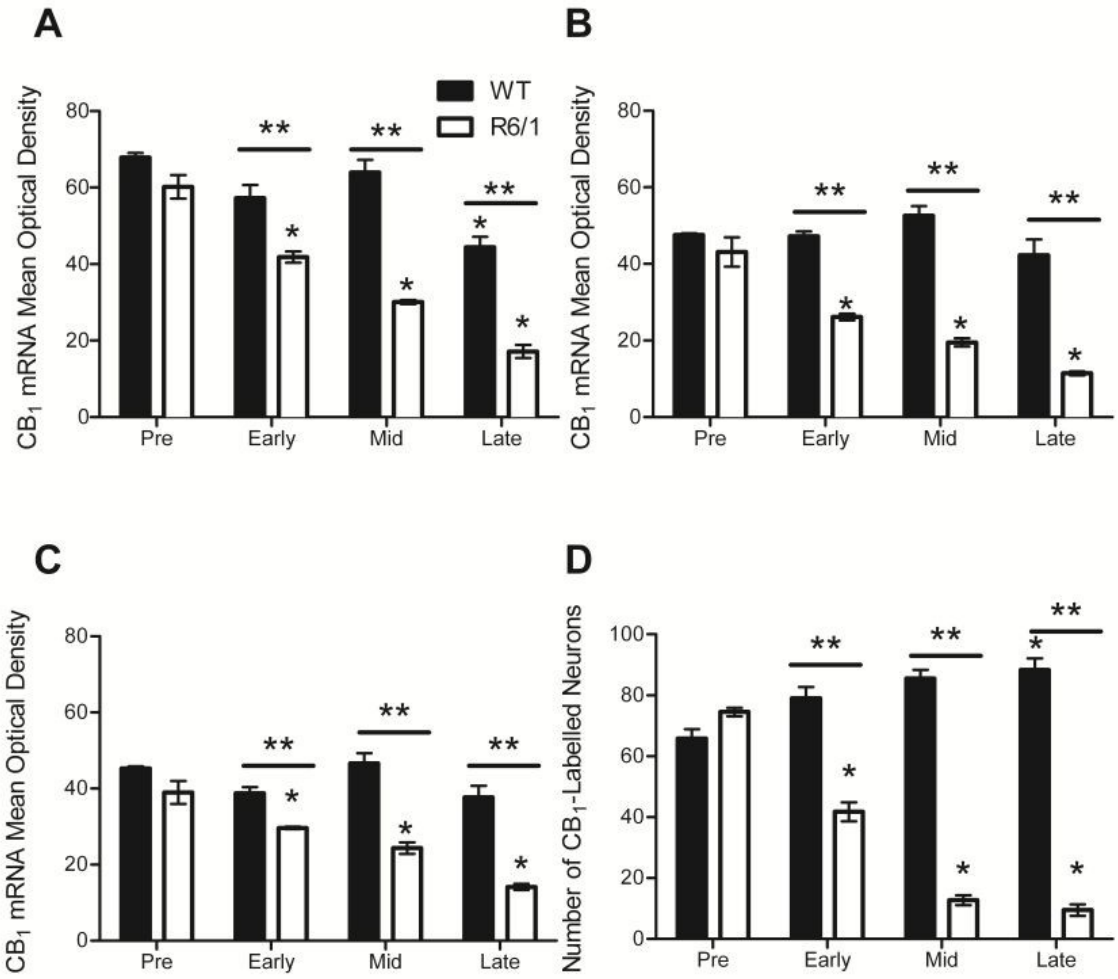

Figure 8. CB_1 mRNA levels were lower in the lateral (A), dorsomedial (B), and ventromedial (C) striatum and cortical neurons (D) of symptomatic R6/1 mice compared to pre-symptomatic R6/1 mice and age-matched WT littermates. OD measurements were collected using Kodak 3D imaging software. Local background was subtracted from each measurement to correct for background variability. CB_1-labelled cortical neurons were counted because cortical mRNA hybridization was punctate rather than homogeneous over a wide area, as in the striatum (Fig. 4). Significance was determined *via* two-way ANOVA for genotype and age followed by *post-hoc* Tukey's test. ** $P < 0.05$ between genotypes within disease stage, * $P < 0.05$ within genotype compared to pre-symptomatic, $n = 4$.

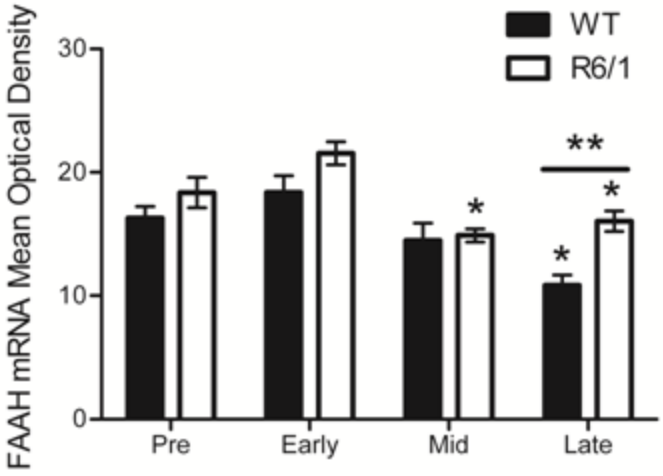

Figure 9. Cortical FAAH mRNA levels were lower in late-stage symptomatic R6/1 mice than in pre-symptomatic R6/1 mice, but greater than in age-matched WT mice. OD measurements were collected using Kodak 3D imaging software. Local background was subtracted from each measurement to correct for background variability. Significance was determined *via* two-way ANOVA for genotype and age followed by *post-hoc* Tukey's test. ** $P < 0.05$ between genotypes within disease stage, * $P < 0.05$ within genotype compared to pre-symptomatic, $n = 4$.

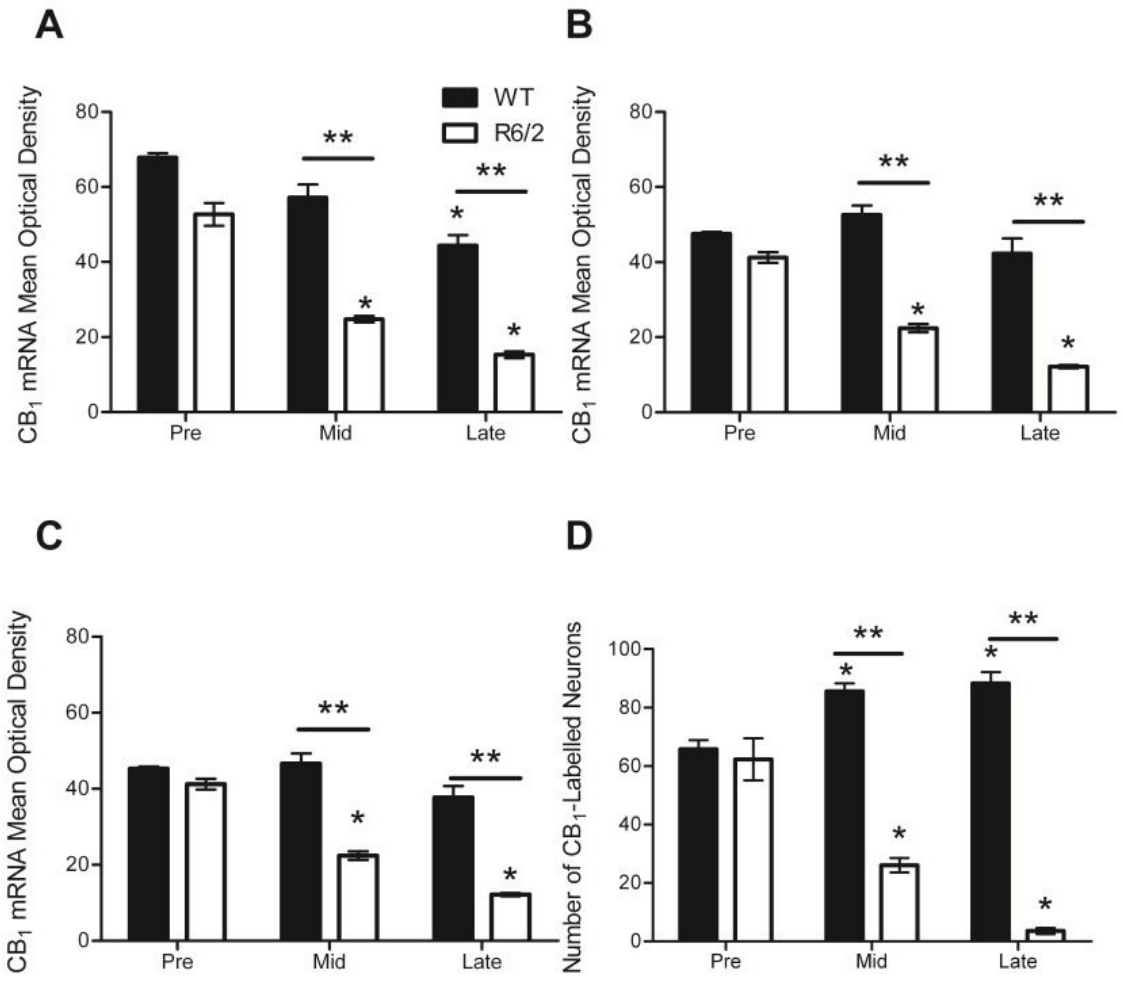

Figure 10. CB_1 mRNA levels were lower in the lateral (A), dorsomedial (B), and ventromedial (C) striatum and cortical neurons (D) of symptomatic R6/2 mice compared to pre-symptomatic R6/2 mice and age-matched WT littermates. OD measurements were collected using Kodak 3D imaging software. Local background was subtracted from each measurement to correct for background variability. CB_1-labelled cortical neurons were counted because cortical mRNA hybridization was punctate rather than homogeneous over a wide area, as in the striatum (Fig. 4). Significance was determined *via* two-way ANOVA for genotype and age followed by *post-hoc* Tukey's test. ** $P < 0.05$ between genotypes within disease stage, * $P < 0.05$ within genotype compared to pre-symptomatic, $n = 4$.

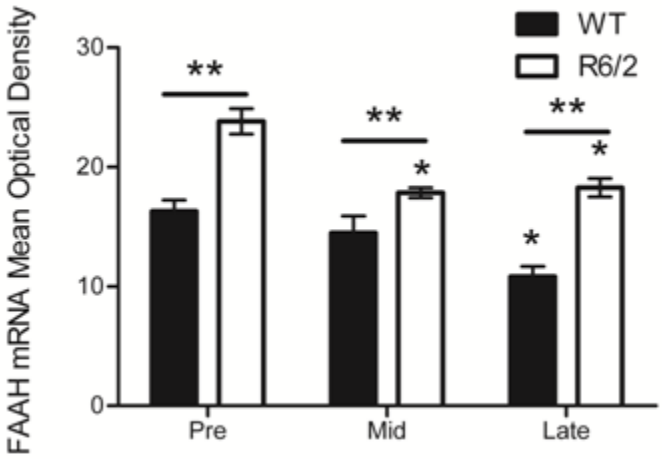

Figure 11. Cortical FAAH mRNA levels were higher in R6/2 mice compared to age-matched WT littermates. OD measurements were collected using Kodak 3D imaging software. Local background was subtracted from each measurement to correct for background variability. Significance was determined *via* two-way ANOVA for genotype and age followed by *post-hoc* Tukey's test. ** $P < 0.05$ between genotypes within disease stage, * $P < 0.05$ within genotype compared to pre-symptomatic, $n = 4$.

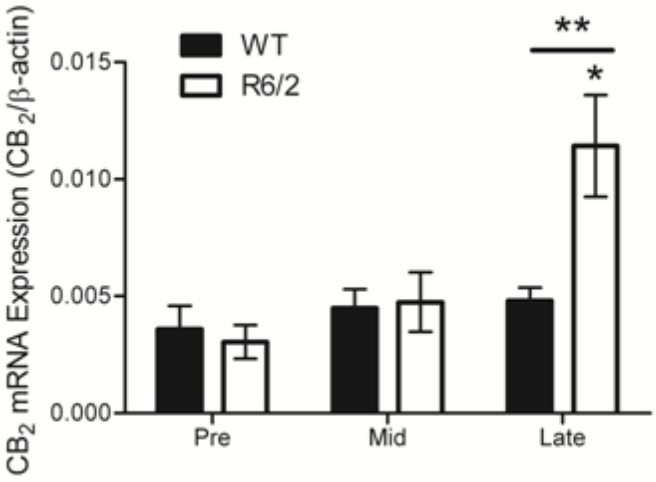

Figure 12. Striatal CB_2 mRNA levels were higher in late-symptomatic R6/2 mice compared to pre-symptomatic R6/2 mice and age-matched WT littermates. Archived striatal mRNA was converted to cDNA. CB_2 mRNA abundance was quantified and normalized to β-actin mRNA levels. Significance was determined *via* two-way ANOVA for genotype and age followed by *post-hoc* Tukey's test. ** $P < 0.05$ between genotypes within disease stage, * $P < 0.05$ within genotype compared to pre-symptomatic, $n = 4$.

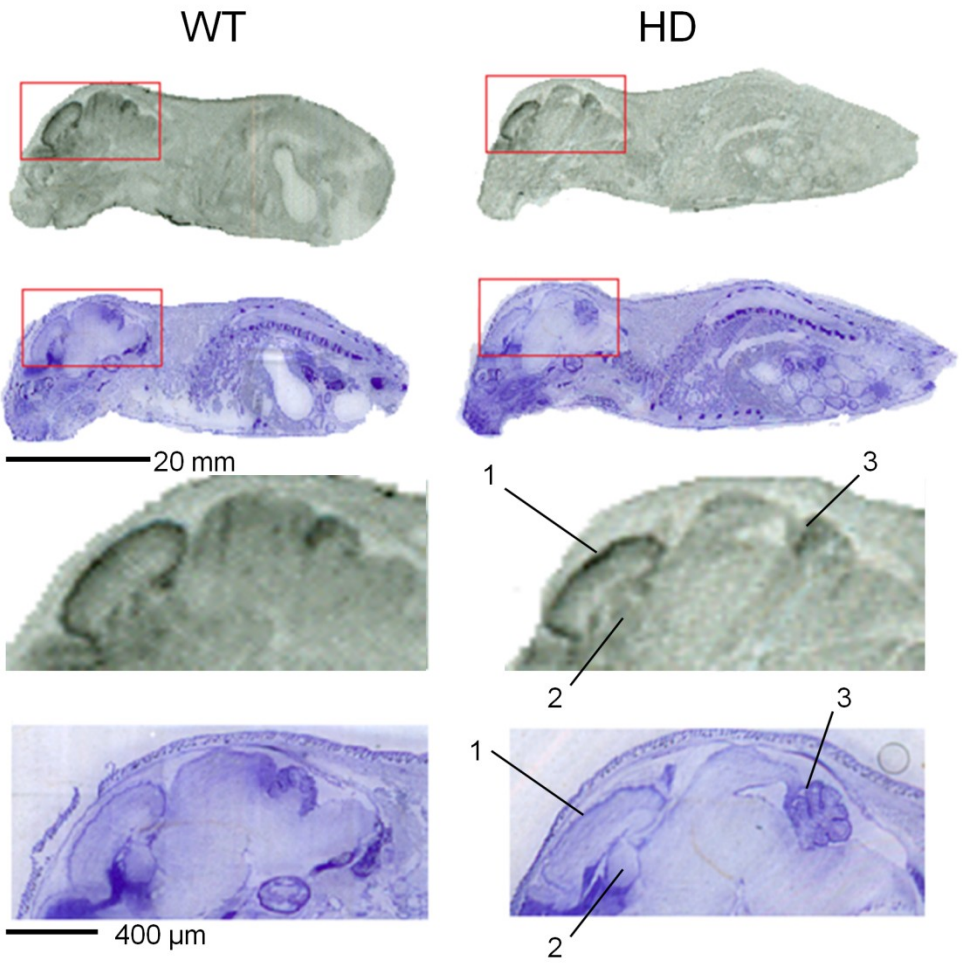

Figure 13. CB_1 mRNA was expressed at highest levels in the primary motor cortex and dorsal cerebellum inferior colliculus (DCIC), not the lateral striatum, of P1 R6/2 and WT mice. *In situ* hybridization for CB_1 in sagittal sections derived from P 1 WT and R6/2 mice. Sections were counter-stained with cresyl violet for the identification of specific anatomical features. 1. Layer II & III Primary motor cortex. 2. Lateral striatum. 3. DCIC.

3.2 *CNR1* Promoter Activity was Lower in 7/111 and 111/111 Cells Expressing mHtt.

The number of primary CB_1 mRNA transcripts is reduced in 6 week-old R6/1 and 4 week-old R6/2 transgenic mice, which indicates that, in adult mice, mHtt affects the rate of CB_1 transcription in adult HD mice (McCaw *et al*., 2004). To determine whether mHtt directly decreased activity of the CB_1 gene promoter (*CNR1*), we transfected serum-deprived 7/7, 7/111, and 111/111 cells with a promoter-reporter vector containing a 904 bp fragment of the human CB_1 promoter driving expression of the *Renilla* luciferase enzyme (pCNR1). 7/7, 7/111, and 111/111 cells express 2 copies of wild-type mouse *huntingtin* containing 7 CAG repeats (7/7), 1 copy of wild-type *huntingtin* and 1 copy of mouse *huntingtin* where exon 1 is replaced with exon 1 of the human *huntingtin* gene containing 111 CAG repeats (HD; 7/111), or 2 copies of mouse *huntingtin* containing the human mutant *huntingtin* exon 1 allele (111/111). The mouse and human/mouse *huntingtin* genes are under the control of the mouse *huntingtin* promoter. Twenty-four hours of serum deprivation causes ST*Hdh* cells to exit the cell cycle, increase neurite outgrowth, and express D_2 and DARPP-32 (Paoletti *et al*., 2008). Consequently, serum deprivation produces a 'MSN' phenotype (Trettel *et al*., 2000; Paoletti *et al*., 2008). *Renilla* luciferase activity was quantified and normalized to the total protein in each cell lysate. The pELS promoter-less plasmid was used as a negative control. *CNR1* promoter activity was lower in 7/111 and 111/111 cells compared to 7/7 cells ($n = 12$, $P < 0.05$, Fig. 14). That is, *CNR1* promoter activity was negatively correlated to the relative levels of mHtt in cells modeling 'MSNs'.

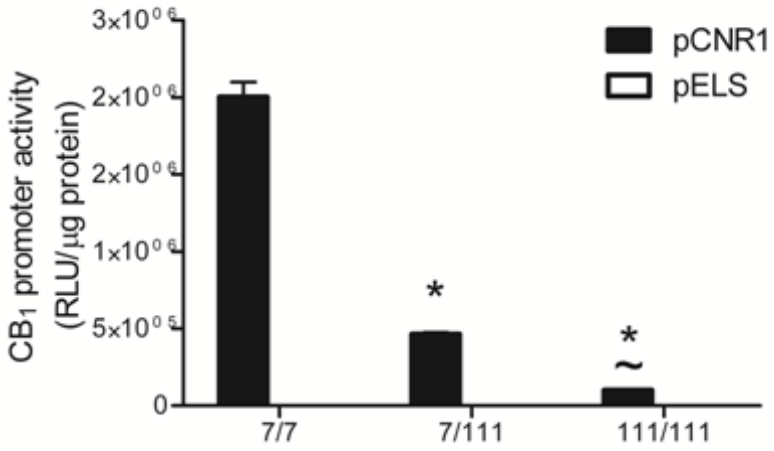

Figure 14. Human CB_1 promoter (*CNR1*) activity was lower in the 7/111 and 111/111 cells than 7/7 cells. A 904 bp *CNR1* promoter-*Renilla* luciferase construct (pCNR1) was transfected into serum-deprived 7/7, 7/111, and 111/111 cells. Eighteen hours post-transfection promoter activity was quantified *via* luciferase assay and relative light units (RLU) were normalized to total protein on a per sample basis. The promoter-less control pELS-*Renilla* luciferase plasmid served as a negative control. Significance was determined *via* one-way ANOVA followed by *post-hoc* Tukey's test. * $P < 0.01$ relative to 7/7, ~ $P < 0.01$ relative to 7/111, $n = 12$.

3.3 CB_1 mRNA Levels were Lower in 7/111 and 111/111 Cells Expressing mHtt.

CNR1 promoter activity was lower in the presence of mHtt than in wild-type cells in a reporter assay and CB_1 mRNA levels were lower in transgenic HD mice than in wild-type mice. We wanted to determine whether endogenous CB_1 mRNA levels were lower in mHtt-expressing 7/111 and 111/111 cells compared to 7/7 cells. We used RT-PCR and agrose gel electrophoresis to show that CB_1 mRNA was expressed in 7/7, 7/111, and 111/111 cells and that primers were sufficiently specific to generate a single product of the expected size and sequence for CB_1 (Fig. 15). qRT-PCR was used to determine CB_1 mRNA levels in 7/7, 7/111, and 111/111 cells. Hypoxanthine ribosyltransferase (HPRT) has been used to normalize gene expression in animal and cell models of HD (McCaw *et al.* 2004; Gomez *et al*., 2006). However, HPRT levels varied between 7/7, 7/111, and 111/111 cells ($n = 12$; $P < 0.01$, Fig. 16). An alternative house-keeping gene for these cells is β-actin (Blazquez *et al*., 2011). We were able to confirm that β-actin levels were constant relative to total RNA in 7/7, 7/111, and 111/111 cells ($n = 12$; $P < 0.01$, Fig. 16). We then quantified relative CB_1 mRNA levels in dividing and post-mitotic 7/7, 7/111, and 111/111 cells. Levels of CB_1 mRNA were not different in dividing 7/7, 7/111, and 111/111 cells (Fig. 17A). In post-mitotic cells, CB_1 mRNA levels were reduced in a mHtt gene dose-dependent manner ($n = 12$; $P < 0.01$, Fig. 17A). CB_1 mRNA levels were elevated in post-mitotic 7/7 cells relative to dividing 7/7 cells ($n = 12$; $P < 0.01$, Fig. 17B). However, the relative increase in CB_1 mRNA abundance in post-mitotic cells compared to dividing cells was attenuated in cells expressing mHtt. Striatal CB_1 levels appeared lower at P1 compared to adulthood (Figs. 7 and 13). Therefore, the transition from low- to high-level CB_1 expression when 7/7 cells enter a post-mitotic state from a dividing state may model the transition from an 'embryonic' to an 'adult' neuronal phenotype. From these data two important points were drawn. First, mHtt affected CB_1

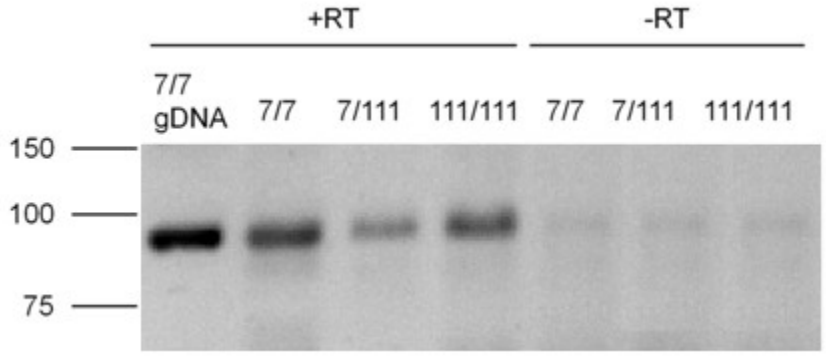

Figure 15. 7/7, 7/111, and 111/111 cells endogenously expressed CB_1 mRNA. RNA was harvested, converted to cDNA, and amplified by PCR before being resolved on a 2% agarose gel. Genomic DNA (gDNA) was used as a positive control, and –RT reactions were used as negative controls. An 89 bp band, the expected product size for CB_1, is shown here.

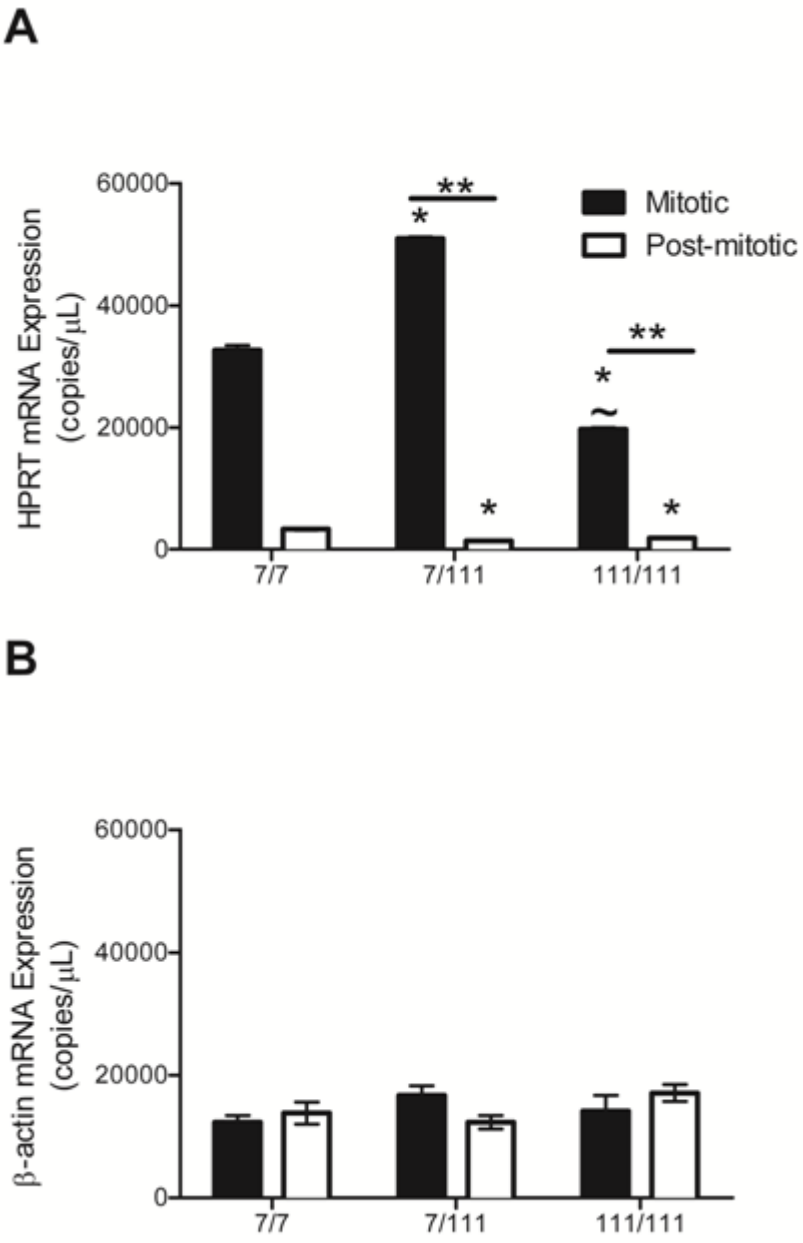

Figure 16. β-actin, not HPRT, was a house-keeping gene in 7/7, 7/111, and 111/111 cells. RNA was harvested from cells grown with (mitotic) or without (post-mitotic) serum-containing media, converted to cDNA, amplified and quantified by qRT-PCR. Significance was determined *via* two-way ANOVA for genotype and treatment followed by *post-hoc* Tukey's test. ** $P < 0.01$ between treatments within genotype, * $P < 0.01$ relative to 7/7 within treatment, ~ $P < 0.01$ relative to 7/111 within treatment, $n = 12$.

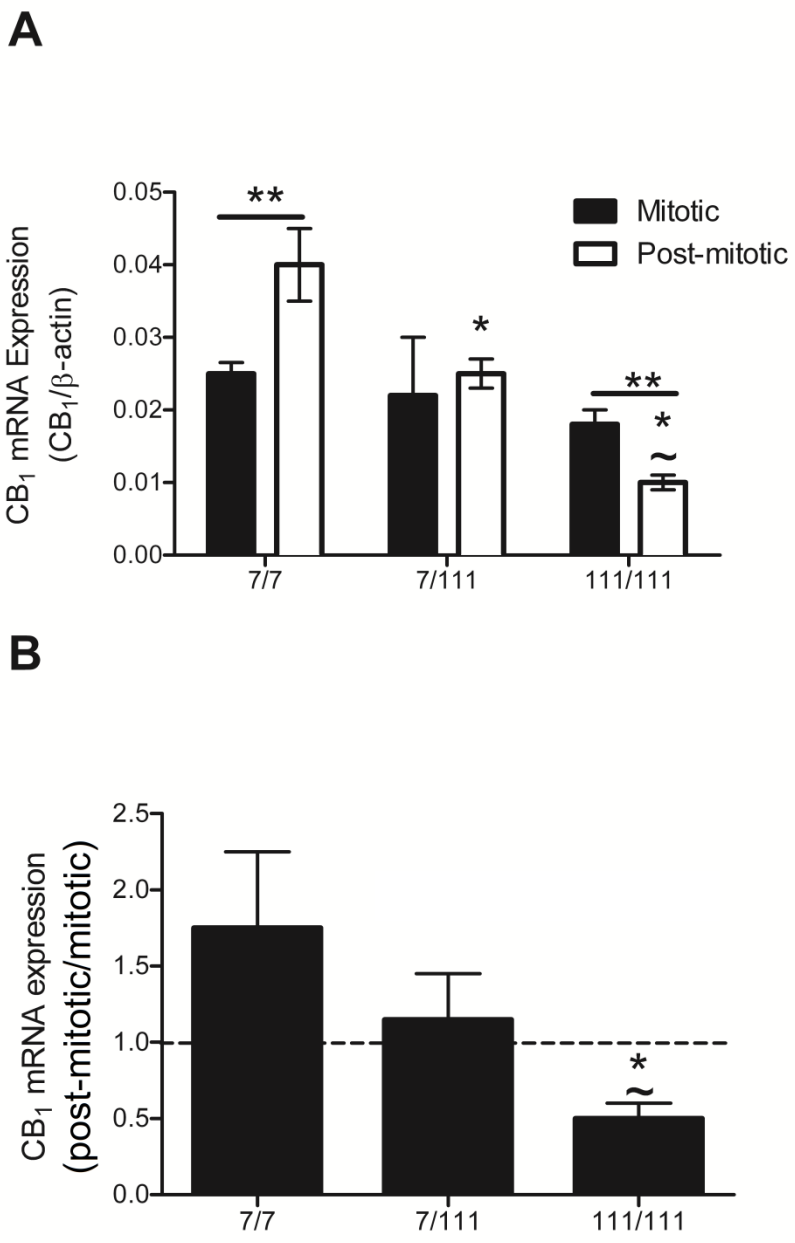

Figure 17. Endogenous CB_1 mRNA levels were lowered in the presence of mHtt in post-mitotic 7/111 and 111/111 cells. A) RNA was harvested and converted to cDNA, which was quantified by qRT-PCR. Expression data were normalized to β-actin mRNA levels. B) The fold-increase in CB_1 mRNA levels following serum-deprivation (*i.e.* post-mitotic/mitotic) were calculated for 7/7, 7/111, and 111/111 cells. Significance was determined *via* two-way ANOVA for genotype and treatment (A), or one-way ANOVA (B), followed by *post-hoc* Tukey's test. ** $P < 0.05$ between treatments within genotype, * $P < 0.05$ relative to 7/7 within treatment, ~ $P < 0.05$ relative to 7/111 within treatment, $n = 12$.

expression at the level of transcription because both promoter activity and endogenous mRNA expression were reduced in the presence of mHtt, and second, mHtt reduced CB_1 expression in post-mitotic 7/111 and 111/111 cells. In all subsequent experiments, we chose to focus our attention on serum-deprived, post-mitotic, 7/7, 7/111, and 111/111 cells because they model adult striatal neurons, which are the sub-population of neurons most severely degenerated over the course of HD pathogenesis (Trettel *et al*., 2000; Kim *et al.*, 2011).

3.4 CB_1 Protein Levels were Lower in 7/111 and 111/111 Cells Expressing mHtt.

To determine whether CB_1 protein levels were also lower in cells expressing mHtt we used an on- and in-cell western approach, rather than a traditional western blot methodology, because on- and in-cell westerns can be used to gather information about the cellular localization of GPCRs (Hudson *et al*., 2010; Wright *et al*., 2011) Moreover, anti-CB_1 antibodies were not amenable to traditional western blot approaches. The on- and in-cell western technique utilized primary antibodies directed against the N-terminal of CB_1 (Howlett *et al*., 1998), and fluorescent secondary antibodies directed against the anti-CB_1 antibodies to detect and quantify CB_1 protein abundance at the plasma membrane and, following permeabilization, total CB_1 levels in cells (Hudson *et al*., 2010). We found that total CB_1 protein levels were lower in 7/111 and 111/111 cells relative to 7/7 cells ($n = 24$; $P < 0.05$, Fig. 18A,C). There was no difference in CB_1 protein levels in 7/111 and 111/111 cells. The relative percentage of CB_1 protein present at the plasma membrane was greater in 7/111 cells, and greater still in 111/111 cells, compared to 7/7 cells ($n = 24$; $P < 0.05$, Fig. 18B,C). That is, although the total amount of CB_1 protein was lower in the presence of mHtt in 7/111 and 111/111 cells, the relative abundance of protein at the plasma membrane was higher. Therefore, although the mHtt-mediated decrease in CB_1 mRNA translated

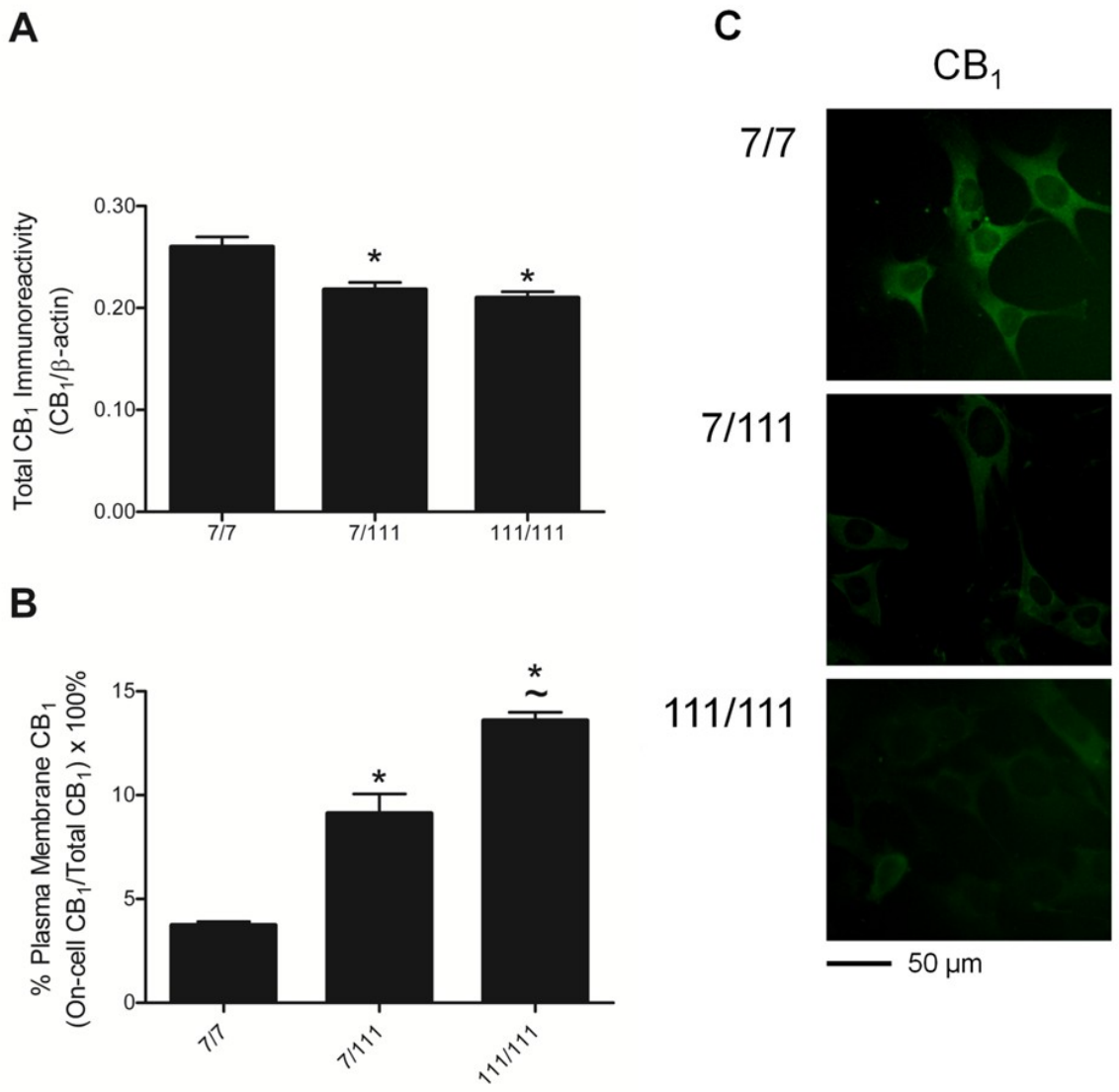

Figure 18. Endogenous CB_1 protein levels were lower in 7/111 and 111/111 cells expressing mHtt. The percentage of CB_1 receptors at the plasma membrane was greater in 7/111 and 111/111 cells. A) Total CB_1 protein abundance was determined *via* in-cell western normalized to β-actin levels. B) The percent of CB_1 protein at the plasma membrane was determined *via* on-cell fluorescence for CB_1 over total CB_1 fluorescence in the same replicate. Significance was determined *via* one-way ANOVA followed by *post-hoc* Tukey's test. * $P < 0.05$ relative to 7/7, ~ $P < 0.05$ relative to 7/111, $n = 24$. C) Representative immunocytochemical staining for CB_1 demonstrating a decrease in the overall abundance of CB_1 in 7/111 and 111/111 cells.

to a lower CB_1 protein level, the fraction of receptors at the plasma membrane was higher in mHtt-expressing cells.

3.5 Cannabinoid Agonists Increased CB_1 Promoter Activity, mRNA and Protein Levels in 7/7, 7/111, and 111/111 Cells

Given the known functional effects of cannabinoid agonism, including neuroprotection and increased expression of pro-survival genes (Fernandez-Ruiz *et al*., 2004), we wanted to determine whether cannabinoid treatment could alter CB_1 levels in 7/7, 7/111, and 111/111 cells. 7/7, 7/111, and 111/111 cells were transfected with pCNR1 and treated with 1 μM ACEA (direct agonist), 1 μM URB-597 (FAAH inhibitor, indirect agonist), or ethanol (vehicle) for 18 h. Eighteen hours is the approximate half-life of ACEA in cell culture (Hillard *et al*.,1999). *Renilla* luciferase activity was quantified and normalized to total protein. Vehicle treatment reduced *CNR1* promoter activity relative to untreated cells (n = 12; $P < 0.05$, Fig. 19A). For this reason, we compared all drug treatments to vehicle treatment. *CNR1* promoter activity was greater in all cells treated with 1 μM ACEA, and 7/111 cells treated with 1 μM URB-597, relative to the vehicle control (n = 12; $P < 0.05$, Fig. 19B,C).

CB_1 mRNA levels were quantified and normalized to β-actin levels in cells treated with 1 μM ACEA, 1 μM URB-597, or vehicle for 18 h. Ethanol (vehicle) treatment reduced CB_1 mRNA levels in 7/7 and 7/111 cells, but these were not reduced in 111/111 cells, which were already low compared to 7/7 and 7/111 cells (n = 16; $P < 0.05$, Fig. 20A). CB_1 mRNA levels were greater in all cell lines treated with 1 μM ACEA and 1 μM URB-597 relative to vehicle (n = 16; $P < 0.05$, Fig. 20B,C). In 111/111 cells treated with ACEA or URB-597, CB_1 mRNA levels were reduced relative to 7/7 cells treated with ACEA or URB-597, respectively. ACEA- or URB-597-mediated fold induction of CB_1 was not different across cell lines (Fig. 20D).

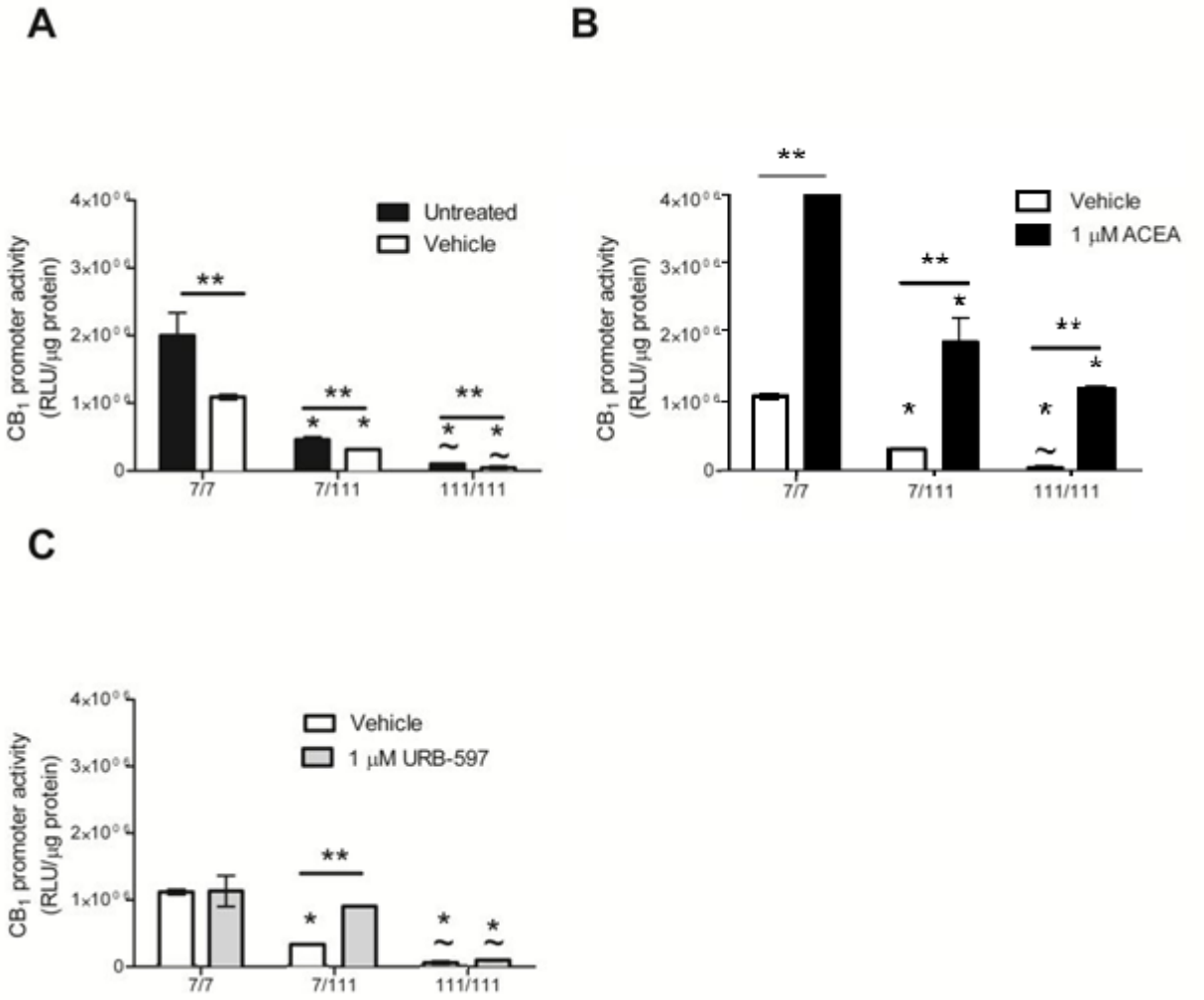

Figure 19. *CNR1* promoter activity was induced by direct (1 μM ACEA) and indirect (1 μM URB-597) cannabinoid agonism in 7/7 and 7/111 cells. Activity of the pCNR1 promoter was quantified in cells treated with ACEA, URB-597 or vehicle control and normalized to total protein. A) Vehicle (ethanol) treatment was associated with lower *CNR1* activity in all cell types. B) 1 μM ACEA induced *CNR1* promoter activity in all cells types. C) 1 μM URB-597 induced *CNR1* promoter activity in 7/111 cells. Significance was determined *via* two-way ANOVA for genotype and treatment group followed by *post-hoc* Tukey's test. ** $P < 0.05$ within genotype between treatments, * $P < 0.05$ relative to 7/7 within treatment group, ~ $P < 0.05$ relative to 7/111 within treatment group, $n = 12$.

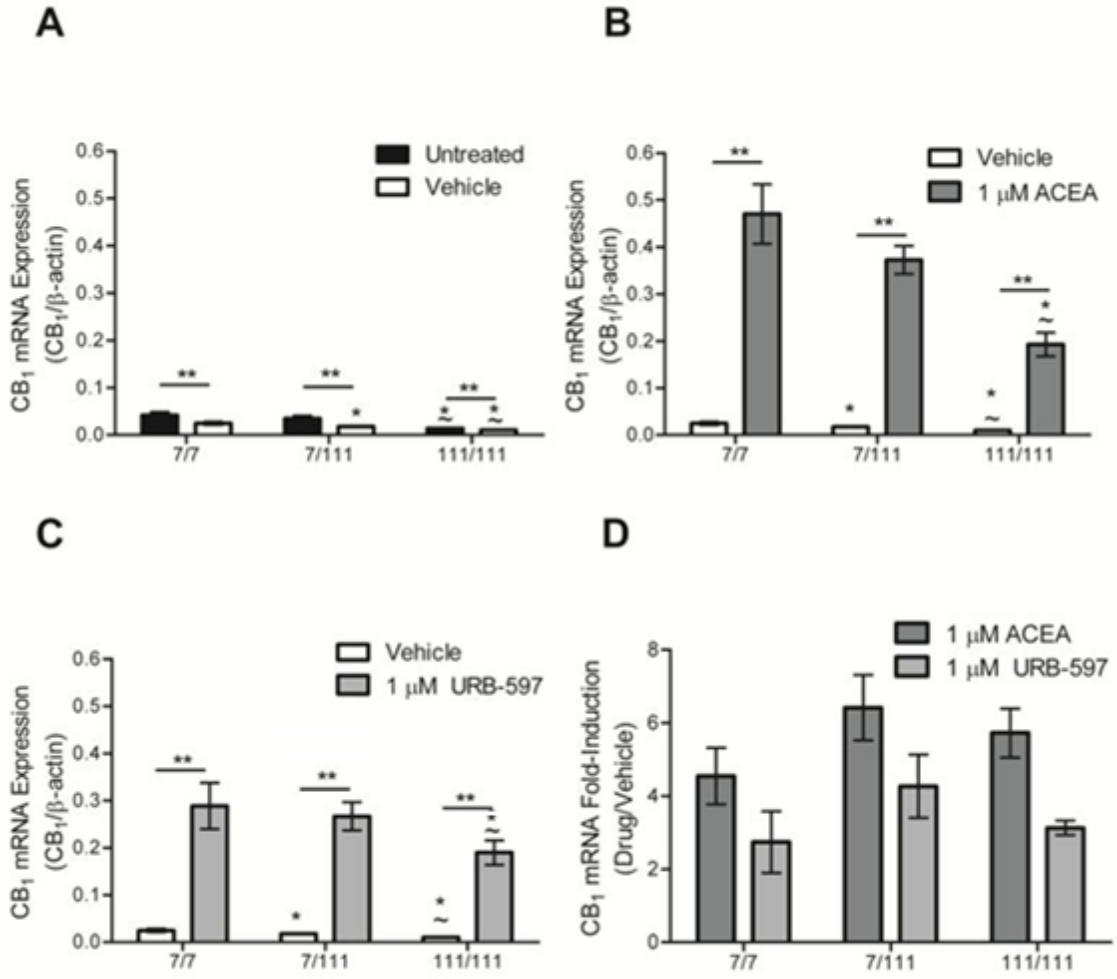

Figure 20. CB_1 mRNA levels were induced by direct (1 μM ACEA) and indirect (1 μM URB-597) cannabinoid agonism in 7/7, 7/111, and 111/111 cells. CB_1 mRNA levels were quantified *via* qRT-PCR. A) Vehicle (ethanol) treatment was associated with lower CB_1 mRNA levels in all cell types. B) 1 μM ACEA treatment induced CB_1 mRNA levels, and C) 1 μM URB-597 treatment also induced CB_1 mRNA levels. D) ACEA- and URB-597-mediated fold induction of CB_1 was not different when cell lines were compared. Significance was determined *via* two-way ANOVA for genotype and treatment group followed by *post-hoc* Tukey's test. ** $P < 0.05$ within genotype between treatments, * $P < 0.05$ relative to 7/7 within treatment group, ~ $P < 0.05$ relative to 7/111 within treatment group, $n = 16$.

Cannabinoid agonism was associated with greater endogenous CB_1 mRNA levels in 7/7, 7/111, and 111/111 cells in the presence of mHtt. However, even when induced by cannabinoid agonism, both promoter activity and mRNA abundance were lower in cells expressing mHtt. That is, the higher steady-state level of CB_1 expression following cannabinoid agonism was reduced by mHtt and the fold induction was not different across cell lines. Therefore, cannabinoid agonism induced CB_1 promoter activity mRNA abundance above a basal level. In the presence of mHtt, the basal level of CB_1 was lower and consequently the induced level was also lower than in 7/7 cells.

Next, we asked whether cannabinoid agonism was associated with elevated CB_1 protein levels in 7/7, 7/111, and 111/111 cells. The half-life of CB_1 receptors is approximately 30 h (ExPASy, 2012) and protein abundance is a less transient measure of cannabinoid-mediated CB_1 induction than mRNA (Howlett *et al.*, 1998). Further, an increase in CB_1 protein may represent an increase in functional receptor abundance. Vehicle treatment did not change total CB_1 protein levels in cells ($n = 24$; Fig. 21A). We found that treatment with 1 μM ACEA was associated with higher CB_1 protein levels, by approximately 2-fold, in all cell lines, relative to the vehicle control ($n = 24$; $P < 0.05$, Fig. 21B). The absolute level of ACEA-mediated CB_1 protein induction was reduced in the presence of mHtt (7/111 and 111/111 cells), relative to 7/7 cells. Additionally, CB_1 protein levels were not altered when cells were treated with 1 μM ACEA and 2 μM O-2050, a specific antagonist of CB_1 receptors ($n = 24$; $P < 0.05$, Fig. 21B). From these observations we concluded that cannabinoid-mediated induction of CB_1 mRNA translated to an increase in CB_1 receptors, and cannabinoid-mediated induction of CB_1 was reduced in the presence of mHtt, as is the basal expression of CB_1 in the presence of mHtt. The cannabinoid antagonist O-2050 blocked

the effect of ACEA on increasing CB_1 protein levels, which suggested that cannabinoids mediated their effect on CB_1 mRNA and protein levels *via* functional CB_1 receptors.

The initial reason for employing O-2050 in these experiments was to understand how CB_1 protein trafficking might differ between 7/7, 7/111, and 111/111 cells. First, we found that the percent of CB_1 at the plasma membrane was reduced in vehicle-treated 7/111 and 111/111 cells, relative to untreated controls ($n = 24$; $P < 0.05$, Fig. 22A). However, the percentage of CB_1 protein present at the plasma membrane remained greater in 7/111 and 111/111 cells compared to 7/7 cells. Treatment of cells with 1 μM ACEA resulted in receptor internalization [*i.e.* a reduction in the percentage of CB_1 protein at the membrane; ($P < 0.05$, Fig. 22B)]. Treatment of cells with 1 μM ACEA and 2 μM O-2050 was associated with a greater (approximately 1.5-fold) percentage of CB_1 protein at the plasma membrane, relative to vehicle-treated cells (Fig. 22B). The percentage of CB_1 protein at the membrane was higher in 7/111 and 111/111 cells treated with 1 μM ACEA and 2 μM O-2050 than in 7/7 cells. Since the percentage of CB_1 protein at the membrane was greater in vehicle-treated 7/111 and 111/111 cells, this trend was anticipated. Therefore, the percentage of total CB_1 receptors present at the plasma membrane was greater in 7/111 and 111/111 cells expressing mHtt than 7/7 cells, yet the processes of CB_1 internalization and recruitment to the plasma membrane were still observed in all the cell types tested.

3.6 CB_1 Receptor Localization and Trafficking were Altered in 7/111 and 111/111 Cells Expressing mHtt

To gain a better understanding of CB_1 receptor trafficking, localization, and abundance, we employed immunocytochemistry and confocal imaging to detect CB_1 in untreated, vehicle-treated, 1 μM ACEA-treated, or 2 μM O-2050-treated 7/7, 7/111, and 111/111 cells. The

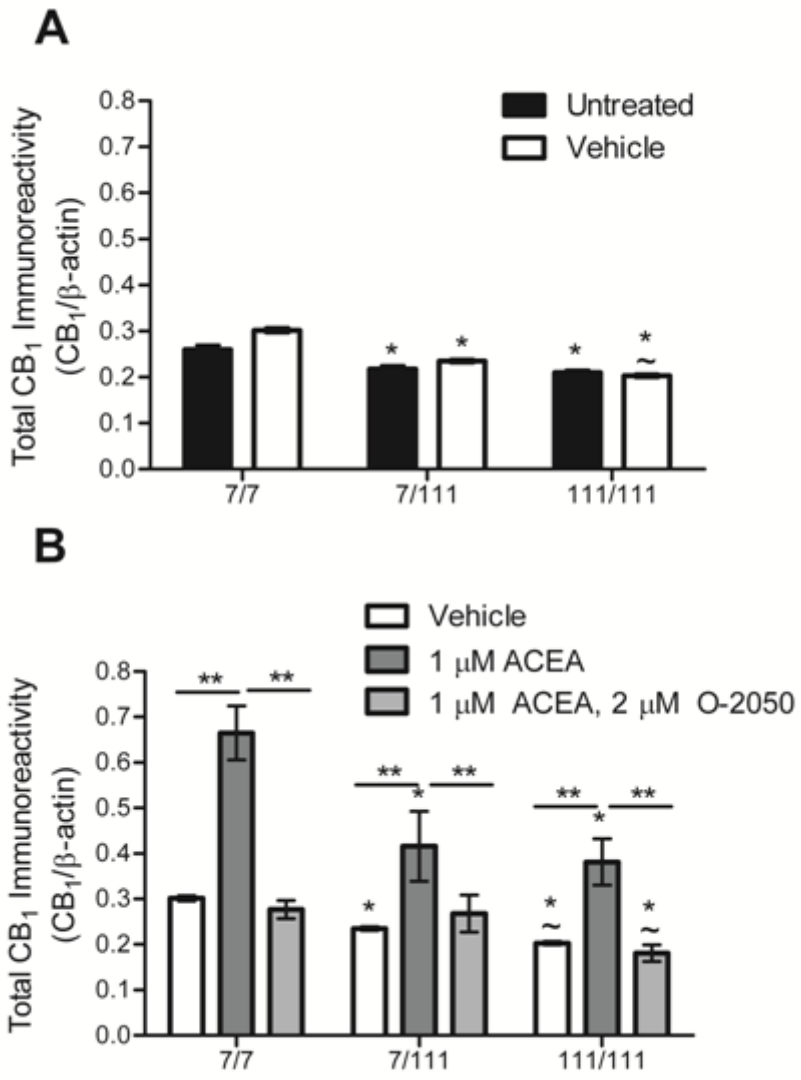

Figure 21. Direct (1 μM ACEA) cannabinoid agonism induced CB_1 protein levels in 7/7, 7/111, and 111/111 cells. CB_1 protein levels were quantified in cells treated wtih 1 μM ACEA or 1 μM ACEA and 2 μM O-2050 or vehicle control *via* in-cell western. A) Vehicle (ethanol) treatment did not change CB_1 protein levels. B) 1 μM ACEA treatment was associated with higher CB_1 protein levels, and this effect was blocked by 2 μM O-2050. Significance was determined *via* two-way ANOVA for genotype and treatment group followed by *post-hoc* Tukey's test. ** $P < 0.05$ within genotype between treatments, * $P < 0.05$ relative to 7/7 within treatment group, ~ $P < 0.05$ relative to 7/111 within treatment group, $n = 24$.

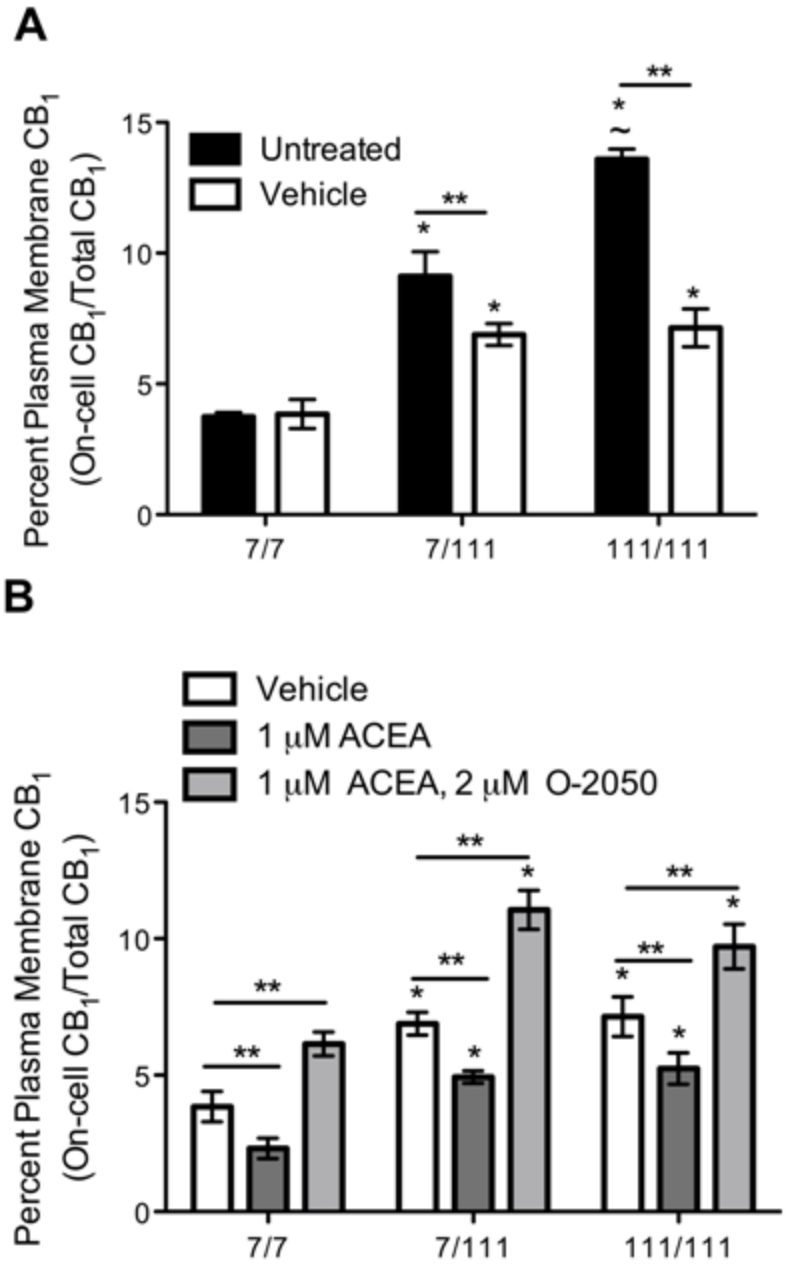

Figure 22. mHtt does not impair CB_1 protein trafficking to the plasma membrane in 7/7, 7/111 and 111/111 cells. Plasma membrane CB_1 protein expression was quantified for cells treated with 1 μM ACEA or 1 μM ACEA and 2 μM O-2050 or vehicle control *via* on- and in-cell western. A) Vehicle-treatment was associated with lower plasma membrane CB_1 protein expression in 7/111 and 111/111 cells. B) 2 μM O-2050 treatment was associated with greater plasma membrane CB_1 expression in all cell types. Significance was determined *via* two-way ANOVA for genotype and treatment group followed by *post-hoc* Tukey's test. ** $P < 0.05$ within genotype between treatments, * $P < 0.05$ relative to 7/7 within treatment group, ~ $P < 0.05$ relative to 7/111 within treatment group, $n = 24$.

intensity of fluorescence corresponding to CB_1 detection was reduced in untreated and vehicle-treated 7/111 and 111/111 cells, relative to 7/7 cells (Fig. 23). Fluorescence was visibly greater in all cells treated with 1 μM ACEA relative to vehicle-treated and untreated cells (Fig. 23). CB_1 fluorescence was not changed in cells treated with 2 μM O-2050 compared to vehicle-treated and untreated cells (Fig. 23). In untreated or vehicle-treated cells, CB_1 appeared evenly distributed throughout the cytoplasm, with slightly more fluorescence present at the plasma membrane. In cells treated with 1 μM ACEA, CB_1 was localized away from the plasma membrane, often in distinct foci, which may represent endoplasmic reticulum or endosomes. Finally, in cells treated with 2 μM O-2050 CB_1 was abundant at the plasma membrane and away from the interior of the cell (Fig. 23).

Fluorescence intensity was measured along a 50 μm line across the cell soma, spanning the nucleus, in 50 cells per treatment group. Fluorescence intensity data gathered per μm were averaged in 5 μm segments (Fig. 6). We observed that CB_1 fluorescence intensity was greater, overall, in untreated 7/7 cells, relative to 7/111 and 111/111 cells (n = 50*;* Fig. 24). In untreated 7/7 cells, CB_1 was evenly distributed throughout the cell, including the nucleus (~15 – 20 μm), although CB_1 fluorescence was greater at the plasma membrane (5 μm and 50 μm; n = 50; $P <$ 0.01). CB_1 was distributed throughout the cytoplasm of untreated 7/111 and 111/111 cells but excluded from the nucleus. Following treatment with 1 μM ACEA, CB_1 levels were lowest at the plasma membrane and greatest at the peri-nuclear region corresponding with the location of the endoplasmic reticulum in all cell types (n = 50; $P < 0.01$; Fig. 24). Finally, in each of the cell lines treated with 2 μM O-2050, the abundance of CB_1 at the plasma membrane was higher and the cytoplasmic fraction was lower (n = 50; $P < 0.01$; Fig. 24). By studying intracellular CB_1 distribution in 7/7, 7/111, and 111/111 cells, we were able to verify a

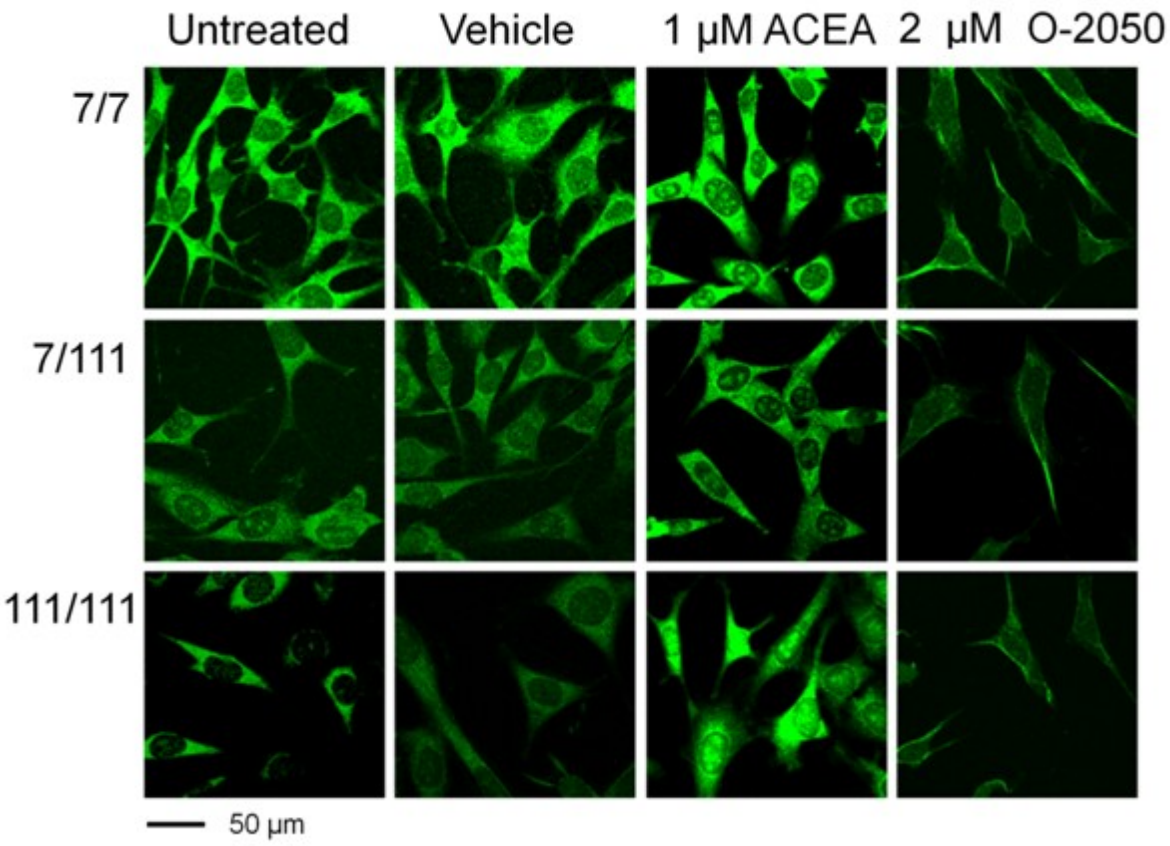

Figure 23. CB_1 protein distribution and response to cannabinoids were similar in 7/7, 7/111, and 111/111 cells despite lower total CB_1 abundance in 7/111 and 111/111 cells. Representative confocal micrographs of CB_1 protein expression in cells treated with 1 µM ACEA or 2 µM O-2050 or vehicle control. Cell types are described to the left of each row and treatments above each column.

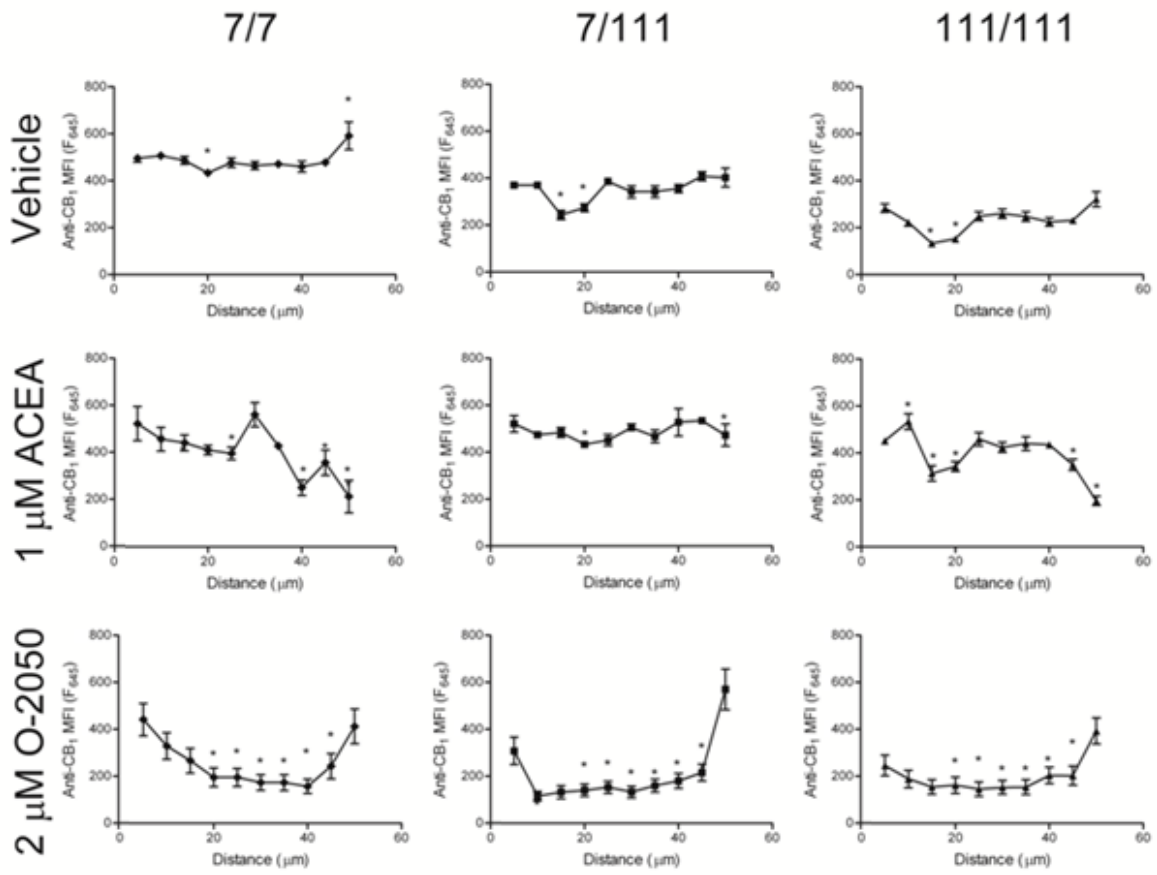

Figure 24. CB_1 protein distribution was altered following cannabinoid agonism (ACEA) or antagonism (O-2050) in 7/7, 7/111, an 111/111 cells. CB_1 protein expression was quantified as mean fluorescece intensity (MFI) along a 50 μm axis in cells treated with 1 μM ACEA or 2 μM O-2050. CB1 protein expression was uniform in vehicle-treated 7/7 cells, but excluded from the nucelus (~15 – 20 μm) in 7/111 and 111/111 cells (top row). 1 μM ACEA treatment was associated with lower plasma membrane CB_1 and higher peri-nuclear CB_1 in all cell types (middle row). 2 μM O-2050 treatment was associated with higher plasma membrane CB1 in all cell types (bottom row). Significance was determined *via* one-way ANOVA followed by *post-hoc* Tukey's test. * $P < 0.01$ across axis relative to the 5 μm point, $n = 50$.

mHtt-dependent decrease in CB_1 protein levels, illustrate the uniform distribution of CB_1 in untreated cells, verify an ACEA-dependent induction of CB_1 expression, demonstrate an agonist-dependent internalization of CB_1 receptors, and an antagonist-dependent localization of CB_1 receptors to the plasma membrane. We also observed the presence of CB_1 in the nucleus of untreated 7/7 cells and not untreated 7/111 or 111/111 cells. The functional significance of this observation is not clear. Treatment with 1 μM ACEA was associated with increased nuclear CB_1 fluorescence in 7/111, but not 111/111, cells. ACEA treatment may, therefore, localize CB_1 receptors to the nucleus. mHtt appears to impair nuclear localization of CB_1 in 111/111, but not 7/111, cells.

3.7 Cannabinoid Agonists Induced CB_1 Levels *Via* Functional CB_1 Receptors

Next, we wanted to determine if cannabinoid-mediated induction of CB_1 mRNA and protein occurred by activation of CB_1 receptors. To do this, we first explored the possibility that other GPCRs could mediate the same induction of CB_1. 7/7, 7/111, and 111/111 cells express dopamine D_2 receptors and CB_2 (Fig. 25A). These receptors are known to be co-expressed with CB_1 *in vivo* (Uriguen *et al*., 2009). CB_2 and CB_1 receptors share 95% sequence similarity. Therefore, even highly selective cannabinoid receptor ligands may interact with both CB_1 and CB_2 receptors (Hillard *et al*., 1999). We used several highly selective CB_1 and CB_2 ligands to determine the cannabinoid receptor that mediated CB_1 mRNA induction. We treated 7/7 cells with the CB_1 agonist ACEA (1 μM, CB_1 K_d = 1.4 nM, CB_2 K_d = 1.9 μM), the CB_1 neutral antagonist O-2050 (1 μM, CB_1 K_d = 2.5 nM, CB_2 K_d = 2.5 μM), the CB_2 agonist HU-308 (1 μM, CB_1 K_d > 10 μM, CB_2 K_d = 22.7 nM), the CB_2 antagonist AM-630 (2 μM, CB_1 K_d = 5.1 μM, CB_2 K_d = 31.2 nM), the D_2 receptor agonist quinipirole (1 μM), the $D_{1/2}$ receptor agonist apo-morphine (1 μM), and vehicle controls and quantified the resulting CB_1 mRNA abundance

(Pertwee *et al*., 1999). The CB_1-selective agonist ACEA induced CB_1 mRNA expression in 7/7 cells while all other compounds employed did not alter CB_1 levels, relative to vehicle (ethanol and DMSO) controls ($n = 12$; $P < 0.05$, Fig. 25B). Therefore, CB_1-specific agonism, and not D_2R or CB_2 agonism, induced CB_1 expression in 7/7cells.

Next, we sought to determine if a general inducer of transcription like a histone deacetylase (HDAC) inhibitor, could also increase CB_1 mRNA levels in cells. Cells were treated with the pan-HDAC inhibitor NaB (100 nM), the type 1 HDAC inhibitor TSA (1 μM), or vehicle (DMSO) for 18 h and CB_1 mRNA abundance was quantified. CB_1 levels were not altered by vehicle or NaB treatment (Fig. 26A,B). TSA treatment was associated with reduced CB_1 mRNA abundance in 7/7 and 7/111 cells, relative to vehicle treatment ($n = 12$, $P < 0.05$; Fig. 26C). Therefore, HDAC inhibition, which is popularly considered an inducer of general transcription (Cui *et al*., 2006), did not induce CB_1 mRNA levels in cells, whether they expressed mHtt or not.

If cannabinoid-mediated induction of CB_1 transcription was CB_1 receptor-dependent, then the induction should be cannabinoid dose-dependent. To test this hypothesis, 7/7 cells were treated with ACEA, mAEA, or AEA at 0.01, 0.10, 0.25, 0.50, 0.75, 1.00, and 5.00 μM for 18 h. Additionally, 7/7 cells were treated with 0.25, 0.50, or 0.75 μM ACEA or mAEA in conjunction with 1.0, 1.5, or 2.0 μM O-2050 (CB_1 neutral antagonist) or AM-281 (CB_1 antagonist/inverse agonist). CB_1 mRNA levels were induced, in a dose-dependent manner by ACEA, mAEA, and AEA (Fig. 27A). When plotted on a logarithmic scale for cannabinoid dose, the data assume a sigmoidal form indicative of a dose-response relationship for a non-linear regression assuming a variable slope (Hill coefficient). The EC_{50} values for ACEA, mAEA, and AEA were 0.36 μM, 0.53 μM, and 0.42 μM, respectively. The E_{max} values for ACEA, mAEA, and AEA were 0.32, 0.26, and 0.29 (CB_1/β-actin), respectively. Therefore, ACEA was the most potent inducer of CB_1

expression tested. This result was expected because ACEA has a greater affinity for CB_1 than mAEA or AEA (K_d = 1.4 for ACEA vs. 20 nM for mAEA or AEA) and a longer half-life in cell culture (18 h for ACEA vs. 12 h for mAEA or AEA; Corchero *et al*., 1999; Pertwee *et al*., 1999).

We wanted to determine how quickly cannabinoid treatment could increase CB_1 mRNA levels. Previously, our experiments had utilized an 18 h treatment period. 7/7 cells were treated with 1 μM ACEA or vehicle control for 0.5, 1, 3, 6, 12, 18, 24, and 30 h and CB_1 mRNA abundance was quantified and normalized to β-actin mRNA levels. CB_1 mRNA levels were increased within 0.5 h of treatment and further increased within 18 h of treatment compared to vehicle control (n = 12; $P < 0.05$; Fig. 28). At 30 h post-ACEA exposure CB_1 mRNA levels were decreased relative to 18 h post-ACEA exposure. Thus, the maximum effect of ACEA treatment was observed at 18 h, which is a single half-life for this drug. After 18 h, CB_1 mRNA levels began to decline. From these data two hypotheses were formed. First, the down-stream transcription factors that mediated CB_1 induction were likely pre-existing and resident at the promoter and subject to post-translational modification or recruited quickly to the promoter in order to have facilitated the rapid (0.5 h) increase in CB_1 mRNA levels. Second, the gradual increase in CB_1 mRNA level during the first 18 h of treatment provided evidence that newly synthesized receptors were activated by the remaining cannabinoids in the media to further induce CB_1 expression.

Next, we wanted to establish whether ACEA and mAEA facilitated a dose-dependent induction of CB_1 mRNA *via* CB_1 receptors. To do this, 7/7 cells were treated with 0.25, 0.50, or 0.75 μM cannabinoid agonist and 1.0, 1.5, or 2.0 μM O-2050 or AM-281. Treatment with O-2050 resulted in an antagonist dose-dependent shift of the cannabinoid agonist-CB_1 mRNA level dose-response curve to the right (n = 16; $P < 0.05$, Fig. 27B,C). A similar result was observed

when AM-281 was employed; however, the magnitude of shift of the curve to the right was not antagonist dose-dependent (n = 16; $P < 0.05$; Fig.27D). AM-281 is known to act as an inverse agonist and this may explain the different results observed (Pertwee *et al.*, 1999). To conclusively demonstrate CB_1 induction was dependent upon the activation of CB_1 receptors, a Schild plot was constructed as the logarithm of the dose-ratio minus 1 against the negative logarithm of the antagonist dose. In the Schild plot, competitive antagonism of a response appears as a linear relationship between the two variables with a slope approaching -1. The x-intercept of a line with a slope approaching -1 represents the dose of antagonist at which a two-fold increase in agonist concentration would be required to evoke the same response in the absence of antagonist (*i.e.* the pA_2). Consequently, O-2050 produced a linear Schild plot with a slope of -1.03 and a pA_2 value of 1.3 μM (Fig. 29). Thus, O-2050 inhibited CB_1 receptor activation, and a consequent increase in CB_1 mRNA levels, in a dose-dependent manner. AM-281 also inhibited CB_1 receptor activation, but AM-281 did not perform as a pure competitive antagonist because the slope of this line was significantly different from 1 ($P < 0.05$). From these data, we had shown that ACEA, mAEA, and AEA induce CB_1 expression in a CB_1 receptor-dependent manner, which can be competitively inhibited by CB_1 antagonism.

Next, we wanted to determine what effect mHtt had on the observed cannabinoid dose-CB_1 induction response relationship. We measured CB_1 mRNA abundance in 7/7, 7/111, and 111/111 cells treated with 0.01, 0.10, 0.25, 0.50, 0.75, 1.00, and 5.00 μM ACEA. Cannabinoid-mediated CB_1 induction was attenuated in 7/111 and 111/111 cells (n = 16; $P < 0.05$, Fig. 30). That is, the E_{max} was reduced in 7/111 and 111/111 cells relative to 7/7 cells while the EC_{50} was

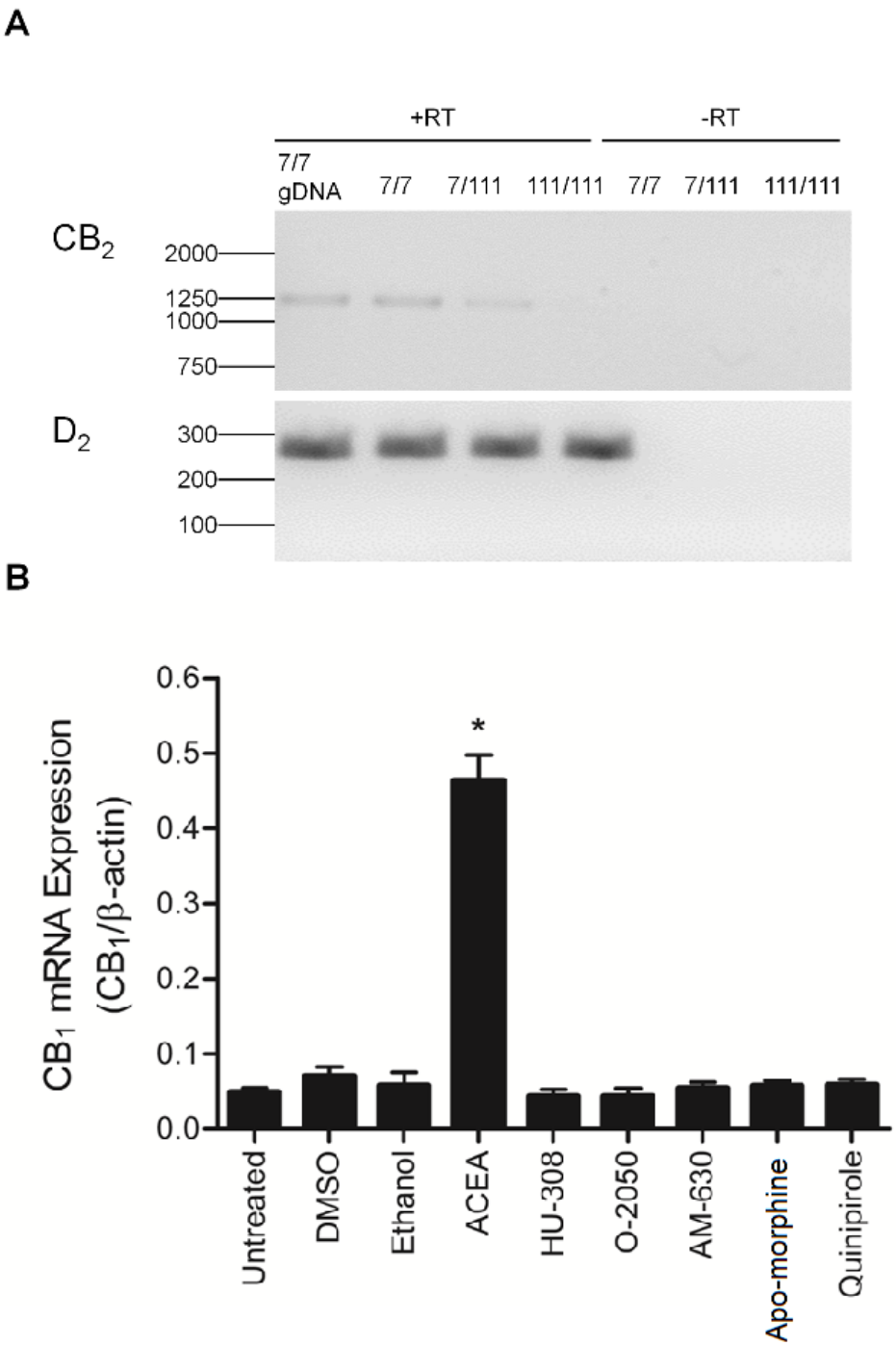

Figure 25. Induction of CB_1 mRNA expression was unique to CB_1 agonism. A) 7/7, 7/111, and 111/111 cells express CB_2 and D_2 receptors (RT-PCR). B) 1 μM ACEA treatment elevated CB_1 mRNA levels in 7/7 cells while 1 μM apo-morphine (D_1/D_2 antagonist), quinipirole (D_2 agonist), HU-308 (CB_2 agonist), O-2050 (CB_1 antagonist), and AM-630 (CB_2 antagonist) did not change CB_1 mRNA abundance. Significance was determined *via* one-way ANOVA followed by *post-hoc* Tukey's test. * $P < 0.05$, $n = 12$.

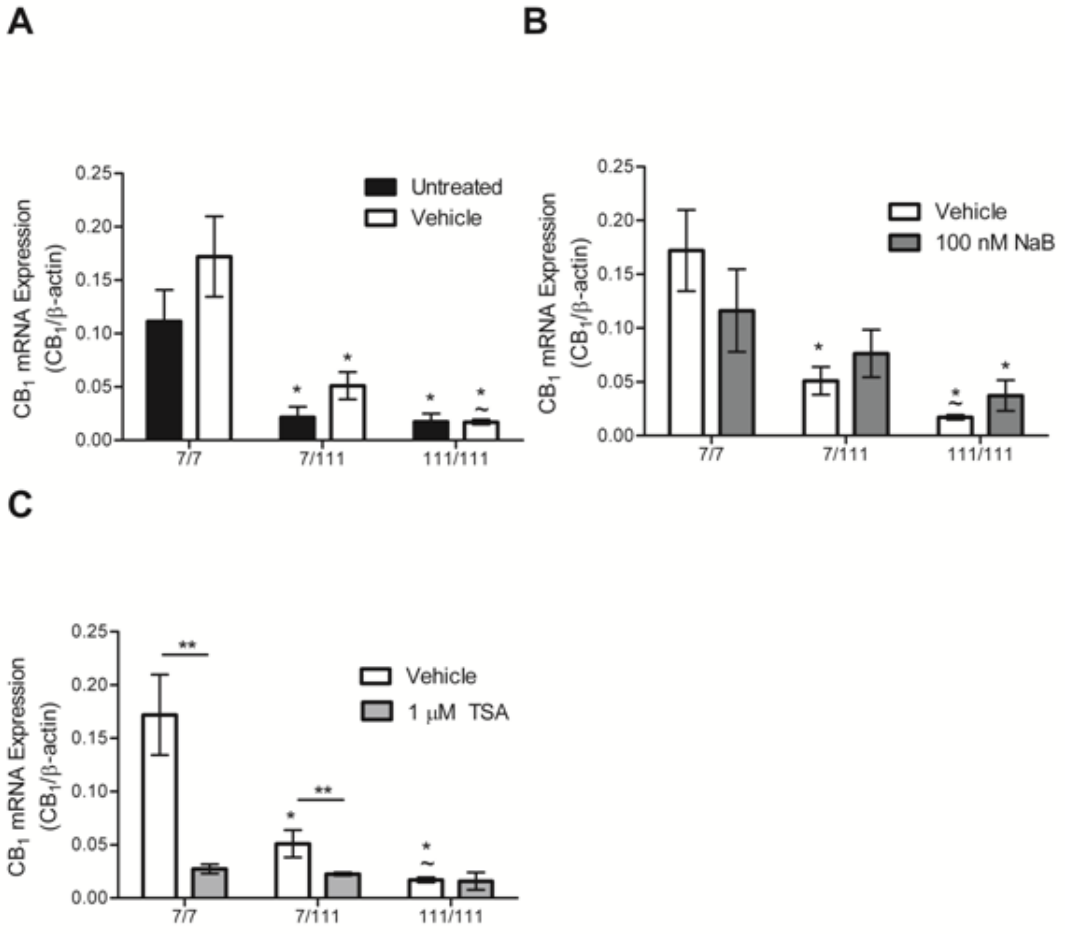

Figure 26. CB_1 mRNA levels were lower following type 1 HDAC inhibition (1 μM TSA) in 7/7 and 7/111 cells. CB_1 mRNA abundance was quantified in cells treated with 100 nM NaB or 1 μM TSA or vehicle control. A) Vehicle (DMSO) treatment did not change CB_1 mRNA level. B) 100 nM NaB did not change CB_1 mRNA level. C) 1 μM TSA treatment was associated with lower CB_1 mRNA levels in 7/7 and 7/111 cells compared to vehicle treatment. Significance was determined *via* two-way ANOVA for genotype and treatment followed by *post-hoc* Tukey's test. ** $P < 0.05$ within genotype between treatments, * $P < 0.05$ relative to 7/7 within treatment group, ~ $P < 0.05$ relative to 7/111 within treatment group, $n = 12$.

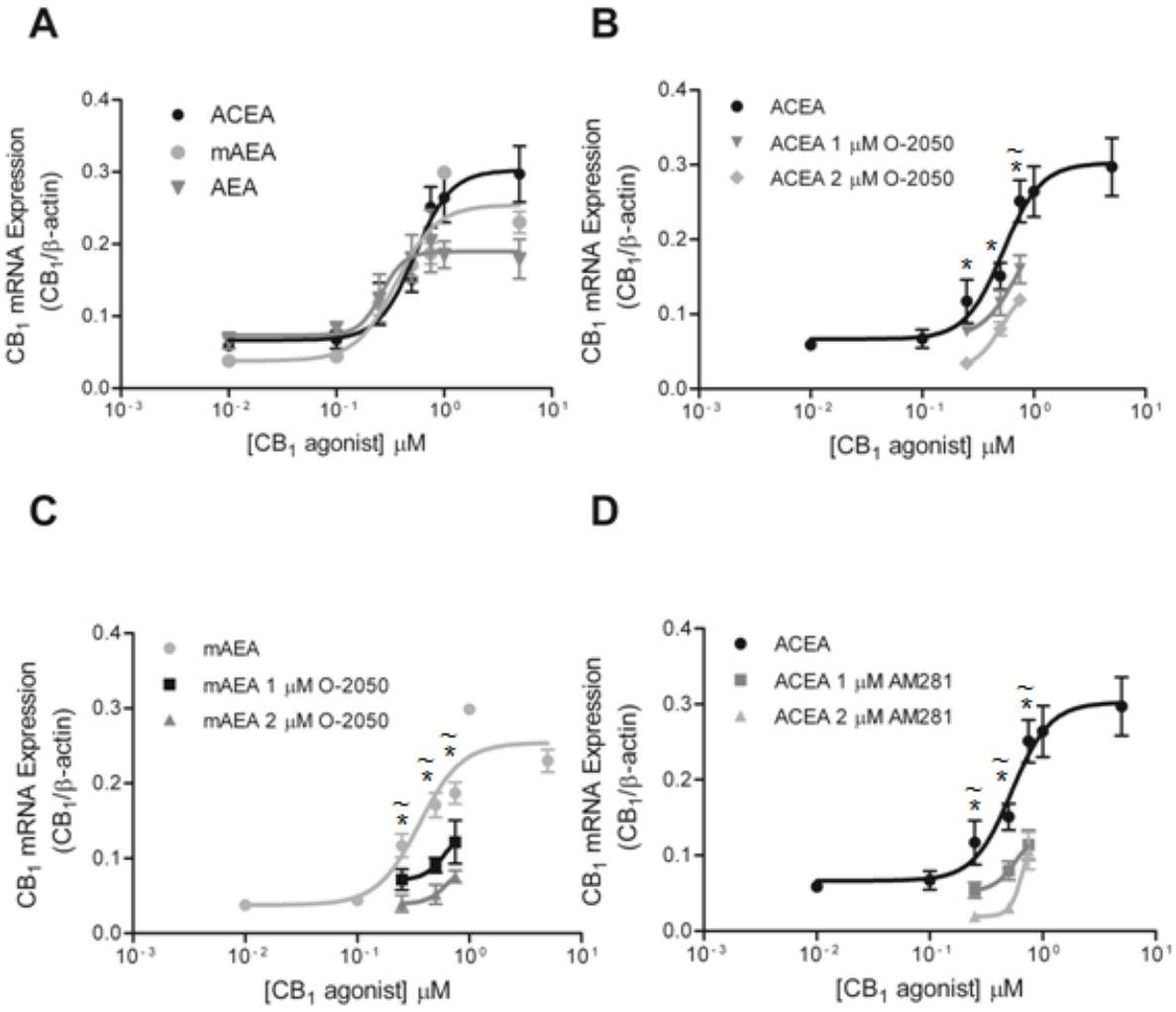

Figure 27. Direct CB_1 receptor agonism induced CB_1 mRNA levels in 7/7 cells. CB_1 mRNA abundance was quantified in 7/7 cells treated with 0.01 – 5.00 μM ACEA, mAEA, or AEA with or without 1 or 2 μM AM-281 or O-2050. A) ACEA, mAEA, and AEA treatment induced CB_1 mRNA levels in a dose-dependent manner in 7/7 cells. O-2050 antagonized the effect of ACEA (B) and mAEA (C) in an antagonist dose-dependent manner. D) AM-281 antagonized the effect of ACEA, but not in an antagonist dose-dependent manner. Significance was determined *via* one-way ANOVA followed by *post-hoc* Tukey's test. $*P < 0.05$ relative to 2 μM antagonist dose, $\sim P < 0.05$ relative to 1 μM antagonist dose, $n = 16$.

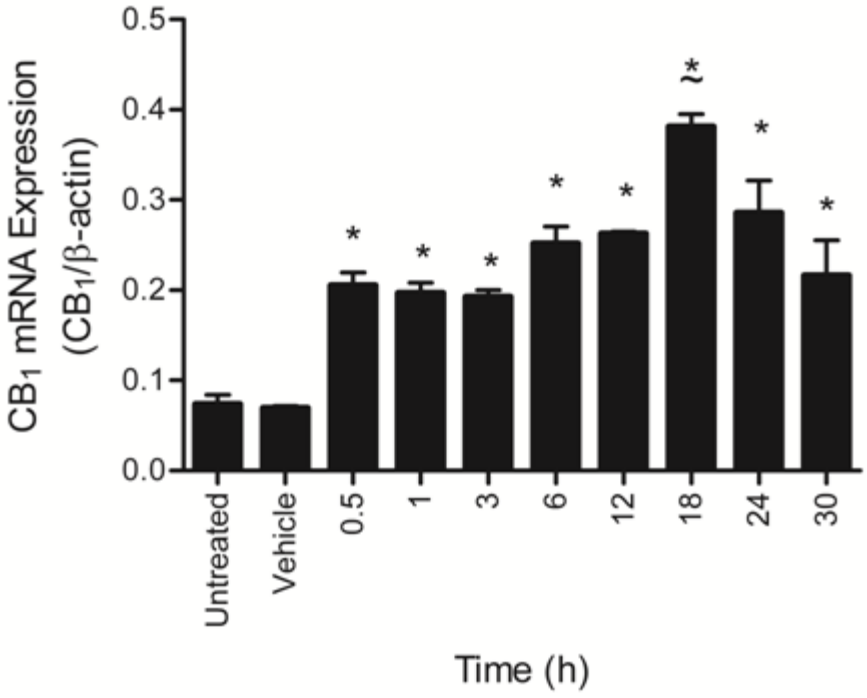

Figure 28. The maximum effect of direct CB_1 receptor agonism on CB_1 mRNA level occured 18 h after drug exposure. CB_1 mRNA abundance was quantified in 7/7 cells treated with 1.00 μM ACEA for 0.5, 1, 3, 6, 12, 18, 24, and 30 h. ACEA treatment was associated with higher-than-basal CB_1 mRNA levels by 0.5 h, with a maximum at 18 h, drug treatment. Significance was determined *via* one-way ANOVA for exposure time followed by *post-hoc* Tukey's test. * $P < 0.05$ relative to 0 h vehicle treatment, ~ $P < 0.05$ relative to 0.5 h ACEA treatment, $n = 12$.

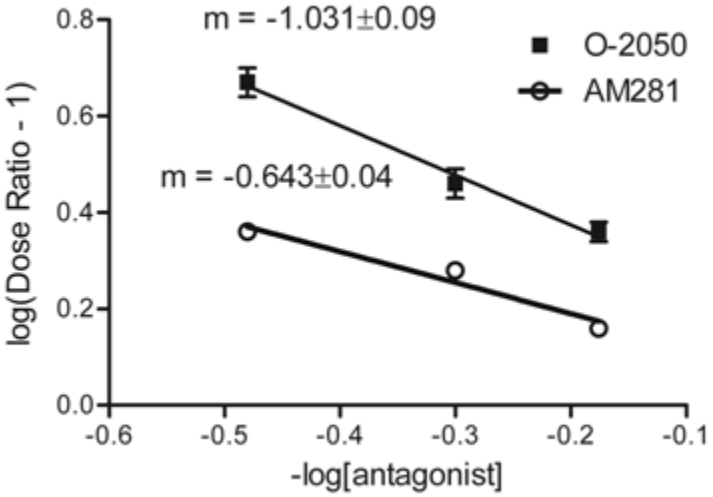

Figure 29. O-2050 competitively antagonized CB_1 receptor agonist-mediated CB_1 mRNA induction in 7/7 cells. A Schild regression was used to demonstrate O-2050, and not AM-281, acts as a competitive inhibitor of ACEA. On the Schild plot a slope approaching -1 represents competitive antagonism. The pA_2 value for a competitive antagonist is the x-intercept of the line whose slope approaches -1. Here, the pA_2 for O-2050 is 1.3 μM. n = 12.

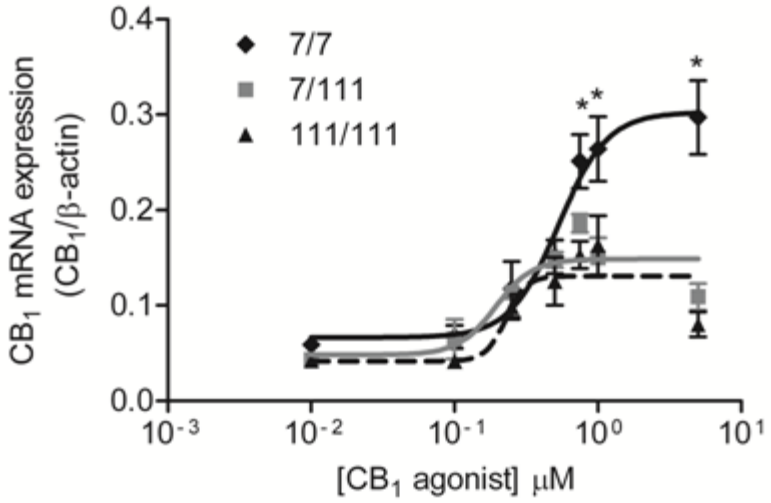

Figure 30. CB_1 mRNA induction was attenuated in the presence of mHtt. CB_1 mRNA abundance was quantified in cells treated with 0.01 – 5.00 μM ACEA. ACEA treatment induced CB_1 mRNA levels in a dose-dependent manner in all cells but E_{max} was lower in 7/111 and 111/111 cells. Significance was determined *via* one-way ANOVA followed by *post-hoc* Tukey's test. * $P < 0.05$, $n = 16$.

not different in each of the three cell lines. Taken together, these two observations demonstrate that mHtt acted as a non-competitive inhibitor of cannabinoid-mediated CB_1 induction. In all cell lines, CB_1 receptors were activated by cannabinoids to induce CB_1 mRNA transcription. In the presence of mHtt, the basal expression of CB_1 was lower and the absolute level of CB_1 receptor-dependent CB_1 mRNA induction, was lower compared to 7/7 cells.

3.8 Activated CB_1 Receptors Signal Through Akt and NF-κB to Induce CB_1 mRNA Transcription.

Our next task was to determine the pathways mediating CB_1 receptor signalling in 7/7, 7/111, and 111/111 cells. CB_1 is classically considered to couple with $G_{i/o}$-proteins (reviewed by Hudson *et al*., 2009; Scotter *et al*., 2010). Downstream of $G_{i/o}$-coupling, ERK2 and PI3K are activated and PKA is inhibited. We chose to measure ERK2 phosphorylation at Tyrosine 204 [pERK2(Y204)], relative to total ERK2, in cells treated with 0.01, 0.10, 0.25, 0.50, 0.75, 1.00, and 5.00 μM ACEA for 18 h. We found that pERK2(Y204) levels increased in an ACEA dose-dependent manner in 7/7 cells (Fig. 31A). The EC_{50} for this dose-response curve was 0.38 μM, which approaches the EC_{50} observed for ACEA-dependent CB_1 mRNA induction (0.36 μM). The dose-response relationships between pERK2(Y204) and ACEA concentration were attenuated in 7/111 and 111/111 cells, in a mHtt-dependent manner ($n = 16$; $P < 0.05$, Fig. 31A). What was unclear, however, was whether reduced pERK2(Y204) was due solely to reduced CB_1 protein levels or if Htt also directly affected pERK2-mediated signal transduction. Treatment with ACEA induced CB_1 mRNA levels in all cell types (Fig. 30). This induction was approximately 50% lower in the presence of mHtt, but not different in 7/111 cells compared to 111/111 cells (Fig. 30). In contrast, pERK2(Y204) levels were induced in an ACEA dose-dependent manner, yet ERK2 phosphorylation was attenuated by approximately 50% in 7/111 cells and approximately 80% in 111/111 cells ($n = 16$; $P < 0.05$; Fig. 31A). If ERK2 mediated

CB_1 induction, then we would not expect to observe an 80% attenuation in CB_1 mRNA induction in 111/111 cells, but this was not the case. Therefore, it did not seem likely that pERK2(Y204) mediated CB_1 mRNA induction downstream of CB_1 receptor activation.

The PI3K/Akt pathway is also downstream of $G_{i/o}$-coupled signalling (Scotter *et al.*, 2010). Moreover, evidence suggests that Akt phosphporylation is unchanged, while ERK2 phosphorylation is lower, in the presence of mHtt (Scotter *et al.*, 2010; Gines *et al.*, 2010). We quantified Akt phosphorylation at Serine 473 [pAkt(S473)], relative to total Akt (panAkt), in cells treated with 0.01, 0.10, 0.25, 0.50, 0.75, 1.00, and 5.00 μM ACEA for 18 h. We found that pAkt(S473) levels increased in an ACEA dose-dependent manner in 7/7, 7/111, and 111/111 cells (Fig. 31B). The common EC_{50} for these dose-response curves was 0.40 μM, which approaches the EC_{50} observed for ACEA-dependent CB_1 mRNA induction (0.36 μM). The E_{max} was not different in 7/7, 7/111 and 111/111 cells. From this result, we concluded that 1) mHtt did not alter Akt phosphporylation and 2) downstream effectors of Akt could facilitate CB_1 induction.

One downstream target of pAkt(S473) is IκB kinase (Iκκ). Activated Iκκ phosphorylates and inactivates the inhibitor of kappa B (IκBα), which normally inhibits the translocation of NF-κB to the nucleus. Once Iκκ is activated, inhibition of NF-κB is relieved and NF-κB translocates to the nucleus to affect gene expression (Reijonen *et al.*, 2011). Activated Iκκ phosphorylates IκB, thereby unmasking the nuclear localization signals of the p50/p52 and p65/RelA subunits of NF-κB (Reijonen *et al.*, 2010). We wanted to determine whether cannabinoid treatment led to greater NF-κB-mediated transcription of CB_1 mRNA. Expression of mHtt is associated with decreased p65/RelA-dependent transcription (Reijonen *et al.*, 2010). We also wanted to determine whether mHtt inhibited NF-κB-dependent transcriptional activation in 7/111 and

111/111 cells. To do this, we co-transfected 7/7, 7/111, and 111/111 cells with pCNR1 and an NF-κB reporter plasmid containing 5 tandem repeats of the NF-κB response element driving expression of firefly luciferase (pNF). In addition, 7/7, 7/111, and 111/111 cells were co-transfected with pCNR1 and an estrogen reporter plasmid containing 5 tandem repeat estrogen response element sites (pERE) because cannabinoids have also been shown to signal *via* ERE-dependent mechanisms (Proto *et al.*, 2011). Transfected cells were untreated, vehicle-treated, 0.01 – 5.00 μM ACEA-treated, 1 μM 17β-estradiol-treated, and 5 ng/mL IL-4-treated for 18 h. 17β-estradiol served as a positive control for ERE induction (Proto *et al.*, 2011) and IL-4 served as a positive control for NF-κB induction (Borner *et al.*, 2007a). CB_1 promoter activity was lower in the presence of mHtt compared to levels observed in 7/7 cells that were untreated, vehicle-treated, and 17β-estradiol-treated ($n = 8$; $P < 0.05$; Fig. 32A). Treatment of cells with 1 μM ACEA or 5 ng/mL IL-4 was associated with an approximately 10-fold induction in CB_1 promoter activity and this induction was attenuated in 7/111 and 111/111 cells ($n = 8$; $P < 0.05$; Fig. 32A). NF-κB promoter activity was lower in the presence of mHtt than in 7/7 cells that were untreated and vehicle-treated ($n = 8$; $P < 0.05$; Fig. 32B). Treatment of cells with 1 μM ACEA or 5 ng/mL IL-4 was associated with an approximately 2- or 5-fold induction, respectively, in NF-κB promoter activity and this induction was attenuated in the presence of mHtt ($n = 8$; $P < 0.05$; Fig. 32B). ERE promoter activity was not different among untreated or vehicle-treated 7/7, 7/111, and 111/111 cells ($n = 8$; $P < 0.05$; Fig. 32C). Treatment of cells with 1 μM 17β-estradiol was associated with greater ERE promoter activity and this induction was attenuated in the presence of mHtt ($n = 8$; $P < 0.05$; Fig. 32C).

ERE promoter activity was induced following treatment with 17β-estradiol, but not ACEA. We had previously shown that CB_1 mRNA levels responded to ACEA in a dose-

dependent manner. We wanted to determine whether CB_1 and NF-κB promoter activity responded to ACEA in a dose-dependent manner. CB_1 promoter activity increased in an ACEA dose-dependent manner and the E_{max} of the dose-response was attenuated by approximately 50% in 7/111 and 111/111 cells expressing mHtt relative to 7/7 cells ($n = 8$; $P < 0.05$; Fig. 33A). The EC_{50} was approximately 0.64 μM ACEA and not different between 7/7, 7/111 and 111/111 cells. Similarly, NF-κB promoter activity increased in an ACEA dose-dependent manner and the E_{max} was also attenuated by approximately 50% in 7/111 and 111/111 cells compared to 7/7 cells ($n = 8$; $P < 0.05$; Fig. 33B). The EC_{50} was approximately 0.82 μM ACEA and not different between cell types. Therefore, the response of the transcription factor NF-κB was ACEA dose-dependent and the dose-response relationship resembled that observed for CB_1 promoter activity and mRNA levels in 7/7, 7/111, and 111/111 cells (Figs. 30, 33A,B). Based on this, we believe NF-κB participated in CB_1 receptor-dependent induction of CB_1 promoter activity and NF-κB promoter activity was inhibited in the presence of mHtt.

3.9 Transcriptional Dysregulation in Heterozygous CB_1 Knock-out Mice ($CB_1^{+/-}$) did not Recapitulate HD Transcriptional Dysregulation.

CB_1 receptor activation is known to effect gene expression *via* up-regulation of ERK- and Akt-mediated signalling and inhibition of cAMP-dependent signalling (Scotter *et al*., 2010; Reijonen *et al*., 2010). Therefore, we sought to determine if decreased CB_1 expression alone affected expression of genes dysregulated in HD. We measured the expression of 12 genes, *via in situ* hybridization, in 10 week-old heterozygous CB_1 knock-out mice ($CB_1^{+/-}$; *i.e.* mice expressing 50% the wild-type level of CB_1). Coronal sections were used for *in situ* hybridization and the radiographic signals corresponding to mRNA hybridization were measured as OD relative to background (Fig. 34). Of these genes, CB_1 ($P < 0.001$), PDE1B ($P < 0.01$), and PGC1α ($P < 0.01$) mRNA levels were lower in the lateral striatum of $CB_1^{+/-}$ mice relative to

wild-type (n = 3; Fig. 35). Dynamin ($P < 0.001$) and Egr-1 ($P < 0.001$) mRNA levels were greater in the cortex of $CB_1^{+/-}$ mice than the cortex of wild-type mice (n = 3; Fig. 35). mRNA levels of the remaining genes, DARPP-32, PDE10A, ppENK, CB_2, FAAH, dopamine D_2 receptor, and β-actin, were not changed (Fig. 35). Therefore, a 50% decrease in CB_1 mRNA level did affect the expression of some, but not all, genes whose expression is altered in HD (Luthi-Carter *et al.*, 2000).

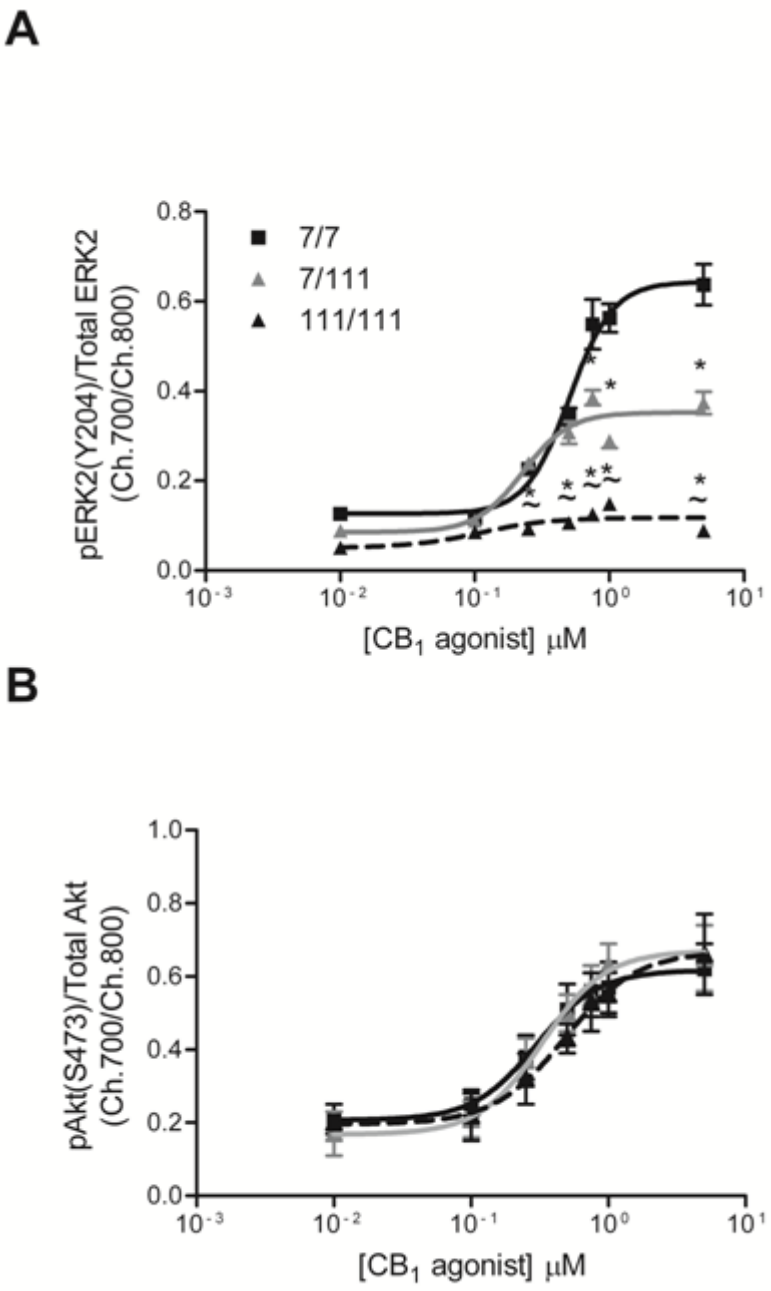

Figure 31. ERK2 phosphorylation [pERK2(Y204)] was attenuated in the presence of mHtt but Akt phosphorylation [pAkt(S473)] was not. pERK2(Y204) relative to total ERK2 and pAkt(S473) relative to total Akt were quantified in 7/7, 7/111, and 111/111 cells treated with 0.01 – 5.00 μM ACEA. A) pERK2(Y204) levels were induced in an ACEA dose-dependent manner but the E_{max} was attenuated in the presence of mHtt. B) pAkt(S473) levels were also induced in an ACEA dose-dependent manner and the E_{max} was not different between cell types. Significance was determined *via* one-way ANOVA within agonist dose followed by *post-hoc* Tukey's test. * $P < 0.05$ relative to 7/7, ~ $P < 0.05$ relative to 7/111, $n = 16$.

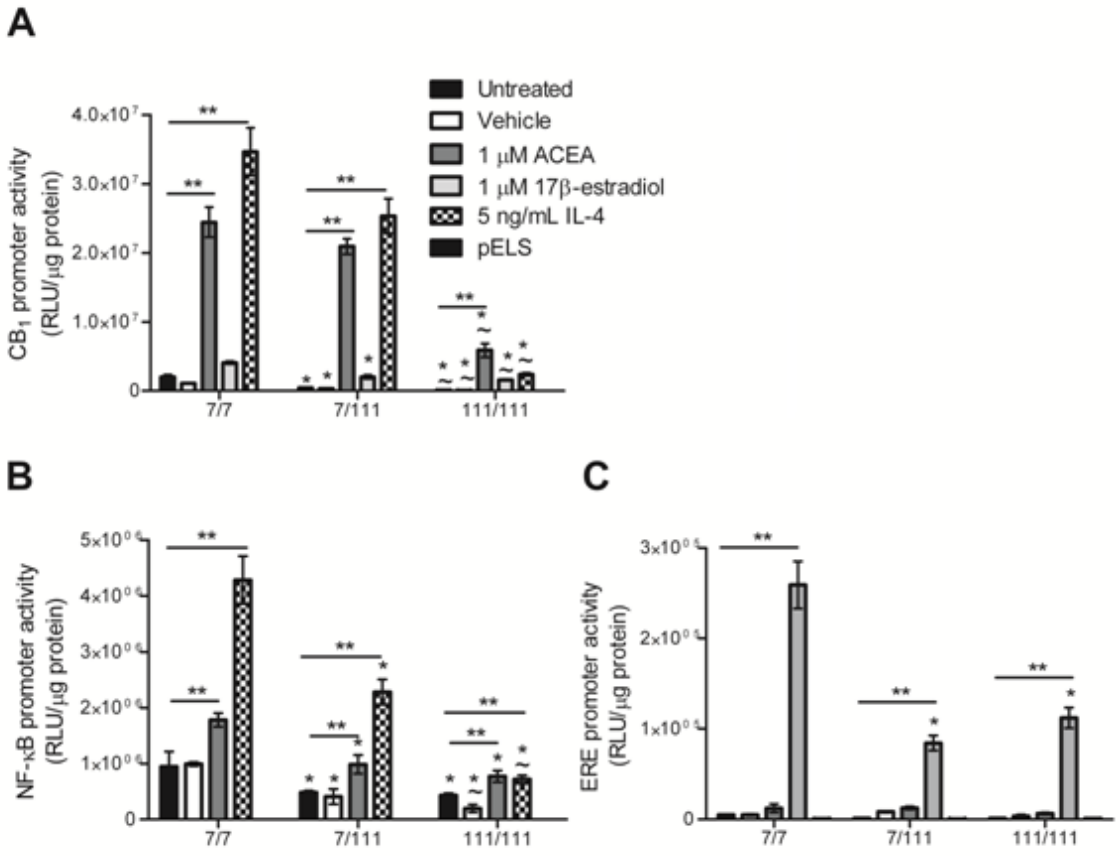

Figure 32. CB_1 receptor agonism induced CB_1 promoter activity *via* NF-κB-dependent signalling. 7/7, 7/111 and 111/111cells were co-transfected with pCNR1, driving *Renilla* luciferase expression, and pNF or pERE, driving firefly luciferase expression, or empty vector control. A) pCNR1 promoter activity was lower in the presence of mHtt and induced by 1 μM ACEA or 5 ng/mL IL-4, but not 1 μM 17β-estradiol. The induced level of pCNR1 activity was attenuated in the presence of mHtt. B) pNF promoter activity was lower in the presence of mHtt and induced by 1 μM ACEA or 5 ng/mL IL-4, but not 1 μM 17β-estradiol. The induced level of pNF activity was attenuated in the presence of mHtt. C) pERE promoter activity was not different in 7/7, 7/111, or 111/111 cells that were untreated, vehicle-treated, or 1 μM ACEA-treated. pERE promoter activity was induced following 1 μM 17β-estradiol treatment and this higher pERE activity was attenuated in the presence of mHtt. Significance was determined *via* two-way ANOVA for cell type and treatment followed by *post-hoc* Tukey's test. ** $P < 0.05$ between treatment groups within genotype, * $P < 0.05$ within treatment relative to 7/7, ~ $P < 0.05$ within treatment relative to 7/111, $n = 8$.

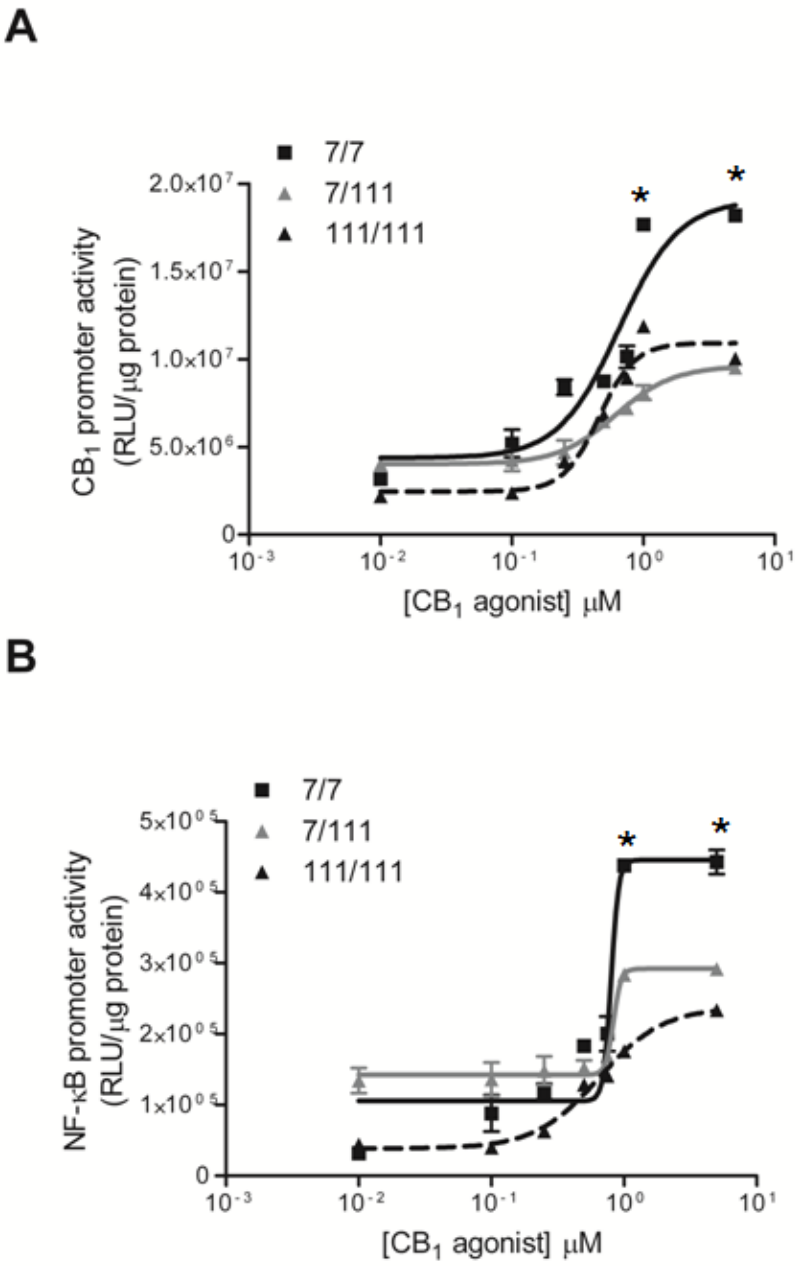

Figure 33. CB_1 receptor agonism induced CB_1 and NF-κB promoter activity in a dose-dependent manner. 7/7, 7/111 and 111/111cells were co-transfected with pCNR1, driving *Renilla* luciferase expression, and pNF, driving firefly luciferase expression. A) pCNR1 promoter activity was induced by ACEA in a dose-dependent manner that was attenuated by mHtt. B) pNF promoter activity was induced by ACEA in a dose-dependent manner that was attenuated by mHtt. Significance was determined *via* one-way ANOVA within dose followed by *post-hoc* Tukey's test. * $P < 0.01$ within treatment relative to 7/111 and 111/111, $n = 8$.

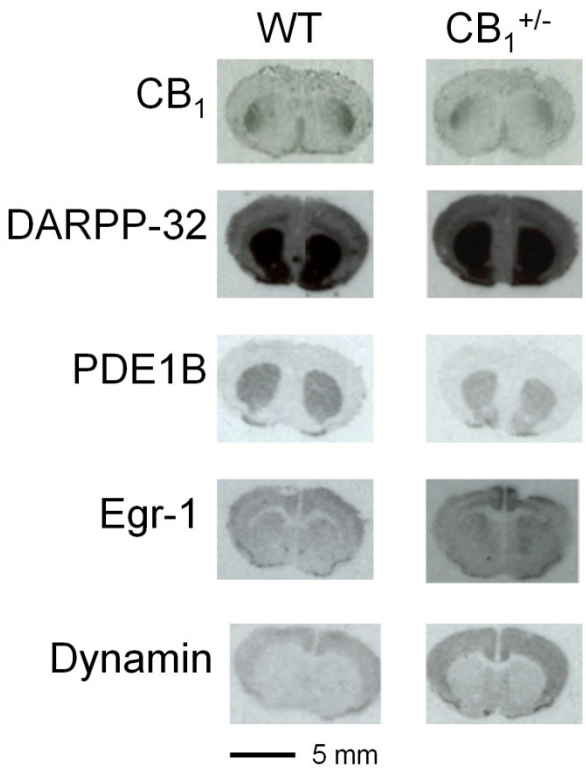

Figure 34. PDE1B, Egr-1 and Dynamin mRNA levels were altered in heterozygous CB_1 knock-out mice ($CB_1^{+/-}$). $CB_1^{+/-}$ mice expressed 50% less CB_1 mRNA than WT litter-mates. Altered CB_1 levels changed the mRNA abundance of some, but not all, genes dysregulated in HD. These are representative coronal sections derived from WT and $CB_1^{+/-}$ mice used for *in situ* hybridization. The probes used are indicated to the left.

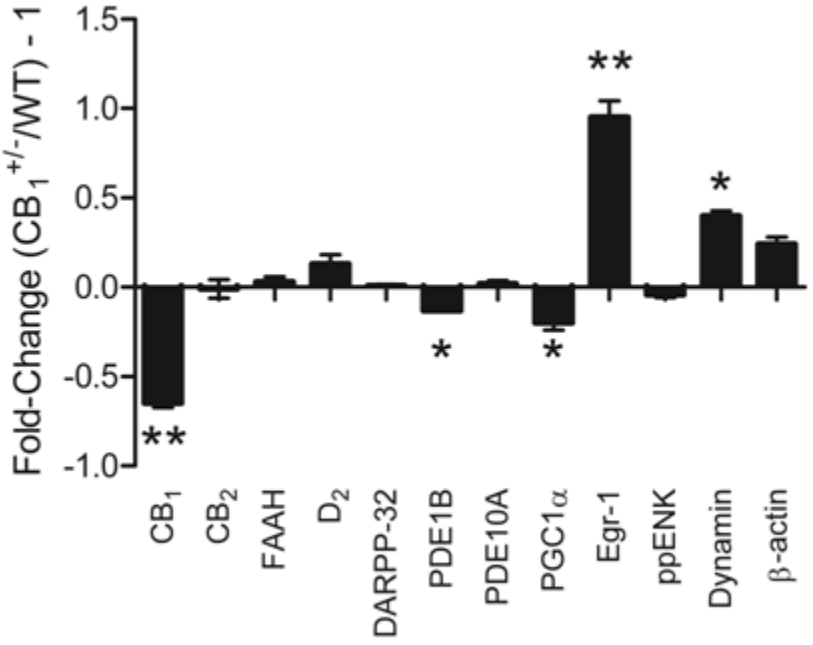

Figure 35. A 50% decrease in CB_1 mRNA altered gene expression but did not recapitulate HD transcriptional dysregulation. OD measurements were collected using Kodak 3D imaging software. Local background was subtracted from each measurement to correct for background variability. This graph presents the fold-change for mRNA hybridization in $CB_1^{+/-}$ relative to WT ($CB_1^{+/-}$/WT). Significance was determined *via* two-tailed Student's *t*-test. * $P < 0.01$, ** $P < 0.001$, n =3.

3.10 Cannabinoid Agonism Improved Cell Functionality and Viability

We wanted to determine if 7/111 and 111/111 cells expressing mHtt were phenotypically distinct from 7/7 cells in terms of their general viability, and whether deficits in cellular viability could be reversed following ACEA treatment. We analyzed the proportion of viable 7/7, 7/111, and 111/11 cells using the Cell Viability kit® (Invitrogen) to quantify and visualize esterase activity and membrane permeability in cells that were untreated, vehicle-treated, or treated with 1 μM ACEA. The cell-permeable dye CalAM is taken up by viable cells and hydrolyzed by esterases to produce green fluorescence. EthD-1 is taken up by cells with compromised membranes. When EthD-1 enters cells, it intercalates with DNA and fluoresces red. The proportion of fluorescent cells and the relative intensity of fluorescence were quantified *via* a plate reader and visualized by fluorescent microscopy, respectively. We found that esterase activity was reduced in 111/111 cells (n = 32; $P < 0.05$, Fig. 36A). The percentage of cells exhibiting EthD-1 intercalation was greater in the presence of mHtt. EthD-1 intercalation was exacerbated by vehicle treatment (n = 32; $P < 0.05$, Fig. 36C). Esterase activity was elevated, although not to levels observed in 7/7 cells, by 1 μM ACEA in 111/111 cells, relative to vehicle treatment (n = 32; $P < 0.05$, Fig. 36B). One micromolar ACEA lowered EthD-1 intercalation, relative to vehicle treatment, to levels similar to untreated cells. However, EthD-1 intercalation was higher in ACEA-treated 7/111 and 111/111 cells than in 7/7 cells (n = 32; $P < 0.05$, Fig. 36D). These quantified data were visually confirmed by fluorescence microscopy (Fig. 37). ACEA treatment visually elevated CalAM staining and reduced EthD-1 intercalation in 7/7, 7/111, and 111/111 cells, relative to vehicle treatment. From these data we concluded that cannabinoid treatment had a beneficial effect on cell viability in 7/111 and 111/111 cells.

HD progression is associated with cellular energy deficit, as demonstrated in MSNs in mouse models of HD and in 7/111 and 111/111 cells (Trettel *et al*., 2000; Cui *et al*., 2006). Specifically, there are deficits in mitochondrial biogenesis, and a reduced ATP/ADP ratio (Gines *et al*., 2003). We wanted to determine whether cannabinoid treatment could improve cellular ATP levels. We quantified ATP concentration in 7/7, 7/111, and 111/111 cells using the CellTiter-Glo® assay (Promega). This assay is based on the conversion of luciferin to oxyluciferin catalyzed by firefly luciferase and dependent on cellular ATP, which is the limiting reagent necessary for the reaction. We found that ATP concentration was reduced in 7/111 and 111/111 cells relative to 7/7 cells in both untreated and vehicle-treated cells (n = 32; $P < 0.05$, Fig. 38A). Following 3 or 24 h of treatment with 1 μM ACEA, ATP concentration was higher in all cell types relative to vehicle control (n = 32; $P < 0.05$, Fig. 38B; 3 h data not shown). ACEA-dependent increases in ATP were attenuated in the presence of mHtt, yet ATP concentration was still greater in cannabinoid-treated 7/111 and 111/111 cells, which suggested improved cellular function following cannabinoid treatment.

Levels of BDNF-2, PGC1α, and DARPP-32 mRNA are, like CB_1, dysregulated early in HD progression (Zuccato *et al*., 2005; Cui *et al*., 2006; Gomez *et al*., 2006). Decreased expression of these genes is thought to contribute to HD pathogenesis *via* neuronal degeneration and mitochondrial dysfunction (Zuccato *et al*., 2005; Cui *et al*., 2006; Gomez *et al*., 2006). In $CB_1^{+/-}$ mice, PGC1α mRNA levels were lower, while DARPP-32 mRNA levels remained unchanged, which suggested that PGC1α levels may have been influenced by CB_1 levels but that DARPP-32 levels were not. Decreased BDNF-2 expression has previously been observed with decreased CB_1 expression (De Chiara *et al*., 2010). We quantified the levels of these transcripts in cells that were untreated, vehicle-treated or treated with 0.01, 0.10, 0.25, 0.50, 0.75, 1.00, and

5.00 μM ACEA for 18 h. We found that BDNF-2 mRNA levels were reduced by mHtt in untreated and vehicle treated cells (n = 12; $P < 0.05$, Fig. 39A). ACEA treatment was associated with elevated BDNF-2 mRNA levels in 7/7 cells (n = 12; $P < 0.05$, Fig. 40A). The EC_{50} for this dose-response relationship was 0.42 μM. ACEA induced BDNF-2 expression in 111/111 cells as well, but the maximal response was less than observed in 7/7 cells (n = 12; $P < 0.05$, Fig. 40A). The EC_{50} for the dose-response relationship in 111/111 cells was 0.38 μM. Only a modest dose-response relationship was observed in 7/111 cells treated with ACEA. Despite this unexpected result, ACEA treatment was associated with a modest induction of BDNF-2 in cells expressing mHtt. It is important to note that the maximal induction, even in 7/111 cells, exceeded BDNF-2 levels measured in untreated 7/7 cells. Therefore, a relative increase of BDNF-2 mRNA abundance to levels observed in 7/7 cells was achieved in 7/111 and 111/111 cells expressing mHtt treated with ACEA.

Next, we measured PGC1α mRNA levels in 7/7, 7/111, and 111/111 cells. PGC1α mRNA levels were reduced in untreated and vehicle-treated 7/111 and 111/111 cells relative to 7/7 cells (n = 12; $P < 0.05$, Fig. 39B). Additionally, vehicle treatment reduced PGC1α levels in 7/7 cells relative to untreated cells (n = 12; $P < 0.05$). PGC1α mRNA abundance was elevated, in an ACEA dose-dependent manner, in all cell types (Fig. 40B). The EC_{50} values for these dose-response relationships were 0.32, 0.56, and 0.79 μM for 7/7, 7/111, and 111/111 cells, respectively. The E_{max} values were 0.39, 0.33, and 0.24 (PGC1α/β-actin) for 7/7, 7/111, and 111/111 cells respectively (Fig. 40B). The shallow dose-response relationship between ACEA dose and PGC1α level, as well as the change in EC_{50} and E_{max} for these dose-response relationships in the presence of mHtt, suggested that PGC1α levels may not be induced by the same mechanism as CB_1, or may be downstream of CB_1 induction. In terms of biological

significance, ACEA treatment was associated with an increase in PGC1α mRNA abundance in the presence of mHtt equal to, or greater than, was observed in untreated 7/7 cells.

Finally, we measured DARPP-32 mRNA levels in 7/7, 7/111, and 111/111 cells. DARPP-32 mRNA expression was reduced in untreated and vehicle-treated 7/111 and 111/111 cells relative to 7/7 cells ($n = 12$; $P < 0.05$, Fig. 39C). Unlike BDNF-2 and PGC1α, DARPP-32 mRNA levels were not altered by ACEA treatment ($n = 12$, data not shown). DARPP-32 mRNA levels were unchanged in the striatum of $CB_1^{+/-}$ mice compared to wild-type mice (Fig. 35). The unresponsiveness of DARPP-32 mRNA levels to ACEA and the observation that DARPP-32 mRNA levels were unchanged in $CB_1^{+/-}$ mice suggested that DARPP-32 was not regulated by CB_1 receptors. In the context of HD this implies that cannabinoid treatment was capable of restoring the expression of some, but not all, of the subset of genes repressed in the presence of mHtt.

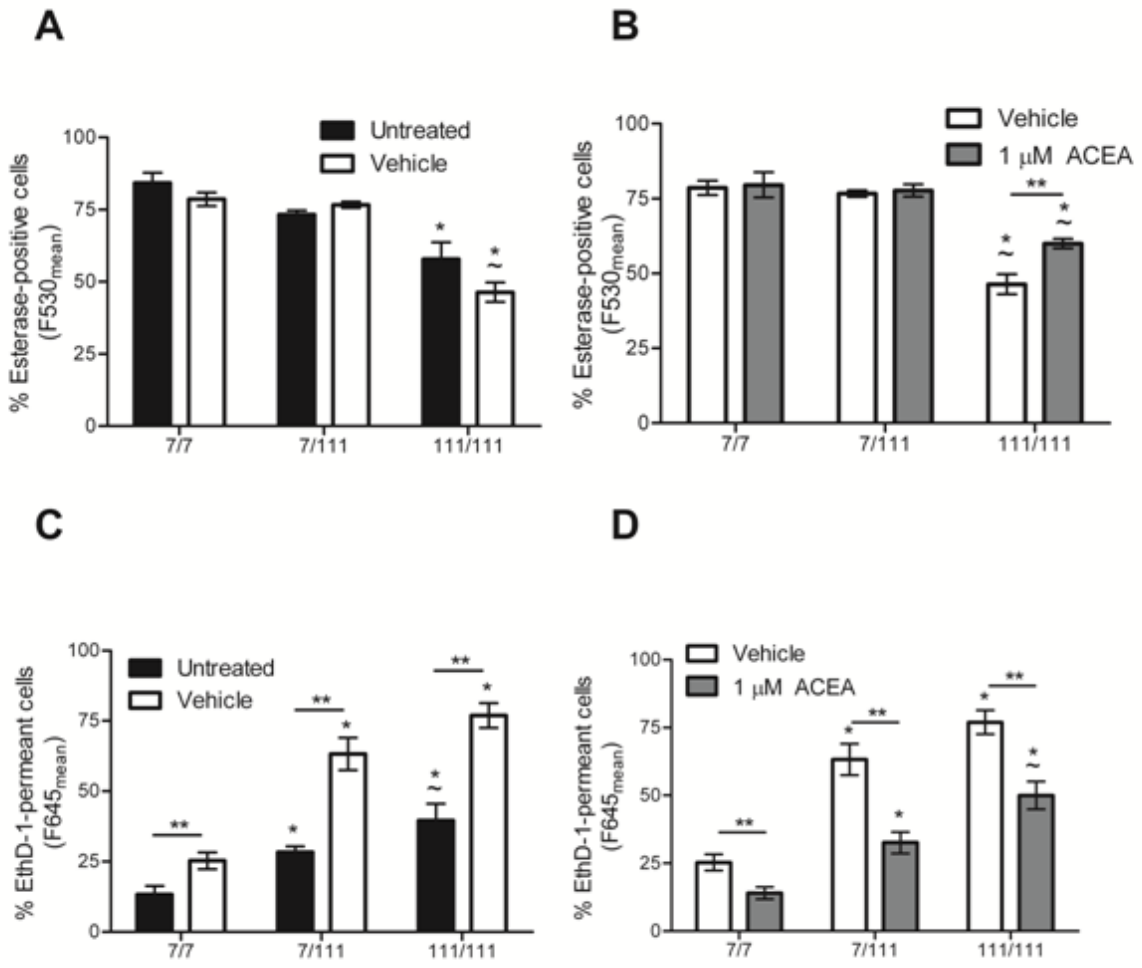

Figure 36. Cell viability was reduced in mHtt-expressing cells and improved following cannabinoid treatment. Cell viability was measured by two methods: esterase activity *via* CalAM fluorescence and membrane permeability *via* EthD-1 fluorescence. A) Esterase activity was lower in the presence of mHtt. B) 1 μM ACEA treatment was associated with higher esterase activity in 111/111 cells compared to vehicle control. C) EthD-1 intercalation was higher in the presence of mHtt and augmented by vehicle treatment. D) 1 μM ACEA reduced EthD-1 intercalation relative to vehicle control in all cell types. Significance was determined *via* two-way ANOVA for cell genotype and treatment followed by *post-hoc* Tukey's test. ** $P < 0.05$ between treatments within genotype, * $P < 0.05$ relative to 7/7 within treatment, ~ $P < 0.05$ relative to 7/111 within treatment, $n = 32$.

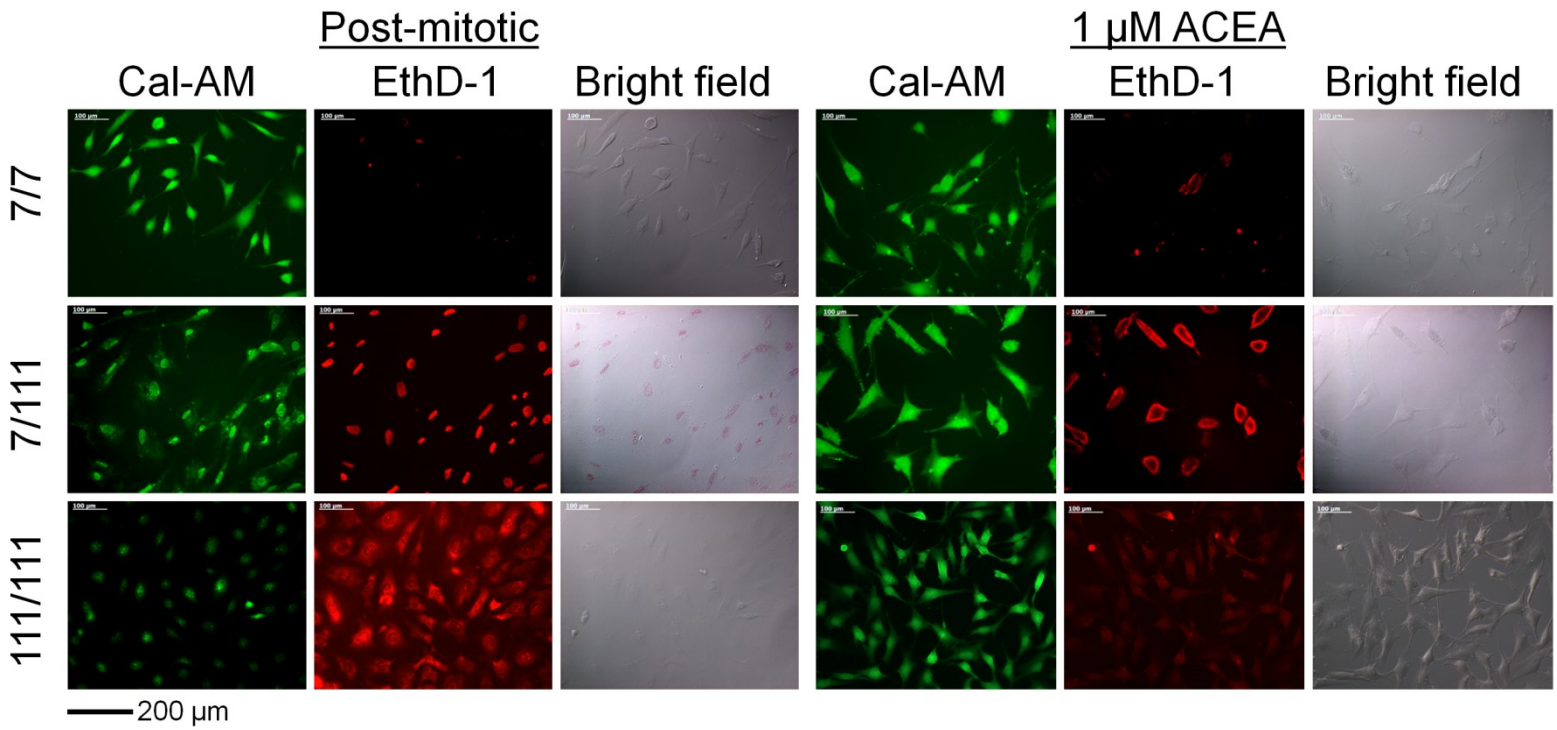

Figure 37. Cell viability was visually lower in the presence of mHtt and higher in cells treated with cannabinoids. Cell viability was measured by two methods: esterase activity *via* CalAM fluorescence and EthD-1 permeability and fluorescence. These representative images depict the effect described and quantified in figure 36.

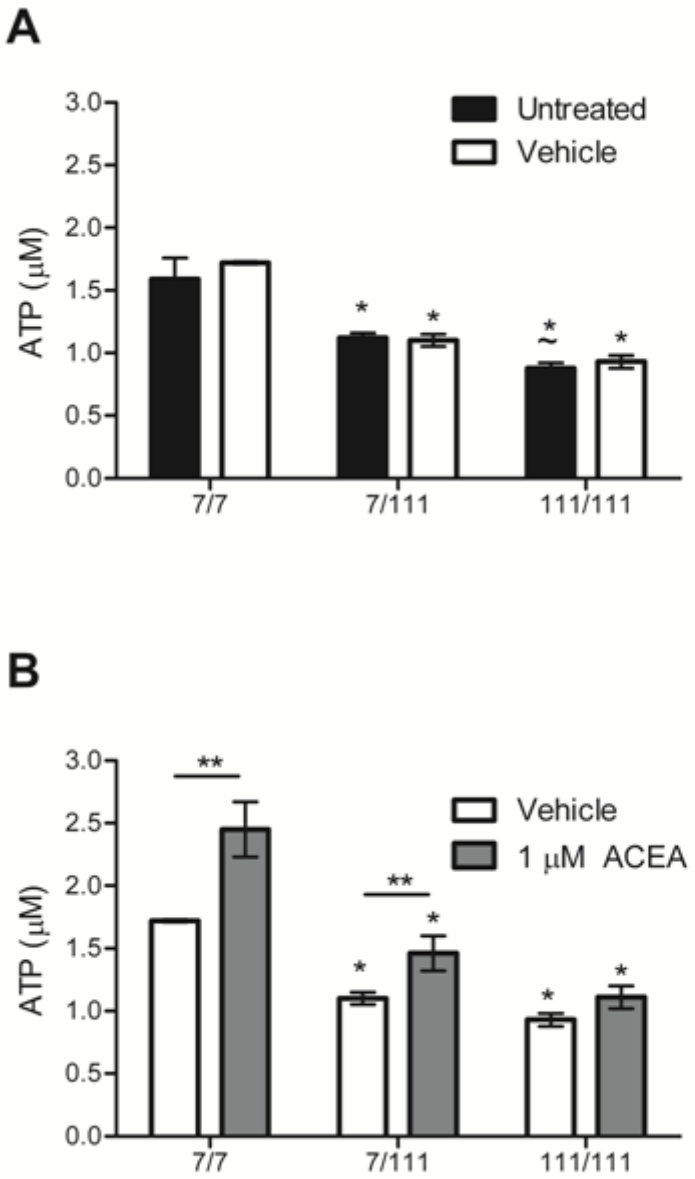

Figure 38. ATP concentration was lower in the presence of mHtt and higher following cannabinoid treatment. ATP concentration was measured using the CellTiter-Glo® assay. A) ATP concentration was lower in 7/111 and 111/111 cells compared to 7/7 cells. B) 1 μM ACEA treatment was associated with higher ATP concentration in 7/7 and 7/111 cells compared to vehicle control. Significance was determined *via* two-way ANOVA for cell genotype and treatment followed by *post-hoc* Tukey's test. ** $P < 0.05$ between treatments within genotype, * $P < 0.05$ relative to 7/7 within treatment, ~ $P < 0.05$ relative to 7/111 within treatment, $n = 32$.

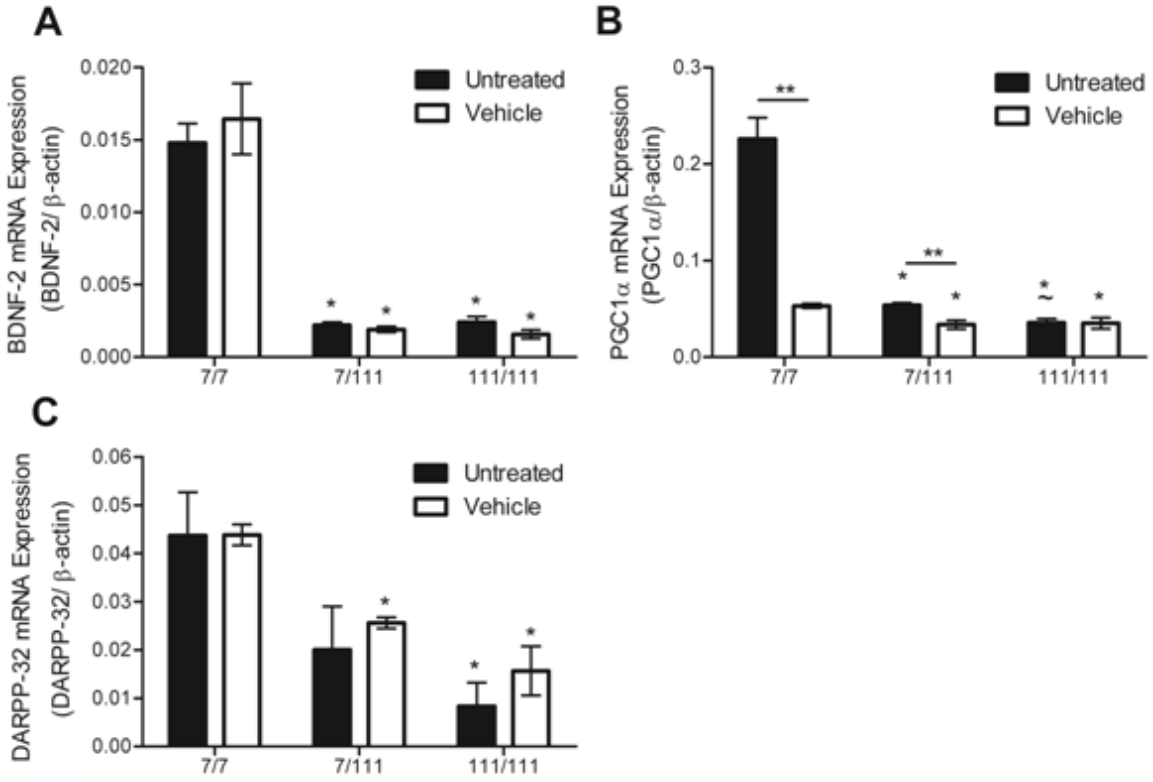

Figure 39. BDNF-2, PGC1α, and DARPP-32 mRNA levels were lower in mHtt-expressing 7/111 and 111/111 cells. BDNF-2, PGC1α, and DARPP-32 mRNA abundance was quantified by qRT-PCR and normalized to β-actin mRNA levels. A) BDNF-2 mRNA levels were lower in the presence of mHtt. B) PGC1α mRNA levels were lower in the presence of mHtt and further reduced by vehicle treatment. C) DARPP-32 mRNA levels were lower in the presence of mHtt. Significance was determined *via* two-way ANOVA for cell genotype and treatment followed by *post-hoc* Tukey's test. ** $P < 0.05$ between treatments within genotype, * $P < 0.05$ relative to 7/7 within treatment, ~ $P < 0.05$ relative to 7/111 within treatment, $n = 12$.

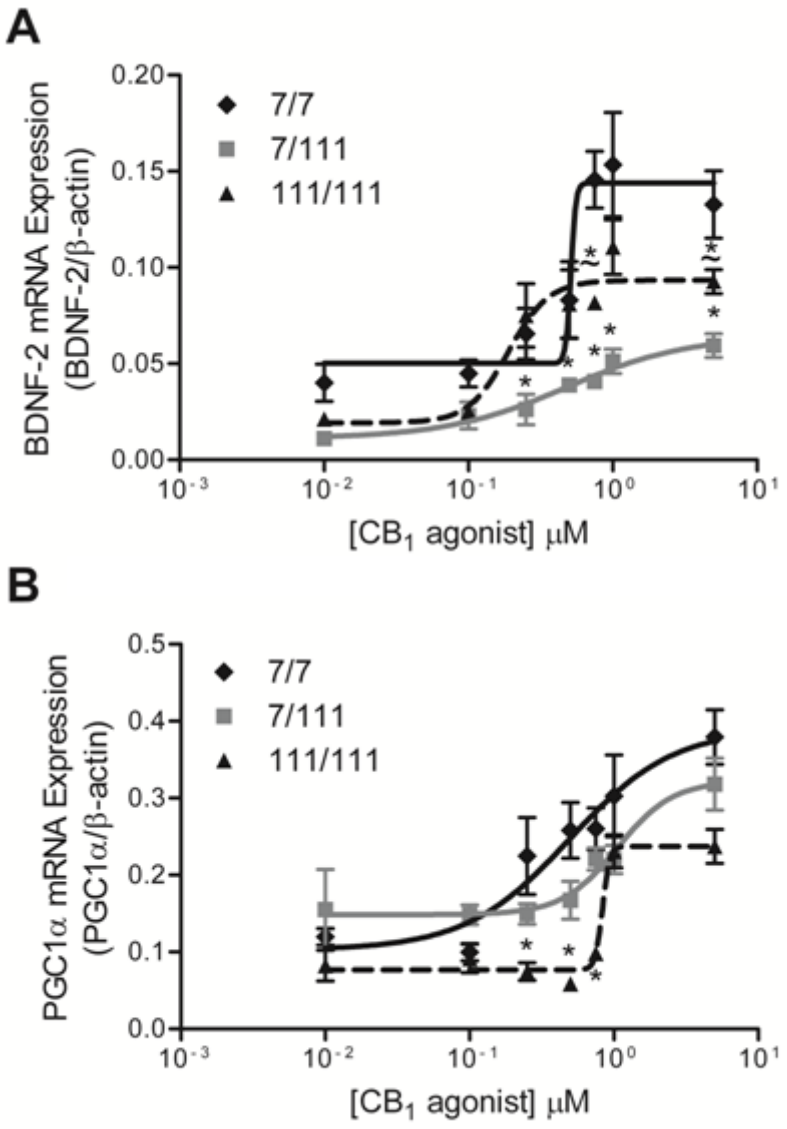

Figure 40. BDNF-2 and PGC1α mRNA levels were increased in an ACEA dose-dependent manner in the presence of mHtt. BDNF-2, and PGC1α mRNA abundance was quantified by qRT-PCR and normalized to β-actin mRNA levels. A) BDNF-2 mRNA levels were increased in an ACEA dose-dependent manner and this effect was attenuated in the presence of mHtt. B) PGC1α mRNA levels were increased in an ACEA dose-dependent manner and this effect was attenuated in the presence of mHtt. Significance was determined *via* one-way ANOVA for ACEA dose followed by *post-hoc* Tukey's test. * $P < 0.05$ relative to 7/7 within treatment, ~ $P < 0.05$ relative to 7/111 within treatment, $n = 12$.

CHAPTER 4

Discussion

4.1 Hypotheses of this Research

We hypothesized that the ECS was dysregulated during HD progression, that treatment of striatal neurons with cannabinoids would induce expression of CB_1, and that, in cells expressing mHtt, increased CB_1 levels would be associated with improved cellular function.

4.2 The Endocannabinoid System was Dysregulated During HD Progression

Prior research concerning repression of CB_1 expression during HD pathogenesis has focused on mRNA and protein abundance in the whole brain (Luthi-Carter *et al*., 2000), GABA-ergic MSNs of the lateral striatum (Denovan-Wright & Robertson, 2000; Blazquez *et al*., 2011; Chiodi *et al.,* 2012), and in cell culture models of HD (Scotter *et al.,* 2010; Blazquez *et al*., 2011). Expression of mHtt is associated with an approximately 50% decrease in CB_1 mRNA expression prior to, or early in, HD symptom onset in all human samples, animal and cell culture models tested to date (reviewed in Pazos *et al*., 2008). Here, we found that CB_1 mRNA levels declined, as part of the normal aging process, in all regions of the striatum of wild-type mice. CB_1 mRNA levels were repressed early in HD progression in HD mice relative to age-matched wild-type mice in all regions of the striatum and in the cortex. Therefore, striatal CB_1 levels declined with age and this decline was exacerbated in the presence of mHtt. Steady-state CB_1 mRNA levels have been shown to decline in the dorso-lateral prefrontal cortex of humans and non-human primates (Eggan *et al*., 2010), the visual cortex of humans (Vitalis *et al*., 2008), and the hippocampus and lateral striatum of mice (NCBI, 2011) as part of the aging process. Neurodegeneration during HD is most pronounced in striatal MSNs, but cortical atrophy also occurs at late stages of HD progression (Vonsattel *et al*., 1985). The mHtt-dependent repression

of CB_1 below wild-type levels in three regions of the striatum and cortical neurons observed here demonstrated that mHtt dysregulated CB_1 expression in two regions of the brain particularly sensitive to mHtt. Because CB_1 levels were decreased early in HD progression in both R6/1 and R6/2 HD mouse models this change was likely a direct consequence of mHtt expression and not a compensatory response to other cellular changes. The early decrease in CB_1 abundance may contribute to other pathogenic changes observed to HD pathogenesis. Mievis *et al*. (2011) found that HD94 tetracycline-inducible HD mice that lacked a full complement of CB_1 ($Htt^{+/+}$/mHtt *x* $CB_1^{+/-}$) exhibited reduced motor coordination and greater striatal atrophy than HD/$CB_1^{+/+}$ mice. We concluded that CB_1 mRNA expression was repressed in the presence of mHtt in a tissue-specific manner in two regions of the brain – the cortex and striatum.

FAAH is the major catabolic enzyme of the ECS. Blazquez *et al*. (2011) found that FAAH mRNA and protein levels are higher in the lateral striatum of late-stage R6/1 HD mice compared to age-matched wild-type controls. Further, FAAH protein levels are higher in the lateral striatum of grade 3 and 4 HD patients compared to age-matched, healthy controls (Blazquez *et al*., 2011). Thus, FAAH expression may change late in the striatum during HD, yet FAAH is more abundant in the cortex than striatum (NCBI, 2011) and cortical neurons expressing FAAH regulate cannabinoid tone within the striatum (Fig. 1). We found that FAAH mRNA levels were higher in late-stage R6/1 mice and at all stages of development in R6/2 mice compared to age-matched wild-type controls. This observation provides evidence for altered endocannabinoid tone during HD progression. Indeed, levels of AEA are lower in the cortex, hippocampus, and striatum of 12 week-old (early symptomatic) R6/1 mice compared to wild-type littermates (Dowie *et al*., 2009). If cannabinoid levels regulate CB_1 expression, these changes may also alter CB_1 levels in the presence of mHtt.

CB_2 mRNA levels are elevated in multiple sclerosis, ischemic stroke, Parkinson's disease, and Alzheimer's disease (Pini *et al*., 2012). We hypothesized that CB_2 mRNA levels would be higher in late-stage HD mice than age-matched wild-type littermates because striatal inflammation would induce CB_2 expression and that was what we observed in R6/2 mice. Induction of CB_2 during late-stage HD pathogenesis may be due to inflammation and altered endocannabinoid tone. Altered CB_2 expression was probably not a direct consequence of mHtt because we observed this change late in HD progression in R6/2 mice. It remains unclear whether CB_2 induction was specific to glia or neurons.

4.3 CB_1 mRNA Abundance and Distribution were Developmental Stage-specific

We had shown that the ECS was dysregulated during HD pathogenesis, but did mHtt alter CB_1 expression early in development? We found that CB_1 mRNA abundance and distribution were similar in wild-type and R6/2 mice at P1. At P1, CB_1 mRNA levels were highest in the cortex and inferior cerebellum. In dividing ST*Hdh* cells, which exist in an embryonic, striatal precursor state, CB_1 mRNA levels were low and expression was not altered by mHtt. In contrast, wild-type, 'adult' striatal neurons expressed CB_1 at higher levels than other regions of the brain and CB_1 expression was higher in post-mitotic ST*Hdh* cells that model adult MSNs compared to dividing ST*Hdh* cells. The observations we made in P1 and adult mice, and dividing and post-mitotic ST*Hdh* cells, prompted us to conclude that CB_1 levels are increased in the striatum as MSNs mature. It is in mature, adult MSNs that specific factors facilitate a relatively high steady-state level of CB_1 expression. Further, it is this high level of CB_1 expression that is repressed by mHtt. CB_1 mRNA abundance has been shown to fluctuate in the human visual cortex such that levels increase and reach a plateau at 1 year, then increase further during puberty, and subsequently decline over the lifespan (Vitalis *et al*., 2008). Similar

fluctuations in CB_1 expression during development have been observed in the *Maccaca mulatta* dorso-lateral prefrontal cortex (Eggan *et al*., 2010). CB_1 levels are also high in rat white matter from embryonic day 14 until P1, after which CB_1 is undetectable (Eggan *et al*., 2010). These findings, as well as our own, demonstrate that CB_1 expression is tissue- and developmental stage-specific. Going forward, we chose to focus on post-mitotic 7/7, 7/111, and 111/111 cells that modelled adult MSNs with high CB_1 expression that was repressed in the presence of mHtt.

4.4 Cannabinoid Treatment Induced CB_1 Expression in the Presence of mHtt

4.4.1 Cannabinoid Treatment was Associated with Elevated CB_1 Promoter Activity, mRNA and Protein Levels

We found that treatment of post-mitotic 7/7, 7/111, and 111/111 cells with direct CB_1 agonists (ACEA, mAEA, AEA) or indirect CB_1 agonists (URB-597) induced CB_1 promoter activity and mRNA expression and elevated CB_1 receptor levels. Cannabinoid treatment has been shown to induce CB_1 mRNA expression in primary hepatocytes (Mukhopadhyay *et al*., 2008), Jurkat and primary T cells (Borner *et al*., 2007a), and colorectcal carcinoma cells (Proto *et al.*, 2011), but this is the first observation of cannabinoid-dependent CB_1 mRNA induction in neuronal cells. ACEA is a potent and selective CB_1 receptor agonist (Pertwee *et al.*, 2010) that was chosen to ensure that a response would be observed if indeed cannabinoid agonism could affect CB_1 expression. URB-597, in contrast, is an indirect cannabinoid agonist that inhibits FAAH and thus increases cannabinoid tone (Pertwee *et al*., 1999; Pertwee *et al*., 2010). The observation that URB-597 induced CB_1 expression suggested this response was relatively sensitive to fluctuations in cannabinoid tone. This result is promising because treatment with potent CB_1 agonists is associated with reduced seizure threshold and hypothermia in animal models of HD (Dowie *et al.*, 2009), while treatment with endogenous or indirect cannabinoid

agonists is associated with improved cell viability and improved motor coordination in models of HD (Scotter *et al*., 2010; Dowie *et al*., 2009).

The magnitude of cannabinoid-mediated CB_1 induction was attenuated in the presence of mHtt. However, the fold-induction of response was not different in 7/7, 7/111, or 111/111 cells, which suggested that mHtt non-competitively inhibited cannabinoid-dependent induction of CB_1 expression. mHtt is known to inhibit transcription of genes by interacting with, and squelching the activity of, many gene-specific co-activators of transcription (Cui *et al*., 2006). mHtt has been shown to repress CB_1 at the level of transcription because the number of primary CB_1 mRNA transcripts is reduced in the presence of mHtt (McCaw *et al*., 2004). Based on this evidence we hypothesized that, in 7/111 and 111/111 cells, mHtt repressed CB_1 promoter activity not CB_1 receptor activity, thereby non-competitively inhibiting cannabinoid-mediated CB_1 mRNA induction.

We also found that ACEA treatment elevated CB_1 protein abundance in 7/7, 7/111, and 111/111 cells and the magnitude of this effect was attenuated in the presence of mHtt. Cannabinoid treatment is associated with a modest increase (3 – 5-fold) in CB_1 protein levels in cultured hepatocytes (Mukhopadhyay *et al*., 2008). Here, CB_1 mRNA levels were induced 4 – 5-fold, and protein levels were induced approximately 2-fold, following cannabinoid treatment. We concluded from this that cannabinoid-mediated CB_1 mRNA induction translated to an increase in CB_1 protein.

4.4.2 CB_1 ReceptorLocalization was Altered in the Presence of mHtt

While examining CB_1 protein abundance following cannabinoid treatment we asked whether cannabinoid treatment altered the localization and trafficking of CB_1 receptors. Using an in- and on-cell western approach, we found that CB_1 receptors were more abundant on the

plasma membrane of 7/111 and 111/111 cells than 7/7 cells. This may have been because the total pool of receptors was lower and therefore the relative fraction of receptors at the plasma membrane appeared higher in the presence of mHtt. Alternatively, CB_1 receptor trafficking and internalization may depend on wild-type Htt protein, which may facilitate receptor trafficking in dendrites and axons (Marcora *et al*., 2010), and was therefore impaired in mHtt-expressing cells in a mHtt dose-dependent manner (Zuccato *et al*., 2008). We explored this observation further using confocal microscopy and found that CB_1 receptors were internalized in respone to ACEA and trafficked to the plasma membrane in response to O-2050 (CB_1 antagonist) in 7/7, 7/111, and 111/111 cells. Therefore, CB_1 receptor trafficking to and from the plasma membrane was not impaired in mHtt-expressing cells. We also observed CB_1 receptors within the nucleus of vehicle- and ACEA-treated 7/7 cells and ACEA-treated 7/111 cells. Our interpretation of these data was that CB_1 receptors were normally present in the nucleus and could be trafficked there in 7/111 cells, but not 111/111 cells, following ACEA treatment. CB_1 receptors have been observed in the nucleus and nuclear membrane of astrocytes and are actively trafficked along actin filaments following cannabinoid treatment (Osborne *et al.,* 2009). Given the lipophillic nature of cannabinoid ligands, the nuclear localization of CB_1 may play an important regulatory role in the signal transduction mediated by these receptors (Osborne *et al*., 2009). In 7/111 and 111/111 cells this trafficking was impaired, which may have resulted from lost wild-type function (Zucatto *et al*., 2008; Marcora *et al*., 2010) because CB_1 receptors were still localized to the nucleus following cannabinoid treatment in heterozygous 7/111 cells. Importantly, these data affirmed our earlier findings that cannabinoids increased CB_1 levels and the magnitude of this increase was lower in the presence of mHtt.

4.4.3 Cannabinoid Treatment Induced CB_1 Expression *Via* Functional CB_1 Receptors

We wanted to determine how cannabinoid agonists induced CB_1 mRNA expression in 7/7, 7/111, and 111/111 cells. We found that CB_1 mRNA abundance was induced in a cannabinoid agonist dose-dependent manner in 7/7 cells treated with ACEA, mAEA, or AEA. The EC_{50} and E_{max} values were not different for the dose-response curves observed for each drug. We also observed that simultaneous treatment with the cannabinoid antagonist O-2050 resulted in an antagonist dose-dependent shift of the dose-response curve to the right. ACEA and mAEA are potent, CB_1-selective, synthetic cannabinoids (Pertwee *et al*., 2010), while AEA is a less potent, less selective, endogenous cannabinoid (reviewed in Howlett *et al*., 1999). The observation that the responses to the three agonists were not different affirmed our hypothesis that cannabinoid-mediated CB_1 mRNA induction was relatively sensitive to fluctuating endocannabinoid tone. Further, the antagonist-dependent shift of the dose-response curve demonstrated the cannabinoid-mediated CB_1 mRNA induction required the activation of functional CB_1 receptors. Mukhopadhyay *et al*. (2008) demonstrated that CB_1 mRNA induction was mediated *via* CB_1 receptors in mouse primary hepatocytes because induction was blocked following treatment with the CB_1-selective inverse agonist AM-281. Similarly, Proto *et al*. (2011) demonstrated cannabinoid-dependent CB_1 mRNA induction occurs through activated CB_1 by blocking these receptors with SR141716 (rimonabant). In contrast, Borner *et al*. (2007a) demonstrated that cannabinoids mediate induction of CB_1 *via* CB_2 receptors, which are activated by JWH-018 and inhibited by AM-630. Here, we demonstrated that CB_1, not CB_2, receptor activation induced CB_1 mRNA expression. To our knowledge, this is the first dose-dependent pharmacological characterization of this phenomenon.

We went on to demonstrate that mHtt non-competitively inhibited cannabinoid-mediated CB_1 mRNA induction because the EC_{50} of the dose-response curve was not different in 7/7, 7/111, and 111/111 cells and the E_{max} was reduced by approximately 50% in 7/111 and 111/111 cells. mHtt dysregulates transcription at many genes *via* interactions with co-activators of transcription (Gafni & Ellerby, 2002). Eukaryotic gene expression is regulated in a combinatorial manner that is dependent upon the activity and localization of multiple proteins. The probability that mHtt represses transcription of a gene depends on the number of mHtt-interacting proteins that regulate that gene and their localization to, or away from, that gene's promoter (Hogel, 2011). Here, steady-state CB_1 mRNA levels were repressed in the presence of mHtt and this repression remained in cells treated with cannabinoid agonists. The maximal cannabinoid-mediated induction of CB_1 expression may have been lower in mHtt-expressing cells because the steady-state level of expression was repressed while the inducibility (*i.e.*fold-induction) was not affected.

We also examined the temporal nature of cannabinoid-mediated CB_1 induction and found that CB_1 mRNA abundance rose within 30 min of cannabinoid treatment, and continued to rise until 18 h post-treatment, after which CB_1 mRNA levels began to decline. The half-life of ACEA in cell culture is approximately 18 h (Pertwee *et al*., 1999). Thus, we propose that ACEA treatment produced a rapid increase in CB_1 expression, new CB_1 receptors were synthesized, and these new CB_1 receptors were activated by remaining ACEA to further increase CB_1 expression. Based on the reported half-life of 18 h for ACEA (Petwee *et al*., 1999), ACEA concentration would have decreased by 50% at 18 h, which was the time that induction of CB_1 expression began to wane. During the period of time that we monitored CB_1 mRNA expression, our data do not indicate that negative feed-back or receptor desensitization, resulting in a decreased response

to ACEA, occurred. If cannabinoid tone regulates CB_1 level *in vivo*, then the response of CB_1 levels to acute or chronic treatments may be highly dependent upon the potency and half-life of the cannabinoid and the frequency of treatment (Pacheco *et al*., 2009; Dowie *et al*., 2009).

4.4.4 CB_1 Promoter Activity was Induced by Akt-dependent Activation of NF-κB

We found that cannabinoid treatment produced a dose-dependent increase in pERK2(Y204) in 7/7 cells but this response was attenuated in the presence of mHtt. Cannabinoid treatment also produced a dose-dependent increase in pAkt(S473) and this response was not changed in the presence of mHtt. ERK1/2-mediated signal transduction is inhibited in PC12 cells expressing mHtt and in YAC128 HD mice (Dowie *et al*., 2009; Marcora *et al*., 2010). Akt-mediated signal transduction, however, is unaffected by mHtt (Dowie *et al*., 2009). The cannabinoid-dose-pERK2(Y204)-response curves and cannabinoid-dose CB_1 mRNA-response curves did not resemble each other (Fig. 30 & 31). pERK(Y204) induction was attenuated in cells expressing one copy of mHtt (7/111) and further attenuated in cells expressing two copies of mHtt (111/111), whereas CB_1 mRNA induction by cannabinoids was attenuated to the same extent in 7/111 and 111/111 cells. If pERK2(Y204) were upstream of CB_1 mRNA expression, than we would not expect CB_1 mRNA expression to be induced to ~50% of wild-type levels in 111/111 cells. Akt-mediated signal transduction, however, is unaffected by mHtt (Dowie *et al*., 2009). We concluded that activated CB_1 receptors mediated CB_1 mRNA induction *via* Akt and that downstream effectors of Akt were inhibited by mHtt.

Activated Akt phosphorylates many proteins that regulate transcription. Borner *et al*. (2007a) demonstrated that cannabinoid-dependent CB_1 induction required binding of NF-κB to the CB_1 promoter. Other authors have demonstrated cannabinoid-mediated CB_1 mRNA induction depends upon RARα/γ or the estrogen receptor (Mukhopadhyay *et al*., 2008; Proto *et*

al., 2011). Of these candidates, only NF-κB is activated downstream of Akt and only NF-κB-mediated transcription has been shown to be inhibited by mHtt (Marcora *et al*., 2010; Reijonen *et al*., 2010; Ghose *et al*., 2011). Therefore, we examined NF-κB-mediated promoter activation using an NF-κB promoter-firefly luciferase reporter and found that activity of this promoter increased in an ACEA dose-dependent manner and the response was inhibited by approximately 50% in the presence of mHtt. Three theories currently exist to explain how mHtt inhibits NF-κB activity. First, wild-type Htt may normally facilitate the trafficking of NF-κB from the dendrites to the nucleus to activate transcription (Marcora *et al*., 2010). Second, mHtt expression is associated with elevated calpain activity and calpain enzymes decrease NF-κB p65 protein abundance (Reijonen *et al*., 2010). Third, the expression of several microRNAs is elevated in the presence of mHtt and these microRNAs suppress expression of the RelA subunit of NF-κB (Ghose *et al*., 2011). Based on our data, we were unable to determine whether mHtt attenuated the NF-κB-mediated increase in promoter activity *via* transcriptional dysregulation of NF-κB genes or *via* decreased activity of the NF-κB protein. Given that transcriptional dysregulation occurs early in HD pathogenesis, CB_1 is one of the genes that is dysregulated early in HD, and NF-κB is a regulator of CB_1, the attenuated NF-κB response we observed may have resulted from mHtt-mediated repression of NF-κB genes. In summary, we observed that cannabinoids activated CB_1 receptors, which stimulated Akt phosphorylation, leading to NF-κB-mediated induction of CB_1 promoter activity and mRNA expression and the translation of CB_1 mRNA to produce new CB_1 receptors (Fig. 41).

4.5 Cannabinoid Treatment Improved Cellular Function

We had shown that cannabinoids could stimulate expression of their cognate receptors. But, if this stimulation conferred no functional benefit to the cells expressing mHtt, then this

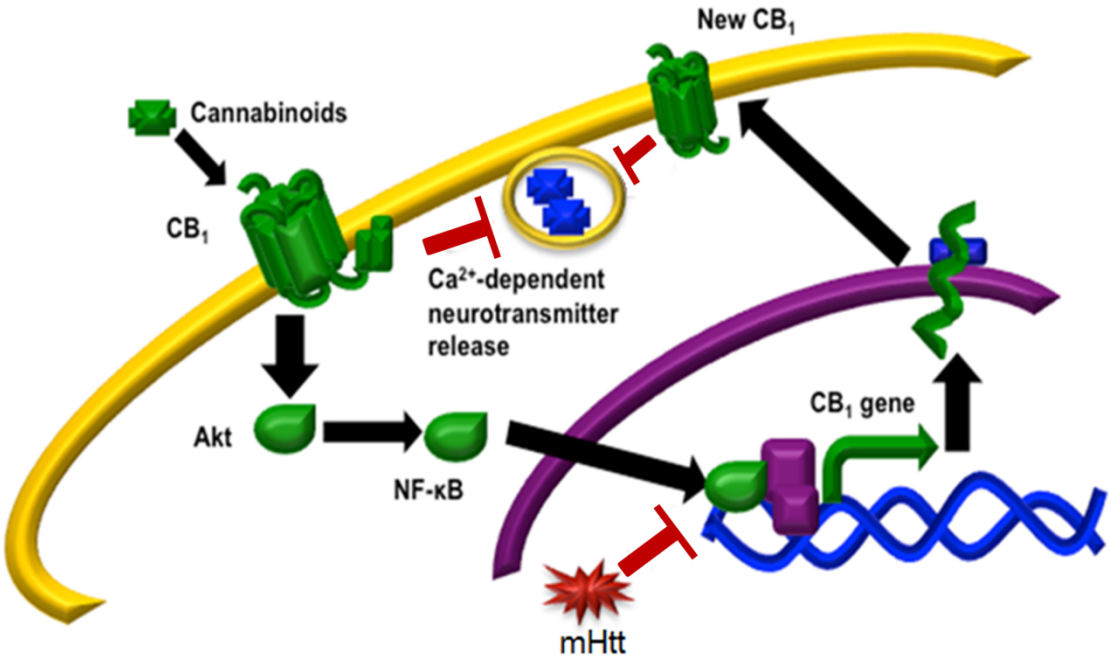

Figure 41. Cannabinoid-mediated induction of CB_1 receptor expression in the presence of mHtt. We found that cannabinoids, such as ACEA, mAEA, and AEA, activated CB_1 receptors leading to the phosphorylation of Akt and activation of NF-κB-mediated transcription. NF-κB induced CB_1 promoter activity. Increased CB_1 promoter activity lead to elevated CB_1 mRNA and protein abundance. Elevated CB_1 levels may augment inhibition of Ca^{2+}-dependent neurotransmitter release. In the presence of mHtt NF-κB-mediated activation of the promoter activity was reduced by approximately 50%.

observation would have limited utility for HD research. CB_1 receptors are considered neuroprotective because they enhance expression of pro-survival genes, inhibit Ca^{2+}-dependent neurotransmitter release, and enhance synaptic plasticity (Fernandez-Ruiz *et al*., 2004). Moreover, cannabinoids display cannabinoid receptor-indpendent antioxidant properties (Pertwee *et al*., 1999). We hypothesized that cannabinoid treatment would improve general cellular viability in the presence of mHtt. Indeed, treatment with 1 μM ACEA increased esterase activity, and decreased membrane permeability. One micromolar ACEA treatment was also associated with elevated ATP levels, which are known to be decreased in the presence of mHtt (Trettel *et al*., 2000; Cui *et al*., 2006). It is unknown whether these effects were CB_1-dependent or –independent. CB_1 receptor activation could have induced pro-survival signalling to yield improved cellular viability (Fernandez-Ruiz *et al*., 2004). Alternatively, ACEA may have acted as an antioxidant and improved mitochondrial activity by absorbing excess reactive oxygen species or, as a lipid, altered the plasma membrane to alter membrane permeability (Pertwee *et al*., 1999).

We also found that treatment of cells with 1 μM ACEA restored expression of BDNF-2 and PGC1α, but not DARPP-32, in a cannabinoid dose-dependent manner. In accordance with this observation, PGC1α mRNA levels were lower in $CB_1^{+/-}$ mice than wild-type mice, yet DARPP-32 mRNA levels were unchanged. Based on these data we concluded that CB_1-mediated signal transduction regulates the expression of a subset of genes, including PGC1α and BDNF-2 and excluding DARPP-32. PGC1α and BDNF-2 mRNA levels were probably not induced *via* the same mechanism as CB_1 as the form of these dose-response curves does not resemble the responses observed for CB_1. Overall, cannabinoid treatment alters the expression of a subset of genes. Similarly, mHtt alters the expression of a subset of genes (Luthi-Carter *et al*., 2000).

Based on our observations we concluded that certain factors that are activated by CB_1-mediated signaling are also inhibited in the presence of mHtt, which yields an overlapping regulatory region in which CB_1, BDNF-2, and PGC1α co-exist (Luthi-Carter *et al*,. 2000; Gafni & Ellerby, 2002; Pazos *et al*., 2008). The crux of these observations is that cannabinoid treatment was associated with normalized expression of two genes that are repressed early in HD pathogenesis.

4.6 Elevated CB_1 Levels Could Affect GPCR Signaling and Pharmacology

Cannabinoids induce expression of their cognate receptors in a cell culture model of 'adult' striatal neurons. Altered endocannabinoid tone could affect CB_1 receptor expression. CB_1 receptors are known to co-localize and dimerize with orexin, μ- and δ-opioid, and dopamine D_2 short receptors in the mammalian brain (Uriguen *et al.,* 2009; Miller & Devi, 2011; Navarro *et al.*, 2009; Bortolato *et al*., 2010). Thus, CB_1 abundance and trafficking could alter the localization and signaling of several other GPCRs depending on the tissue- and cell-specific importance of CB_1 receptors. If cannabinoid treatment can increase CB_1 expression *in vivo*, then cannabinoids may alter their own receptor pharmacology as well the dopaminergic and opiate-mediated signal transduction. In fact, injection of AEA into the mouse median forebrain elevates dopamine concentration and dopamine D_2 receptor binding (Khoury *et al*., 2012). The effect of cannabinoid treatment on the ECS may also be developmental stage-specific because expression of CB_1 fluctuates during developmental (Eggan *et al*., 2010). Cannabinoid treatment, or *cannabis* abuse, may be particularly potent during adolescence because CB_1 mRNA and protein levels peak in several regions of the brain during this stage (Eggan *et al*., 2010; Vitalis *et al*., 2008).

4.7 Cannabinoid-mediated Induction of CB_1 Receptors may Negatively Feedback onto Neurotransmitter Release

Elevated CB_1 receptor expression as a response to cannabinoids seems to represent a positive feedback loop, yet few biological systems operate through positive feedback. The role of acutely activated CB_1 receptors in the central nervous system is the inhibition of Ca^{2+}-dependent neurotransmitter release (Fitzgerald *et al*., 2012). Therefore, a biological system whereby cannabinoids induce expression of their cognate receptors may represent a form of negative feedback on the release of neurotransmitter from the cell. Viewed from this context, elevated CB_1 receptor levels would enhance hypoactivity and analgesia, which are two commonly observed effects of cannabinoid treatment (Mallet *et al*., 2008).

4.8 Cannabinoid-mediated Induction of CB_1 may Hold Therapeutic Benefit for HD

Cannabinoid treatment elevated CB_1 receptor abundance in the presence of mHtt. Although CB_1 induction was attenuated by approximately 50% in 7/111 and 111/111 cells, CB_1 mRNA levels exceeded those observed in untreated wild-type 7/7 cells for all cannabinoid-treated cells. An important point is that this induction was mediated by NF-κB, which is an important factor in the inflammatory response (Borner *et al*., 2007b). CB_1 receptor activation may trigger certain components of the inflammatory response that may be of benefit and detriment depending on the context. Furthermore, cannabinoid treatment improved cellular function and viability. Therefore, although the toxic factor mediating HD pathogenesis, mHtt, was not altered by cannabinoid treatment, the function and viability of 7/111 and 111/111 cells were improved. CB_1 mRNA levels decline by approximately 50% early in HD pathogenesis in human patients and all animal models of HD tested to date (Denovan-Wright & Robertson, 2000; Pazos *et al*., 2008), and decreased CB_1 levels contribute to HD pathogenesis (Blazquez *et al*., 2011; Mievis *et al*., 2011).

Our data provide strong evidence for the utility of cannabinoids as a therapeutic treatment for HD because CB_1 receptor activation may ameliorate transcriptional dysregulation, decrease excitotoxicity, and improve motor coordination and synaptic plastiticty (Fernandez-Ruiz *et al*., 2004; Pazos *et al*., 2008). Further, cannabinoids represent a pharmacologically tractable means of treatment for HD that can be administered orally, nasally, or by inhalation (El Khoury *et al.*, 2012); whereas other putative therapeutics for HD, such as gangliosides (Di Pardo *et* al., 2012) and kinase inhibitors (Atwal *et al.*, 2011) may be limited by their route of administration, bioavailability, and specificity. Other authors have explored cannabinoids as a therapeutic treatment for HD. Treatment of PC12 cells expressing mHtt with direct and indirect cannabinoid agonists improves cell survival (Scotter *et al.*, 2010). Treatment of mice injected with quinolinic acid or 3-nitropropionic acid (models of HD striatal lesions) with cannabinoid agonists reduces striatal atrophy (Lastres-Becker *et al.*, 2003; Lastres-Becker *et al*., 2002; Pintor *et al*., 2006). Short-term (2 week) treatment of R6/2 HD mice with THC is associated with decreased striatal atrophy, improved rotarod performance, and increased lifespan (Blazquez *et al*., 2011). However, chronic (10 week) treatment of R6/2 HD mice with THC lowers the threshold to seizure and does not alter striatal atrophy while AEA or inhibitors of FAAH did not alter seizure threshold or HD progression (Dowie *et al*., 2009). Our study is the first to our knowledge to demonstrate a cannabinoid-mediated induction of CB_1 receptor expression in the presence of mHtt. In light of this observation, the therapeutic benefit of cannabinoids in HD may depend upon the specific cannabinoid used, the dose and frequency of use.

4.9 Conclusions and Future Research

We observed that several components of the ECS, CB_1, CB_2, and FAAH, were dysregulated during HD pathogenesis. We found that treatment of models of adult striatal neurons with

cannabinoids induced expression of CB_1 in a CB_1 receptor-, Akt-, and NF-κB-dependent manner in the presence of mHtt and mHtt non-competitively inhibited this induction. To our knowledge, this is the first demonstration of cannabinoid-mediated CB_1 receptor induction in a neuronal cell model (Borner *et al*., 2007a, Mukhopadhyay *et al*., 2008; Proto *et al*., 2011). This research demonstrates that the pharmacology and expression of GPCRs can be altered by their cognate ligands. In HD therefore, the malleability of CB_1 expression is restricted by the presence of mHtt, but not so restricted that CB_1 expression could not be normalized by cannabinoid treatment. *In vivo*, cannabinoid-mediated induction of cannabinoid receptors may depend on the type of exposure to and potency of the ligand used. We propose that CB_1 agonists of limited potency (Dowie *et al*., 2009), indirect agonists (Kim & Alger, 2010), or allosteric modulators of CB_1 (Ahn *et al*., 2012) hold the most therapeutic potential for the treatment of HD because they appear to promote the desirable affects of cannabinoid treatment, such as improved motor control and reduced striatal atrophy, with fewer detrimental repercussions. The biological significance of our observations is that induction of CB_1 expression by cannabinoids may improve neuronal function in the population of neurons most severely affected by mHtt.

Our future research will explore three major facets of cannabinoid-mediated CB_1 induction. First, we will determine whether cannabinoid treatment affects other components of the ECS, such as CB_2 and FAAH expression, using the ST*Hdh* cell culture model of HD. Second, we will assess the effect of elevated CB_1 receptor levels on Ca^{2+}-dependent neurotransmitter release in ST*Hdh* cells. Finally, we will treat HD mice with cannabinoids, measure expression of several components of the ECS, and evaluate the progression of HD in animals treated with cannabinoids or untreated. Our hypothesis is that cannabinoid treatment will induce the

expression of CB_1 in HD mice and that the magnitude of response to cannabinoid will be dose-, drug-, and developmental stage-specific.

REFERENCES

Ahn KH, Mahmoud MM, Kendall DA (2012). Allosteric modulator ORG27569 induces CB1 cannabinoid receptor high affinity agonist binding state, receptor internalization, and Gi protein-independent ERK1/2 kinase activation. *J Biol Chem* **287**: 12070 – 82.

Allen KL, Waldvogel HJ, Glass M, Faull RL (2009). Cannabinoid (CB(1)), GABA(A) and GABA(B) receptor subunit changes in the globus pallidus in Huntington's disease. *J Chem Neuroanat* **37**: 266 – 81.

Amaya F, Shimosato G, Kawasaki Y, Hashimoto S, Tanaka Y, Ji RR, Tanaka M (2006). Induction of CB1 cannabinoid receptor by inflammation in primary afferent neurons facilitates antihyperalgesic effect of peripheral CB1 agonist. *Pain* **124**: 175 – 83.

Atwal RS, Desmond CR, Caron N, Maiuri T, Xia J, Sipione S, Truant R (2011). Kinase inhibitors modulate huntingtin cell localization and toxicity. *Nat Chem Biol* **7**: 453 – 60.

Atwood BK & Mackie K (2010). CB2: a cannabinoid receptor with an identity crisis. *Br J Pharmacol* **160**: 467 – 79.

Basavarajappa B, Nixon R, Arancio O (2009). Endocannabinoid system: emerging role from neurodevelopment to neurodegeneration. *Min Rev Med Chem* **9**: 448 – 62.

Bjorkqvist M, Fex M, Renstrom E, Wierup N, Petersen A, Gil J, Bacos K, Popovic N, Li JY, Sundler F, Brundin P, Mulder H (2005). The R6/2 transgenic mouse model of Huntington's disease develops diabetes due to deficient beta-cell mass and exocytosis. *Hum Mol Genet* **14**: 565 – 74.

Blázquez C, Chiarlone A, Sagredo O, Aguado T, Pazos MR, Resel E, Palazuelos J, Julien B, Salazar M, Börner C, Benito C, Carrasco C, Diez-Zaera M, Paoletti P, Díaz-Hernández M, Ruiz C, Sendtner M, Lucas JJ, de Yébenes JG, Marsicano G, Monory K, Lutz B, Romero J, Alberch J, Ginés S, Kraus J, Fernández-Ruiz J, Galve-Roperh I, Guzmán M (2011).Loss of striatal type 1 cannabinoid receptors is a key pathogenic factor in Huntington's disease. *Brain* **134**: 119 – 36.Bonelli (2003)

Borner C, Holt V, Kraus J (2007). Activation of human T cells induces upregulation of cannabinoid type 1 transcription. *Neuroimmunomodulation* **14**: 281 – 6.

Borner C, Holt V, Kraus J (2007). Transcriptional regulation of the cannabinoid receptor type 1 gene in T cells by cannabinoids. *J Leukoc Biol* **81**: 336 – 43.

Borner C, Bedini A, Holt V, Kraus J (2008). Analysis of promoter regions regulating basal and interleukin-4 inducible expression of the human CB1 receptor gene in T lymphocytes. *Mol Pharmacol* **73**: 1013 – 9.

Bortolato M, Frau R, Bini V, Luesu W, Loriga R, Collu M, Gessa GL, Ernas MG, Castelli MP (2010).Methamphetamine neurotoxicity increase brain expression and alters behavioural functions of CB1 cannabinoid receptors. *J Psychiatr Res* **44**: 944 – 55.

Bosier B, Sarre S, Smolders I, Michotte Y, Hermans E, Lambert DM (2010). Revisiting the complex influences of cannabinoids on motor functions unravels pharmacodynamic differences between cannabinoid agonists. *Neuropharmacology* **59**: 503 – 10.

Calkins RA & Van Allen MW (1967). Huntington's chorea. *J Iowa Med Soc* **57**: 336 – 40.

Casteels C, Martinez E, Bormans G, Camon L, de Vera N, Baekelandt V, Planas AM, Van Laere K (2010). Type 1 cannabinoid receptor mapping with [18F]MK-9470 PET in the rat brain after quinolinic acid lesion: a comparison of dopamine receptors and glucose metabolism. *Eur J Nuc Med Mol Imaging* **37**: 2354 – 63.

Chiodi V, Uchigashima M, Beggiato S, Ferrante A, Armida A, Matire A, Potenza RL, Ferraro L, Tanganelli S, Watanabe M, Domenici MR, Popoli P (2012). Unbalance of CB1 receptors expressed in GABAergic and glutamatergic neurons in a transgenic mouse models of Huntington's disease. *Neurobiol Dis* **45**: 983 – 91.

Conneally PM (1984). Huntington's disease: genetics and epidemiology. *Am J Hum Genet* **36**: 506 – 26.

Corchero J, Romero J, Berrendero F, Fernandez-Ruiz J, Ramos JA, Fuentes JA, Manzanares J (1999). Time-dependent differences of repeated administration with Delta9-tetrahydrocannabinol in proenkephalin and cannabinoid receptor gene expression and G-protein activation by mu-opiod and CB1-cannabinoid receptors in the caudate-putamen. *Brain Res Mol Brain Res* **67**: 148 – 57.

Cravatt BF, Giang DK, Mayfield SP, Boger DL, Lerner RA, Gilula NB (1996). Molecular characterization of an enzyme that degrades neuromodulatory fatty-acid amides. *Nature* **384**: 83 – 7.

Cui L, Jeong H, Borovecki F, Pakhurst CN, Tanese N, Krainc D (2006). Transcriptional repression of PGC1-alpha by mutant huntingtin leads to mitochondrial dysfunction and neurodegeneration. *Cell* **127**: 58 – 69.

de Lago E & Fernandez-Ruiz J (2007). Cannabinoids and neuroprotection in motor-related disorders. *CNS Neurol Disord Drug Targets* **6**: 377 – 87.

Denovan-Wright EM & Robertson HA (2000). Cannabinoid receptor messenger RNA levels decrease in a subset of neurons of the lateral striatum, cortex, and hippocampus of transgenic Huntington's disease mice. *Neuroscience* **98**: 705 – 13.

Di Marzo V, Fontana A, Cadas H, Schinelli S, Cimino G, Schwartz JC, Piomelli D (1994). Formation and inactivation of endogenous cannabinoid anandamide in central neurons. *Nature* **372**: 686 – 91.

Di Pardo A, Maglione V, Alpaugh M, Horkey M, Atwal RS, Sassone J, Ciammola A, Steffan JS, Fouad K, Turant R, Sipione S (2012). Ganglioside GM1 induces phosphorylation of mutant huntingtin and restores normal motor behaviour in Huntington disease mice. *Proc Natl Acad Sci USA* **109**: 3528 – 33.

Djousse L, Knowlton B, Cupples LA, Marder K, Shoulson I, Myers RH (2002). Weight loss in early stage of Huntington's disease. *Neurology* **59**: 1325 – 30.

Dowie MJ, Bradshaw HB, Howard ML, Nicholson LF, Faull RL, Hannan AJ, Glass M (2009). Altered CB1 receptor and endocannabinoid levels precede motor symptom onset in a transgenic mouse model of Huntington's disease. *Neuroscience* **163**: 456 – 65.

Dowie MJ, Howard ML, Nicholson LF, Faull RL, Hannan AJ, Glass M (2010). Behavioural and molecular consequences of chronic cannabinoid treatment in Huntington's disease transgenic mice. *Neuroscience* **170**: 324 – 36.

Dragatsis I, Efstradiadis A, Zeitlin S (1998). Mouse mutant embryos lacking huntingtin are rescued from lethality by wild-type extraembryonic tissues. *Development* **125**: 1529 – 39.

Eggan SM, Melchitsky DS, Sesack SR, Fish KN, Lewis DA (2010). Relationship of cannabinoid CB1 receptor and cholecystokinin immunoreactivity in monkey dorsolateral prefrontal cortex. *Neuroscience* **169**: 1651 – 61.

El Khoury MA, Gorgievski V, Moutsimilli L, Giros B, Tzavara ET (2012). Interactions between the cannabinoid and dopaminergic systems: Evidence from animal studies. *Prog Neuropsychopharmacol Biol Psychiatry* **E-pub ahead of print**.

ExPASYy (2012) [http://expasy.org/proteomics/protein_characterisation_and_function]

Fernandez-Ruiz J, Gomez M, Hernandez M, de Miguel R, Ramos JA (2004). Cannabinoids and gene expression during brain development. *Neurotox Res* **6**: 389 – 401.

Fitzgerald ML, Chan J, Mackie K, Lupica CR, Pickel VM (2012). Altered dendritic distribution of dopamine D2 receptors and reduction in mitochondrial number in parvalbumin-containing interneurons in medial prefrontal cortex of cannabinoid-1 (CB1) receptor knockout mice. *J Comp Neurol* **E-pub ahead of print**.

Fong TM & Heymsfield SB (2009). Cannabinoid-1 receptor inverse agonists : current understanding of mechanism of action and unanswered questions. *Int J Obes (Lond)* **33**: 947 – 55.

Gafni J, & Ellerby LM (2002). Calpain activation in Huntington's disease. *J Neuroscience* **22**: 4842 – 9.

Ghose J, Sinha M, Das E, Jana NR, Battacharyya NP (2011). Regulation of miR-146a by RelA/NFkB and p53 in STHdh(Q111)/Hdh(Q111) cells, a cell model of Huntington's disease. *PLoS One* **6**: e23837.

Gines S, Ivanova E, Seong IS, Saura CA, MacDonald ME (2003). Enhanced Akt signal is an early pro-survival response that reflects N-methyl-D-aspartate receptor activation in Huntington's disease knock-in striatal cells. *J Biol Chem* **278** : 50514 – 22.

Gines S, Paoletti P, Alberch J (2010). Impaired TrkB-mediated ERK1/2 activation in Huntington disease knock-in striatal cells involves reduced p52/p46 Shc expression. *J Biol Chem* **285**: 21537 – 48.

Glass M, van Dellen A, Blakemore C, Hannan AJ, Faull RL (2004). Delayed onset of Huntington's disease in mice in an enriched environment correlates with delayed loss of cannabinoid CB1 receptors. *Neuroscience* **123**: 207 – 12.

Gomez GT, Hu H, McCaw EA, Denovan-Wright EM (2006). Brain-specific factors in combination with mutant huntingtin induce gene-specific transcriptional dysregulation. *Mol Cell Neurosci* **31**: 661 – 75.

Graham RK, Deng Y, Slow EJ, Haigh B, Bissada N, Lu G, Pearson J, Shehadeh J, Bertram L, Murphy Z, Warby SC, Doty CN, Roy S, Wellington CL, Leavitt BR, Raymond LA, Nicholson DW, Hayden MR (2006). Cleavage at the caspase-6 site is required for neuronal dysfunction and degeneration due to mutant huntingtin. *Cell* 125: 1179 – 91.

Gustafsson K, Wang X, Severa D, Eriksson M, Kimby E, Merup M, Christensson B, Flygare J, Sander B (2008). Expression of cannabinoid receptors type 1 and type 2 in non-Hodgkin lymphoma: growth inhibition by receptor activation. Int J Cancer **123**: 1025 – 33.

Gutekunst CA, Li SH, Yi H, Mulroy JS, Kuemmerle S, Jones R, Rye D, Ferrante RJ, Hersch SM, Li XJ (1999). Nuclear and neuropil aggregates in Huntington's disease: relationship to neuropathology. *J Neurosci* **19**: 2522 – 34.

Gutierrez T, Farthing JN, Zvonok AM, Makriyannis A, Hohmann AG (2006). Activation of peripheral CB1 and CB2 receptors suppresses the maintenance of inflammatory nociception: a comparative analysis. *Br J Pharamcol* **150**: 153 – 63.

Hebb AL, Robertson HA, Denovan-Wright EM (2004). Striatal phosphodiesterase mRNA and protein levels are reduced in Huntington's disease transgenic mice prior to the onset of motor symptoms. *Neuroscience* **123**: 967 – 81.

Heng L, Beverley JA, Steiner H, Tseng KY (2011). Differential developmental trajectories for CB1 cannabinoid receptor expression in limbic/associative and sensorimotor cortical areas. *Synapse* **65**: 278 – 86.

Hermel E, Gafni J, Propp SS, Leavitt BR, Wellington CL, Young JE, Hackam AS, Logvinova AV, Peel AL, Chen SF, Hook V, Singaraja R, Krajewski S, Goldsmith PC, Ellerby HM, Hayden MR, Bredesen DE, Ellerby LM (2004). Specific caspase interactions and amplification are involved in selective neuronal vulnerability in Huntington's disease. *Cell Death Differ* 11: 424 – 38.

Hill MN, Hillard CJ, McEwen BS (2011). Alterations in corticolimbic dendritic morphology and emotional behaviour in cannabinoid CB1 receptor-deficient mice parallel the effects of chronic stress. *Cereb Cortex* **21**: 2056 – 64.

Hillard CJ, Manna S, Greenberg MJ, DiCamelli R, Ross RA, Stevenson LA, Murphy V, Pertwee RG, Campbell WB (1999). Synthesis and characterization of potent and selective agonists of the neuronal cannabinoid receptor (CB1). *J Pharmacol Exp Ther* **289**: 1427 – 33.

Hodges A, Strand AD, Aragaki AK, Kuhn A, Sengstag T, Hughes G, Elliston LA, Hartog C, Goldstein DR, Thu D, Hollingsworth ZR, Collin F, Synek B, Holmans PA, Young AB, Wexler NS, Delorenzi M, Kooperberg C, Augood SJ, Faull RL, Olson JM, Jones L, Luthi-Carter R (2006). Regional and cellular gene expression changes in human Huntington's disease brain. *Hum Mol Genet* 15:965 – 77.

Hogel M (2011). Investigating the mechanism of promoter-specific N-terminal mutant huntingtin-mediated transcriptional dysregulation. *Dalhousie University thesis.*

Howlett AC, Song C, Berglund BA, Wilken GH, Pigg JJ (1998). Characterization of CB1 cannabinoid receptors using receptor peptide fragments and site-directed antibodies. *Mol Pharmacol* **53**: 504 – 10.

Howlett AC, Barth F, Bonner TI, Cabral G, Casellas P, Devane WA, Felder CC, Herkenham M, Mackie K, Martin BR, Mechoulam R, Pertwee RG (2002). International Union of Pharmacology. XXVII. Classification of Cannabinoid Receptors. *Pharmacol Rev* **54**: 161 – 202.

Hudson BD, Hebert TE, Kelly ME (2010). Physical and functional interaction between CB1 cannabinoid receptors and beta2-adrenoceptors. *Br J Pharmacol* **160**: 627 – 42.

Huffman JW (2000). The search for selective ligands for the CB2 receptor. *Curr Pharm Des* **6**: 1323 – 37.

Huntington's Disease Collaborative Research Group (HDCRG, 1993). A novel gene containing a trinucleotide repeat that is expanded and unstable on Huntington's disease chromosomes. The Huntington's Disease Collaborative Research Group. *Cell* **72**: 971 – 83.

Killoran A & Biglan KM (2012). Therapeutics in Huntington's disease. *Curr Treat Options Neurol* **E-pub ahead of print**.

Kim J & Alger BE (2010). Reduction in endocannabinoid tone is a homeostatic mechanism for specific inhibitory synapses. *Nat Neurosci* **13**: 592 – 600.

Kim K, Lee SG, Kegelman TP, Su ZZ, Das SK, Dash R, Dasgupta S, Barral PM, Hedvat M, Diaz P, Reed JC, Stebbins JL, Pellecchia M, Sarkar D, Fisher PB (2011). Role of excitatory amino acid transporter-2 (EAAT2) and glutamate in neurodegeneration: opportunities for developing novel therapeutics. *J Cell Physiol* **226** : 2484 – 93.

Krainc D (2007). Clearance of mutant proteins as a therapeutic target for neurodegenerative diseases. *Arch Neurol* **67**: 388 – 92.

Kremer HP, Roos RA, Dingjan G, Marani E, Bots GT (1990). Atrophy of the hypothalamic lateral tuberal nucleus in Huntington's disease. *J Neuropathol Exp Neurol* **49**: 371 – 82.

Lambert DM & Fowler CJ (2005). The endocannbinoid system : drug targets, lead compounds, and potential therapeutic applications. *J Med Chem* **48**: 5059 – 87.

Landwehrmeyer GB, Standaert DG, Testa CM, Penney JB Jr, Young AB (1995). NMDA receptor subunit mRNA expression by projection neurons and interneurons in rat striatum. *J Neurosci* **15**: 5297 – 307.

Lastres-Becker I, Gómez M, De Miguel R, Ramos JA, Fernández-Ruiz J (2002). Loss of cannabinoid CB(1) receptors in the basal ganglia in the late akinetic phase of rats with experimental Huntington's disease. *Neurotox Res* **4**: 601 – 608.

Li SH, Lam S, Cheng AL, Li XJ (2000). Intranuclear huntingtin increases the expression of caspase-1 and induces apoptosis. *Hum Mol Genet* **9**: 2859 – 67.

Li JY, Popovic N, Brundin P (2005). The use of the R6 transgenic mouse models of Huntington's disease in attempts to develop novel therapeutic strategies. *NeuroRx* **2**: 447 – 64.

Li JL, Hayden MR, Warby SC, Durr A, Morrison PJ, Nance M, Ross CA, Margolis RL, Rosenblatt A, Squitieri F, Frati L, Gómez-Tortosa E, García CA, Suchowersky O, Klimek ML, Trent RJ, McCusker E, Novelletto A, Frontali M, Paulsen JS, Jones R, Ashizawa T, Lazzarini A, Wheeler VC, Prakash R, Xu G, Djoussé L, Mysore JS, Gillis T, Hakky M, Cupples LA, Saint-Hilaire MH, Cha JH, Hersch SM, Penney JB, Harrison MB, Perlman SL, Zanko A, Abramson RK, Lechich AJ, Duckett A, Marder K, Conneally PM, Gusella JF, MacDonald ME, Myers RH (2006). Genome-wide significance for a modifier of age at neurological onset in Huntington's disease at 6q23-24: the HD MAPS study. *BMC Med Genet* **17**: 71.

Lin S, Zhang Y, Dodel R, Farlow MR, Paul SM, Du Y (2009). Minocycline blocks nitric oxide-induced neurotoxicity by inhibition p38 MAP kinase in rat cerebellar granule neurons. *Neurosci Lett* **315**: 61 – 4.

Luthi-Carter R, Strand A, Peters NL, Solano SM, Hollingsworth ZR, Menon AS, Frey AS, Spektor BS, Pennery EB, Schilling G, Ross CA Borchelt DR, Tapscott SJ, Young AB, Cha JH, Olson JM (2000). Decreased expression of striatal signaling genes in a mouse model of Huntington's disease. *Hum Mol Genet* **9**: 1259 – 71.

Mallet N, Pogosyan A, Márton LF, Bolam JP, Brown P, Magill PJ (2008). Parkinsonian beta oscillations in the external globus pallidus and their relationship with subthalamic nucleus activity. *J Neurosci* **28**: 14245 – 58.

Mangiarini L, Bates GP, Davies SW (1996). Transgenic mice in the study of polyglutamine repeat expansion diseases. *Brain Pathol* **8**: 699 – 714.

Marcora & Kennedy MD (2010). The Huntington's disease mutation impairs huntingtin's role in the transport of NF-kB from the synapse to the nucleus. *Hum Mol Genet* **19**: 4373 – 84.

Martin BR, Mechoulam R, & Razdan RK (1999). Discovery and characterization of endogenous cannabinoids. *Life Sci* **65**: 573 – 95.

Matsuda LA, Lolait SJ, Brownstein MJ, Young AC, Bonner TI (1990). Structure of a cannabinoid receptor and functional expression of the cloned cDNA. *Nature* **346**: 561 – 4.

McCaw EA, Hu H, Gomez GT, Hebb AL, Kelly ME, Denovan-Wright EM (2004). Structure, expression, and regulation of the cannabinoid receptor gene (CB1) in Huntington's disease transgenic mice. *Eur J Biochem* **271**: 4909- 20.

Meade CA, Deng YP, Fusco FR, Del Mar N, Hersch S, Goldowitz D, Reiner A (2002). Cellular localization and development of neuronal intranuclear inclusions in striatal and cortical neurons in R6/2 transgenic mice. *J Comp Neurol* **449**: 241 – 69.

Mechoulam R & Hanu L (2001). The cannabinoids: an overview. Therapeutic implications in vomiting and nausea after cancer chemotherapy, in appetite promotion, in multiple sclerosis, and in neuroprotection. *Pain Res Manag* **6:** 67 – 73.

Mechoulam R, Peters M, Murillo-Rodriguez E, Hanus LO (2007). Cannabidiol – recent advances. *Chem Biodivers* **4:** 1678 – 92.

Mestre T, Ferreira J, Coelho MM, Rosa M, Sampaio C (2009). Therapeutic interventions for symptomatic treatment in Huntington's disease. *Cochrane Database Syst Rev* **8**: CD006456.

Mievis S, Blum D, Ledent C (2011). Worsening of Huntington's disease phenotype in CB1 receptor knockout mice. *Neurobiol Dis* **42**: 524 – 9.

Miller LK & Devi LA (2011). The highs and lows of cannabinoid receptor expression in disease: mechanisms and their therapeutic implications. *Pharmacol Rev* **63**: 461 – 70.

Mukhopadhyay B, Liu J, Osei-Hyiaman D, Godlewski G, Mukhopadhyay P, Wang L, Jeong WI, Gao B, Duester G, Mackie K, Kojima S, Kunos G (2010). Transcriptional regulation of cannabinoid receptor-1 expression in the liver by retinoic acid acting via retinoic acid receptor-gamma. *J Biol Chem* **285**: 19002 – 11.

Munro S, Thomas KL, Abu-Shaar M (1993). Molecular characterization of a peripheral receptor for cannabinoids. *Nature* **365**: 61 – 5.

National Centre for Biotechnology Information (NCBI) (2011). Database of Expressed Sequence Tags (dbEST). [http://www.ncbi.nlm.nih.gov/nucest?term=CB1]

Navarro G, Carriba P, Gandia J, Ciruela F, Casado V, Cortes A, Mallol J, Canela EI, Lluis C, Franco R. (2008). Detections of heteromers formed by cannabinoid CB1, dopamine D2, and adenosine A2A G-protein-coupled receptors by combining bimolecular fluorescence complementation and bioluminescence energy transfer. *ScientificWorldJournal* **11**: 1088 – 97.

Navarro HA, Howard JL, Pollard GT, Carroll FI (2009). Positive allosteric modulation of the human cannabinoid (CB) receptor by RTI-371, a selective inhibitor of the dopamine transporter. *Br J Pharmacol* **156**: 1178 – 84.

Newcombe RG (1981). A life table for onset of Huntington's chorea. *Ann Hum Genet* **45**: 375 – 85.

Orth M, Schippling S, Schneider SA, Bhatia KP, Talelli P, Tabrizi SJ, Rothwell JC (2010). Abnormal motor cortex plasticity in premanifest and very early manifest Huntington disease. *J Neruol Neurosurg Psychiatry* **81**: 267 – 70.

Pacheco DF, Klein A, Perez AC, Pacheco CM, de Francischi JN, Reis GM, Duarte ID (2009). Central antinociception induced by mu-opioid receptor agonist morphine, but not delta- or kappa-, is mediated by cannabinoid CB1 receptor. *Br J Pharmacol* **158**: 225 – 231.

Palermo FA, Angelini M, Cottone E, Virgili M, Franzoni MF, Mosconi G, Polzonetti-Magni AM (2009). Involvement of endocannabinoid CB1 receptor in the modulation of stress responses related to xenoestrogen exposure. *Ann N Y Acad Sci* **1163**: 504 – 507.

Paoletti P, Vila I, Rifé M, Lizcano JM, Alberch J, Ginés S (2008). Dopaminergic and glutamatergic signaling crosstalk in Huntington's disease neurodegeneration: the role of p25/cyclin-dependent kinase 5. *J Neurosci* **28**: 10090 – 101.

Pazos MR, Sagredo O, Fernandez-Ruiz J (2008). The endocannabinoid system in Huntington's disease. *Curr Pharm Des* 2008 **14**: 2317 – 25.

Pertwee RG (1999). Pharmacology of cannabinoid receptor ligands. *Curr Med Chem* **6**: 635 – 64.

Pertwee RG, Howlett AC, Abood ME, Alexander SP, Di Marzo V, Elphick MR, *et al*. (2010). International Union of Basic and Clinical Pharmacology. LXXIX. Cannabinoid receptors and their ligands: beyond CB1 and CB2. *Pharmacol Rev* **62**: 588 – 631.

Pini A, Mannaioni G, Pellegrini-Giampietro D, Passani MB, Mastroianni R, Bani D, Masini E (2012). The role of cannabinoids in inflammatory modulation of allergic respiratory disorders, inflammatory pain and ischemic stroke. *Curr Drug Targets* **13**: 984 – 93.

Pinto JG, Hornby KR, Jones DG, Murphy KM (2010). Developmental changes in GABAergic mechanisms in human visual cortex across the lifespan. *Front Cell Neurosci* **4**: 16.

Proto MC, Gazzerro P, Di Croce L, Santoro A, Malfitano AM, Pisanti S, Laezza C, Bifulco M (2011). Interaction of endocannabinoid system and steroid hormones in the control of colon cancer cell growth. *J Cell Physiol* **In-press**.

Puente N, Elezgarai I, Lafourcade M, Reguero L, Marsicano G, Georges F, Manzoni OJ, Grandes P (2010). Localization and function of the cannabinoid CB1 receptor in the anterolateral bed nucleus of the stria terminalis. **5:e8869**.

Quarrell OW, Rigby AS, Barron L, Crow Y, Dalton A, Dennis N, Fryer AE, Heydon F, Kinning E, Lashwood A, Losekoot M, Margerison L, McDonnell S, Morrison PJ, Norman A, Peterson M, Raymond FL, Simpson S, Thompson E, Warner J (2007). Reduced penetrance alleles for Huntington's disease: a multi-centre direct observational study. *J Med Genet* **44**: e68.

Racette BA Perlmutter JS (1998). Levodopa responsive parkinsonism in an adult with Huntington's disease. *J Neurol Neurosurg Psychiatry* **65**: 577 – 9.

Rajesh M, Mukhopadhyay P, Haskó G, Huffman JW, Mackie K, Pacher P (2008). CB2 cannabinoid receptor agonists attenuate TNF-alpha-induced human vascular smooth muscle cell proliferation and migration. *Br J Pharmacol* **153**: 347 – 57.

Ravina B, Romer M, Constantinescu R, Biglan K, Brocht A, Kieburtz K, Shoulson I, McDermott MP (2008). The relationship between CAG repeat length and clinical progression in Huntington's disease. *Mov Disord* **23**: 1223 – 7.

Reijonen S, Kukkonen JP, Hyrskyluoto A, Kivinen J, Kairisalo M, Takei N, Lindholm D, Korhonen L (2010). Downregulation of NF-kappaB signaling by mutant huntingtin proteins induces oxidative stress and cell death. *Cell Mol Life Sci* **67**: 1929 – 41.

Reuter I, Hu MT, Andrews TC, Brooks DJ, Clough C, Chaudhuri KR (2000). Late onset levodopa responsive Huntington's disease with minimal chorea masquerading as Parkinson plus syndrome. *J Neurol Neurosurg Psychiatry* **68**: 238 – 41.

Rinaldi-Carmona M, Calandra B, Shire D, Bouaboula M, Oustric D, Barth F, Casellas P, Le Fur G (1996). Characterization of two cloned human CB1 receptor isoforms. *J Pharmacol Exp Ther* **278**: 871 – 8.

Rosenblatt A, Liang KY, Zhou H, Abbott MH, Gourley LM, Margolis RL, Brandt J, Ross CA (2006). The association of CAG repeat length with clinical progression in Huntington disease. *Neurology* **66**: 1016 -20.

Rozenfeld R, Bushlin I, Gomes I, Tzavaras N, Gupta A, Neves S, Battini L, Gusella GL, Lachmann A, Ma'ayan A, Blitzer RD, Devi LA (2011). Receptor heteromerization expands the repertoire of cannabinoid signaling in rodent neurons. *PLoS One* **7** E-pub ahead of print.

Russo EB, Burnett A, Hall B, Parker KK (2005). Agonistics properties of canabidiol of 5-HT1a receptors. *Neurochem Res* **30:** 1037 – 43.

Ryberg E, Vu HK, Larsson N, Groblewski T, Hjorth S, Elebring T, Sjogren S, Greasley PJ (2005). Identification and characterisation of a novel splice variant of the human CB1 receptor. *FEBS Lett* **579**: 259 – 64.

Sagredo O, García-Arencibia M, de Lago E, Finetti S, Decio A, Fernández-Ruiz J (2007). Cannabinoids and neuroprotection in basal ganglia disorders. *Mol Neurobiol* **36**: 82 – 91.

Sapp E, Ge P, Aizawa H, Bird E, Penney J, Young AB, Vonsattel JP, DiFiglia M (1995). Evidence for a preferential loss of enkephalin immunoreactivity in the external globus pallidus in low grade Huntington's disease using high resolution image analysis. *Neuroscience* **64**: 397 – 404.Schagat *et al*. (2007)

Scott LJ (2011). Tetrabenazine: for chorea associated with Huntington's disease. *CNS Drugs* **25**: 1073 – 85.

Scotter EL, Goodfellow CE, Graham ES, Dragunow M, Glass M (2010). Neuroprotective potential of CB1 receptor agonists in an in vitro model of Huntington's disease. *Br J Pharmacol* **160**: 747 – 61.

Shire D, Calandra B, Rinaldi-Carmona M, Oustric D, Pessègue B, Bonnin-Cabanne O, Le Fur G, Caput D & Ferrara P (1996). Molecular cloning, expression and function of the murine CB2 peripheral cannabinoid receptor. *Biochim Biophys Acta* **1307**: 132- 136.

Sipione S, Rigamonti D, Valenza M, Zuccato C, Conti L, Pritchard J, Kooperberg C, Olson JM, Cattaneo E (2002). Early transcriptional profiles in huntingtin-inducible striatal cells by microarray analyses. *Hum Mol Genet* **11**: 1953 – 65.

Slow EJ, Graham RK, Osmand AP, Devon RS, Lu G, Deng Y, Pearson J, Vaid K, Bissada N, Wetzel R, Leavitt BR, Hayden MR (2005). Absence of behavioral abnormalities and neurodegeneration in vivo despite widespread neuronal huntingtin inclusions. Proc Natl Acad Sci U S A **102**: 11402 – 7.

Spires TL, Grote HE, Garry S, Cordery PM, Van Dellen A, Blakemore C, Hannan AJ (2004). Dendritic spine pathology and deficits in experience-dependent dendritic plasticity in R6/1 Huntington's disease transgenic mice. *Eur J Neurosci* **19**: 2799 – 807.

Stadel D, Cristofanon S, Abhari BA, Deshayes K, Zobel K, Vucic D, Debatin KM, Fulda S (2011). Requirement of nuclear factor κB for Smac mimetic-mediated sensitization of pancreatic carcinoma cells for gemcitabine-induced apoptosis. *Neoplasia* **13**: 1162 – 70.

Strand AD, Baquet ZC, Aragaki AK, Holmans P, Yang L, Cleren C, Beal MF, Jones L, Kooperberg C, Olson JM, Jones KR (2007). Expression profiling of Huntington's disease models suggests that brain-derived neurotrophic factor depletion plays a major role in striatal degeneration. *J Neurosci* **27**: 11758 – 68.

Strong TV, Tagle DA, Valdes JM, Elmer LW, Boehm K, Swaroop M, Kaatz KW, Collins FS, Albin RL (1993). Widespread expression of the human and rat Huntington's disease gene in brain and nonneuronal tissues. *Nat Genet* **5**: 259 – 65.

Thompson JC, Harris J, Sollom AC, Stopford CL, Howard E, Snowden JS, Craufurd D (2012). Longitudinal evaluation of neuropsychiatric symptoms in Huntington's disease. *J Neuropsychiatry Clin Neurosci* **24**: 53 – 60.

Trejo A, Tarrats RM, Alonso ME, Boll MC, Ochoa A, Velasquez L (2004). Assessment of the nutrition status of patients with Huntington's disease. *Nutrition* **20**: 192 – 6.

Trettel F, Rigamonti D, Hilditch-Maguire P, Wheeler VC, Sharp AH, Persichetti F, Cattaneo E, MacDonald ME (2000). Dominant phenotypes produced by the HD mutation in STHdh(Q111) striatal cells. *Hum Mol Genet* **9**: 2799 – 809.

Uriguen L, Garcia-Fuster MJ, Callado LF, Morentin B, La Harpe R, Cassado V, Lluis C, Franco R, Garcia-Sevilla JA, Meana JJ (2009). Immunodensity and mRNA expression of A2A adenosine, D2 dopamine, and CB1 cannabinoid receptors in post-mortem frontal cortex of subjects with schizophrenia: effect of antipsychotic treatment. Psychopharmacology *(Berl)* **206**: 313 – 24.

Valenza M, Rigamonti D, Goffredo D, Zuccato C, Fenu S, Jamot L, Strand A, Tarditi A, Woodman B, Racchi M, Mariotti C, Di Donato S, Corsini A, Bates G, Pruss R, Olson JM, Sipione S, Tartani M, Cattaneo E (2005). Dysfunction of the cholesterol biosynthetic pathway in Huntington's disease. *J Neurosci* **25**: 9932 – 9.

van Duijn E, Kingma EM, van der Mast RC (2007). Psychopathology in verified Huntington's disease carriers. *J Neuropsychiatry Clin Neurosci* **19**: 441 – 8.

Van Raamsdonk JM, Murphy Z, Slow EJ, Leavitt BR, Hayden MR (2005). Selective degeneration and nuclear localization of mutant huntingtin in the YAC128 mouse model of Huntington disease. *Hum Mol Genet* **14**: 3823 – 35.

Vitalis T, Laine J, Simon A, Roland A, Leterrier C, Lenkei Z (2008). The type 1 cannabinoid receptor is highly expressed in embryonic cortical projection neurons and negatively regulates neurite growth in vitro. *Euro J Neurosci* **28**: 1705 – 18.

Vonsattel JP, Myers RH, Stevens TJ, Ferrante RJ, Bird ED, Richardson EP Jr (1985). Neuropathological classification of Huntington's disease. *J Neuropathol Exp Neurol* **44** : 559 – 77.

Vonsattel JP, Keller C, Cortes Ramirez EP (2011). Huntington's disease – neuropathology. *Handb Clin Neurol* **100**: 83 – 100.

Walker FO (2007). Huntington's disease. *Semin Neurol* **27**: 143 – 50.

Whittier J, Haydu G, Crawford J (1961). Effect of imipramine (Tofranil) on depression and hyperkinesia in Huntington's disease. *Am J Psychiatry* **118**: 79.

Wright CD, Wu SC, Dahl EF, Sazama AJ, O'Connell TD (2011). Nuclear localization drives alpha1-adrenergic receptor oligomerization and signalling in cardiac myocytes. *Cell Signal* **24**: 794- 802.

Xiao JC, Jewell JP, Lin LS, Hagmann WK, Fong TM, Shen CP (2008). Similar in vitro pharmacology of human cannabinoid CB1 receptor variants expressed in CHO cells. *Brain Res* **1238**: 36 – 43.

Zeng BY, Dass B, Owen A, Rose S, Cannizzaro C, Tel BC, Jenner P (1999). Chronic L- DOPA treatment increases striatal cannabinoid CB1 receptor mRNA expression in 6-hydroxydopamine-lesioned rats. *Neurosci Lett* **276**: 71 – 4.

Zeron MM, Hansson O, Chen N, Wellington CL, Leavitt BR, Brundin P, Hayden MR, Raymond LA (2002). Increased sensitivity to N-methyl-D-aspartate receptor-mediated excitotoxicity in a mouse model of Huntington's disease. *Neuron* **33**: 849 – 60.

Zhang F, Hong S, Stone V, Smith PJ (2007). Expression of cannabinoid CB1 receptors in models of diabetic neuropathy. *J Pharmacol Exp Ther* **323**: 508 – 15.

Zimmer A, Zimmer AM, Hohmann AG, Herkenham M, Bonner TI (1999). Increased motality, hypoactivity, and hypoalgesia in cannabinoid CB1 receptor knockout mice. *Proc Natl Acad Sci U.S.A*. **96**: 5780 – 5.

Zuccato C, Liber D, Ramos C, Tarditi A, Rigamonti D, Tartari M, Valenza M, Cattaneo E (2005). Progressive loss of BDNF in a mouse model of Huntington's disease and rescue by BDNF delivery. *Pharmacol Res* **52**: 133 – 9.

Zuccato C, Marullo M, Conforti P, MacDonald ME, Tartari M, Cattaneo E (2008). Systematic assessment of BDNF and its receptor levels in human cortices affected by Huntington's disease. *Brain Pathol* **18**: 225 – 38.

Zurolo E, Iyer AM, Spliet WG, Van Rijen PC, Troost D, Gorter JA, Aronica E (2010). CB1 and CB2 cannabinoid receptor expression during development and in epileptogenic development pathologies. *Neuroscience* **170**: 28 – 41.